$\mathcal{L}_1$ Adaptive Control for Safety Critical Systems

Guaranteed robustness with fast adaptation

Naira Hovakimyan, Chengyu Cao, Evgeny Kharisov,

Enric Xargay and Irene Gregory

Safety critical systems appear in several application areas, including transportation and air–traffic control systems, nuclear plants, space systems, operation rooms in the hospitals, to name a few. Reliable control of these systems requires not only meeting different performance specifications simultaneously in the presence of multiple constraints, which would together ensure predictable response of the overall system and safe operation of it, but also graceful degradation of the performance when the underlying assumptions leading to the main result are violated. Figure 1 explains this requirement for flight control applications. The green area of angle of attack and angle of sideslip represents the normal flight envelope, where the airplane usually flies in the absence of abnormalities. The gray area represents the configurations for which there are sufficiently adequate models developed based on wind–tunnel data. Outside this wind–tunnel envelope, the aerodynamic models available are usually obtained by extrapolation of wind–tunnel test data, and hence are highly uncertain. Moreover, the pilots are not trained to fly in these conditions. The main objective of the flight control system therefore — from the safety

considerations — is to ensure that an aircraft, suddenly experiencing an adverse flight regime or an unexpected failure, does not "escape" its α–β wind–tunnel data envelope, provided that some control redundancy remains. This objective requires that the control system quickly adapt to the failure with guaranteed and uniform transient performance specifications to ensure the safety of the aircraft.

Typical performance specifications in the majority of control applications include transient and steady–state performance, and robustness margins that the control engineer must be able to trade off in a systematic way, subject to the given hardware constraints such as CPU, sampling rates of sensors and actuators, and control channel bandwidth. This viewpoint has led, as an example, to certification of flight control laws for commercial aviation, where the certification protocols rely on the gain and the phase margins of the gain–scheduled controllers computed for all the operating points [1]. This process is repeated for every aircraft and every route, rendering the overall verification and validation (V&V) overly expensive. The price of the process continues to grow with the growing complexity of the systems.

$\mathcal{L}_1$ adaptive control theory was motivated by the emerging need for certification of advanced flight critical systems with an objective to render the V&V process more affordable. On one hand, this objective required development of a control architecture with a priori quantifiable transient and steady–state performance specifications and robustness margins. On the other hand, achieving the objective appeared to be possible with an architecture that enables fast adaptation with uniform performance bounds without losing robustness. Because the emphasis is on uniform performance bounds for transient and steady–state, the sufficient condition for stability and performance is derived in terms of $\mathcal{L}_1$–norms of underlying transfer functions, which leads to

uniform bounds on the $\mathcal{L}_\infty$–norms of the input–output signals. Therefore the underlying theory is named as $\mathcal{L}_1$ *adaptive control theory*. For definition and properties of the $\mathcal{L}_1$–norm of a system see "$\mathcal{L}_1$–Norm of a System".

The key feature of $\mathcal{L}_1$ adaptive control architectures is the guaranteed robustness in the presence of fast adaptation, which leads to uniform performance bounds both in transient and steady state, and therefore eliminating the need for gain scheduling of the controller parameters [2]. These properties can be achieved by appropriate formulation of the control objective with the understanding that the uncertainties in a feedback loop can be compensated within only the bandwidth of the control channel. By explicitly building the robustness specification into the problem formulation it is possible to decouple adaptation from robustness with continuous feedback and increase the speed of adaptation, subject only to hardware limitations. With $\mathcal{L}_1$ adaptive control architectures, fast adaptation appears to be beneficial both for performance and robustness, while the tradeoff between the two is resolved by means of selection of the underlying filtering structure. The latter, in its turn, is a linear problem and can be addressed using conventional methods from classical and robust control. Moreover, the performance bounds of $\mathcal{L}_1$ adaptive control architectures can be analyzed to determine the extent of the modeling of the system that is, required for the given set of hardware.

From the "Brave Era" to $\mathcal{L}_1$ Adaptive Control

Research in adaptive control was motivated in mid fifties by the design of autopilots for highly agile aircraft that need to operate at a wide range of speeds and altitudes, experiencing large parametric variations. In the early 1950s adaptive control was conceived and put forward

as a technology for automatically adjusting the controller parameters in the face of changing aircraft dynamics [3, 4]. In [5], that period is called the *brave era* because “there was a very short path from idea to flight test with very little analysis in between.” The tragic flight test of the X–15 was the proof of it [6].

The initial results in adaptive control were motivated by system identification [7], which led to an architecture consisting of an on–line parameter estimator combined with automatic control design [8, 9]. Two architectures of adaptive control emerged, namely, the direct method, where only controller parameters were estimated, and the indirect method, where process parameters were estimated and the controller parameters were obtained using some design procedure. The relationships between the architectures are clarified in [10].

The progress in systems theory led to fundamental results for development of stable adaptive control architectures [10–20]. The proofs of stability were accompanied by several examples, including Rohrs’s example, challenging the robustness of adaptive controllers in the presence of unmodeled dynamics [21]. Although [21] includes a proof of the existence of two infinite–gain operators in the closed–loop adaptive system, the explanation given for the phenomena observed in the simulations, which was based on qualitative considerations, was not complete. A more detailed explanation can be found in [22, 23]. Nevertheless, [21] emphasizes a key point, namely, the available adaptive control algorithms to that date were unable to adjust the bandwidth of the closed–loop system and guarantee its robustness. The results and conclusions of [21] motivated numerous investigations of robustness and stability issues of adaptive control systems. In [24–29], causes of instability are analyzed and damping–type modifications of adaptive laws are suggested to prevent them. The basic idea of these

modifications is to limit the gain of the adaptation loop and to eliminate its integral action. Examples of these modifications are the σ–modification [26] and the e–modification [29]. All these modifications address the problem of parameter drift, however they do not directly address the architectural problem identified by Rohrs. An overview of robustness and stability issues of adaptive controllers can be found in [23].

In adaptive control, the nature of the adaptation process plays a central role in both robustness and performance. Ideally, adaptation is expected to correctly respond to all the changes in initial conditions, reference inputs, and uncertainties, by quickly identifying a set of control parameters that provide a satisfactory system response. This fact demands fast estimation schemes with high adaptation rates, and as a consequence, leads to the fundamental question of determining the upper bound on the adaptation rate that would not result in poor robustness characteristics. We notice that the results available in the literature consistently limit the rate of variation of uncertainties, by providing examples of destabilization due to fast adaptation [30, p. 549], while the transient performance analysis is continually reduced to persistency of excitation–type assumption [31], which, besides being a highly undesirable phenomenon, cannot be verified a priori. The lack of analytical quantification of the relationship between the rate of adaptation, the transient response and the robustness margins led to gain–scheduled designs of adaptive controllers, examples of which are the flight tests of late 1990s by Air Force and Boeing [32, 33]. These flight tests relied on intensive Monte–Carlo analysis for determination of the "best" rate of adaptation for various flight conditions. It was apparent that fast adaptation was leading to high frequencies in control signals and increased sensitivity to time delays. The fundamental question was thus reduced to determining an architecture, which would allow for fast adaptation without losing robustness. It was understood that this architecture can reduce the amount of

gain scheduling, and possibly eliminate it, since fast adaptation — in the presence of guaranteed robustness — is able compensate for the negative effects of rapid variation of uncertainties on the system response.

The $\mathcal{L}_1$ adaptive control theory addresses this question by setting in place an architecture for which the estimation loop is decoupled from the control loop. This decoupling allows for arbitrary increase of the estimation rate, limited by only the available hardware, that is, CPU clock speed, while robustness is limited by the available control channel bandwidth and can be addressed by conventional methods from classical and robust control. The architectures of $\mathcal{L}_1$ adaptive control theory have guaranteed transient performance and guaranteed robustness in the presence of fast adaptation, without introducing or enforcing persistence of excitation, without gain scheduling in the controller parameters, without control reconfiguration and without resorting to high–gain feedback. With $\mathcal{L}_1$ adaptive controller in the feedback loop, the response of the closed–loop system can be predicted a priori, thus reducing the amount of Monte–Carlo analysis required for verification and validation of these systems. These features of $\mathcal{L}_1$ adaptive control theory are verified — consistently with the theory — in flight tests and in mid–to–high fidelity simulation environments [34–55].

In the remaining sections of this article we present the two basic architectures of adaptive control, direct and indirect, and use the indirect architecture for transition to $\mathcal{L}_1$ adaptive control. We discuss various insights and properties by analyzing two benchmark problems, specifically, Rohrs's example and two–cart system. Flight tests of NASA's AirSTAR testbed conclude the article.

Limitations and Opportunities Induced by Architectures

In this section we place the focus on the architecture. We first present the direct MRAC architecture using a scalar system. We proceed by considering its state predictor based reparametrization and give a preview of the $\mathcal{L}_1$ adaptive controller. We emphasize the role of the predictor in the architecture.

Thus, consider the first–order system dynamics

$$\dot{x}(t) = -a_m x(t) + b(u(t) + \theta x(t)) \,, \quad x(0) = x_0 \,, \tag{1}$$

where $x(t) \in \mathbb{R}$ is the state of the system, $u(t) \in \mathbb{R}$ is the control input, $a_m \in (0,\ \infty)$, and $b \in (0,\ \infty)$ are known system parameters, and $\theta \in \mathbb{R}$ is a constant system uncertainty with a known (conservative) bound

$$|\theta| \leq \theta_{\max} \,. \tag{2}$$

The control objective is to define the feedback signal $u(t)$ such that $x(t)$ tracks a given uniformly bounded piecewise continuous input $r(t) \in \mathbb{R}$ with quantifiable performance bounds. Let $\|r\|_{\mathcal{L}_\infty} \leq \bar{r}$.

The MRAC architecture proceeds by considering the *nominal controller*

$$u_{\rm nom}(t) = -\theta x(t) + k_g r(t) \,, \tag{3}$$

where

$$k_g \triangleq \frac{a_m}{b} \tag{4}$$

ensures that $x(t)$ tracks step reference inputs with zero steady–state error. This nominal controller assumes perfect cancelation of uncertainties in (1) and leads to the *ideal system*

$$\dot{x}_m(t) = -a_m x_m(t) + bk_g r(t)\,, \quad x_m(0) = x_0\,, \tag{5}$$

where $x_m(t) \in \mathbb{R}$ is the state of the ideal system.

Model Reference Adaptive Control

The model reference adaptive controller is obtained by replacing the unknown parameter θ in the nominal controller (3) by its estimate

$$u(t) = -\hat{\theta}(t)x(t) + k_g r(t)\,, \tag{6}$$

where $\hat{\theta}(t) \in \mathbb{R}$ is the estimate of θ. Substituting (6) into (1) yields the closed–loop system dynamics

$$\dot{x}(t) = -a_m x(t) - b\tilde{\theta}(t)x(t) + bk_g r(t)\,, \quad x(0) = x_0\,,$$

where $\tilde{\theta}(t) \triangleq \hat{\theta}(t) - \theta$ denotes the parametric estimation error.

Letting $e(t) \triangleq x_m(t) - x(t)$ be the tracking error signal, the tracking error dynamics can be written as

$$\dot{e}(t) = -a_m e(t) + b\tilde{\theta}(t)x(t)\,, \quad e(0) = 0\,. \tag{7}$$

The update law for the parametric estimate is given by

$$\dot{\hat{\theta}}(t) = -\Gamma x(t)e(t)\,, \quad \hat{\theta}(0) = \hat{\theta}_0\,, \tag{8}$$

where $\Gamma \in (0,\ \infty)$ is the adaptation gain, and the initial conditions for the parametric estimate $\hat{\theta}_0$ are selected according to (2). The architecture of the closed–loop system is given in Figure 2a.

To analyze the asymptotic properties of this adaptive scheme, consider the Lyapunov function candidate

$$V(e(t), \tilde{\theta}(t)) = \frac{1}{2}e^2(t) + \frac{b}{2\Gamma}\tilde{\theta}^2(t)\,. \tag{9}$$

The time–derivative of $V(e(t), \tilde{\theta}(t))$ along the system trajectories (7)–(8) is given by

$$\begin{aligned}\dot{V}(t) &= e(t)(-a_m e(t) + b\tilde{\theta}(t)x(t)) + \frac{b}{\Gamma}\tilde{\theta}(t)\dot{\tilde{\theta}}(t) \\ &= -a_m e^2(t) + b\tilde{\theta}(t)x(t)e(t) + \frac{b}{\Gamma}\tilde{\theta}(t)\dot{\hat{\theta}}(t)\,.\end{aligned}$$

Using the adaptation law in (8), we obtain

$$\dot{V}(t) = -a_m e^2(t) \leq 0\,.$$

Hence, the equilibrium of (7)–(8) is Lyapunov stable, that is, the signals $e(t)$, $\tilde{\theta}(t)$ are bounded. Since $x(t) = x_m(t) - e(t)$, and $x_m(t)$ is the state of the stable ideal model, then $x(t)$ is bounded. To show that the tracking error converges to zero asymptotically, we compute the second derivative

$$\ddot{V}(t) = -2a_m e(t)\dot{e}(t)\,.$$

It follows from (7) that $\dot{e}(t)$ is uniformly bounded, and hence $\ddot{V}(t)$ is bounded, implying that $\dot{V}(t)$ is uniformly continuous. Application of Barbalat's lemma, stated in "Barbalat's lemma", yields

$$\lim_{t\to\infty} \dot{V}(t) = 0\,,$$

which consequently proves that $e(t) \to 0$ as $t \to \infty$. Thus, $x(t)$ asymptotically converges to $x_m(t)$, which follows $r(t)$ with desired specifications. However, nothing can be claimed regarding the transient behavior of $x(t)$.

Notice that asymptotic convergence of parametric estimation errors to zero is not guaranteed. The parametric estimation errors are guaranteed only to stay bounded.

Model Reference Adaptive Control with State Predictor

Next, we consider a reparametrization of the above architecture using a state predictor, given by

$$\dot{\hat{x}}(t) = -a_m \hat{x}(t) + b(u(t) + \hat{\theta}(t)x(t)) \,, \quad \hat{x}(0) = x_0 \,, \tag{10}$$

where $\hat{x}(t) \in \mathbb{R}$ is the state of the predictor. The system in (10) replicates the system structure from (1), with the unknown parameter θ replaced by its estimate $\hat{\theta}(t)$. Notice that since the state of the plant in (1) is measured, we can initialize the state predictor as $\hat{x}(0) = x_0$. By subtracting (1) from (10), we obtain the *prediction error dynamics*, independent of the control choice

$$\dot{\tilde{x}}(t) = -a_m \tilde{x}(t) + b\tilde{\theta}(t)x(t) \,, \quad \tilde{x}(0) = 0 \,, \tag{11}$$

where $\tilde{x}(t) \triangleq \hat{x}(t) - x(t)$ and $\tilde{\theta}(t) \triangleq \hat{\theta}(t) - \theta$. Notice that these error dynamics are identical to the error dynamics in (7), and is independent of the control signal.

Let the adaptation law for $\hat{\theta}(t)$ be given as

$$\dot{\hat{\theta}}(t) = -\Gamma x(t)\tilde{x}(t) \,, \quad \hat{\theta}(0) = \theta_0 \,, \tag{12}$$

where $\Gamma \in (0,\ \infty)$, and the initial conditions for the parameter estimate $\hat{\theta}_0$ are selected according to (2). This adaptive law is similar to (8) in its structure, except that the tracking error $e(t)$ is replaced by the prediction error $\tilde{x}(t)$. The choice of the Lyapunov function candidate

$$V(\tilde{x}(t), \tilde{\theta}(t)) = \frac{1}{2}\tilde{x}^2(t) + \frac{1}{2\Gamma}\tilde{\theta}^2(t)$$

leads to

$$\dot{V}(t) = -a_m \tilde{x}^2(t) \leq 0\,,$$

implying that the errors $\tilde{x}(t)$ and $\tilde{\theta}(t)$ are uniformly bounded. Moreover, from the fact that

$$\frac{1}{2}\tilde{x}^2(t) \leq V(t) \leq V(0) = \frac{\tilde{\theta}^2(0)}{2\Gamma}\,, \tag{13}$$

we obtain

$$|\tilde{x}(t)| \leq \frac{|\tilde{\theta}(0)|}{\sqrt{\Gamma}}\,, \quad \text{for all} \quad t \geq 0\,.$$

Taking into account that

$$|\tilde{\theta}(0)| = |\hat{\theta}(0) - \theta| \leq 2\theta_{\max}\,,$$

this bound can be rewritten as

$$|\tilde{x}(t)| \leq \frac{2\theta_{\max}}{\sqrt{\Gamma}}\,, \quad \text{for all} \quad t \geq 0\,. \tag{14}$$

Notice, however, that without introducing the feedback signal $u(t)$ we cannot apply Barbalat's lemma to conclude asymptotic convergence of $\tilde{x}(t)$ to zero. Both $x(t)$ and $\hat{x}(t)$ can diverge at the same rate, keeping $\tilde{x}(t)$ uniformly bounded.

If we use (6) in (10), the closed–loop state predictor replicates the bounded ideal system of (5)

$$\dot{\hat{x}}(t) = -a_m \hat{x}(t) + b k_g r(t)\,, \quad \hat{x}(0) = x_0\,. \tag{15}$$

Hence, Barbalat's lemma can be invoked to conclude that $\tilde{x}(t) \to 0$ as $t \to \infty$. The architecture of the closed–loop system with the predictor is given in Figure 2b.

Comparing the closed–loop state predictor in (15) with the ideal model in (5), and the error dynamics in (7) with (11), we see that the state predictor parametrization of MRAC is equivalent to the MRAC architecture. However, Figures 2a and 2b illustrate the fundamental difference between the MRAC and the predictor–based MRAC. In Figure 2b, the control signal is provided as input to both systems, the system and the predictor, while in Figure 2a, the control signal serves only as input to the system. Therefore in the predictor–based MRAC the control signal can be redefined without affecting the proof of stability, as long as the state predictor with the redefined controller remains bounded. Exactly this feature is explored in details toward obtaining the first architecture of $\mathcal{L}_1$ adaptive control theory [56].

Tuning Challenges

From (14) it follows that the prediction error, or equivalently the tracking error can be arbitrarily reduced for all $t \geq 0$ (including the transient phase) by increasing the adaptation gain Γ. However, from the control law in (6) and the adaptive laws in (8) and (12), it follows that large adaptive gains result in high–gain feedback control, which manifests itself by high–frequency oscillations in the control signal and reduced tolerance to time delays. Moreover, applications requiring identification schemes with time scales comparable with those of the

closed–loop dynamics appear to be challenging due to undesirable interactions of the two processes [23]. Due to the lack of systematic design guidelines to select an adequate adaptation gain, tuning of such applications is done by either computationally expensive Monte–Carlo simulations or trial–and–error methods following some empirical guidelines or engineering intuition. As a consequence, proper tuning of MRAC architectures represents a major challenge and has largely remained an open question in the literature.

$\mathcal{L}_1$ Adaptive Control

The $\mathcal{L}_1$ adaptive controller is obtained from the predictor–based MRAC by setting the $\mathcal{L}_1$ control law to be the output of a stable, strictly proper transfer function $C(s)$

$$u(s) = C(s)\hat{\eta}(s)\,, \tag{16}$$

where $\hat{\eta}(s)$ is the Laplace transform of

$$\hat{\eta}(t) \triangleq -\hat{\theta}(t)x(t) + k_g r(t)\,.$$

The architecture of the $\mathcal{L}_1$ adaptive controller is shown in Figure 2c.

Unlike the predictor–based MRAC, the closed–loop system with $\mathcal{L}_1$ adaptive controller does not behave similar to the ideal system in (5), due to the limited bandwidth of the control channel enforced by $C(s)$. Instead, the closed–loop system is approximating the $\mathcal{L}_1$ *reference system*. To derive the dynamics of the reference system for the $\mathcal{L}_1$ controller, consider the case

when the system parameters are precisely known. Then, the controller in (16) takes the form

$$u_{\rm ref}(s) = C(s)(k_g r(s) - \theta x_{\rm ref}(s))\,. \tag{17}$$

Notice that this control law as compared to the nominal control law in (3) aims for only partial compensation of uncertainties, namely, for only those that are within the bandwidth of the control channel. Substituting the *reference controller* into the system dynamics in (1) leads to the closed–loop $\mathcal{L}_1$ reference model, which incorporates the filter

$$x_{\rm ref}(s) = H(s)C(s)k_g r(s) + H(s)(1 - C(s))\theta x_{\rm ref}(s) + x_{\rm in}(s)\,, \tag{18}$$

where

$$H(s) \triangleq \frac{b}{s + a_m}\,, \quad x_{\rm in}(s) \triangleq \frac{1}{s + a_m} x_0\,.$$

We notice that $x_{\rm in}(s)$ is the Laplace transform of the ideal system's response to the initial condition. The first term in (18) contains the ideal system (5) and the filter, which corresponds to the desired behavior of the system in the absence of uncertainties. The second term, as we see, depends on the uncertainty θ. The transfer function $1 - C(s)$ is a highpass filter, which attenuates the low frequency content of the uncertainties. This approach differs from the MRAC schemes above, where the nominal controller in (3) attempts to follow the ideal system and to compensate for the uncertainties in the entire frequency range. The $\mathcal{L}_1$ adaptive controller pursues a less ambitious, yet practically achievable objective, namely, compensation of the uncertainties within only the bandwidth of the control channel. We notice that the $\mathcal{L}_1$ reference system is equivalent to a disturbance observer (DOB) type closed–loop system. For more details see "Bridging Adaptive and Robust Control".

Notice, however, that the consequence of the lowpass filter in the control channel is that the stability of the $\mathcal{L}_1$ reference system is not guaranteed a priori, as it is for the ideal system in (5). Using the $\mathcal{L}_1$–norm of the transfer functions, we obtain the upper bound from (18)

$$\|x_{\rm ref}\|_{\mathcal{L}_\infty} \leq \|H(s)C(s)k_g\|_{\mathcal{L}_1} \|r\|_{\mathcal{L}_\infty} + \|H(s)(1-C(s))\theta\|_{\mathcal{L}_1} \|x_{\rm ref}\|_{\mathcal{L}_\infty} + \|x_{\rm in}\|_{\mathcal{L}_\infty} ,$$

which can be rewritten as

$$\|x_{\rm ref}\|_{\mathcal{L}_\infty} \leq \frac{\|H(s)C(s)k_g\|_{\mathcal{L}_1} \|r\|_{\mathcal{L}_\infty} + \|x_{\rm in}\|_{\mathcal{L}_\infty}}{1 - \|G(s)\theta\|_{\mathcal{L}_1}} , \tag{19}$$

where

$$G(s) \triangleq H(s)(1-C(s)) . \tag{20}$$

We see that the denominator of (19) must be positive in order to make the bound feasible. Thus, we obtain the sufficient condition

$$\|G(s)\theta\|_{\mathcal{L}_1} < 1 \tag{21}$$

for stability of the $\mathcal{L}_1$ reference system. The question of the filter design to satisfy the condition in (21) is discussed in "Verifying the $\mathcal{L}_1$–Norm Bound".

Next, we rewrite the control signal in (16) as

$$u(s) = C(s)(k_g r(s) - \theta x(s) - \tilde{\eta}(s)) , \tag{22}$$

where $\tilde{\eta}(t) \triangleq \tilde{\theta}(t)x(t)$. Rewriting the system dynamics (1) in frequency domain, we obtain

$$\begin{aligned} x(s) &= \frac{b}{s+a_m}(u(s)+\theta x(s)) + x_{\rm in}(s) \\ &= H(s)\bigg(C(s)k_g r(s) + (1-C(s))\theta x(s) - C(s)\tilde{\eta}(s)\bigg) + x_{\rm in}(s)\,. \end{aligned} \tag{23}$$

Subtracting (23) from (18) gives

$$x_{\rm ref}(s) - x(s) = G(s)\theta(x_{\rm ref}(s) - x(s)) + H(s)C(s)\tilde{\eta}(s)\,,$$

which further can be rewritten as

$$x_{\rm ref}(s) - x(s) = \frac{C(s)}{1-G(s)\theta}H(s)\tilde{\eta}(s)\,.$$

Notice that from the prediction error dynamics in (11) it follows that

$$\tilde{x}(s) = \frac{b}{s+a_m}\tilde{\eta}(s)\,, \tag{24}$$

which leads to

$$x_{\rm ref}(s) - x(s) = \frac{C(s)}{1-G(s)\theta}\tilde{x}(s)\,.$$

Using the bound on $|\tilde{x}(t)|$ in (14), we obtain the upper bound

$$\|x_{\rm ref} - x\|_{\mathcal{L}_\infty} \leq \left\|\frac{C(s)}{1-G(s)\theta}\right\|_{\mathcal{L}_1}\|\tilde{x}\|_{\mathcal{L}_\infty} \leq \left\|\frac{C(s)}{1-G(s)\theta}\right\|_{\mathcal{L}_1}\frac{2\theta_{\max}}{\sqrt{\Gamma}}\,. \tag{25}$$

This upperbound implies that the error between the states of the closed–loop system with the $\mathcal{L}_1$ adaptive controller and the $\mathcal{L}_1$ reference system, which uses the reference controller, can be uniformly bounded by a constant inverse proportional to the square root of the rate of adaptation.

Similarly, using (22), (17), and (24), we can derive

$$\begin{aligned} u_{\rm ref}(s) - u(s) &= C(s)(-\theta(x_{\rm ref}(s) - x(s)) + \tilde{\eta}(s)) \\ &= -C(s)\theta(x_{\rm ref}(s) - x(s)) + C(s)\frac{s + a_m}{b}\tilde{x}(s)\,. \end{aligned} \tag{26}$$

Because $C(s)$ is strictly proper and stable, $C(s)(s + a_m)/b$ is proper and stable, and hence it has bounded $\mathcal{L}_1$–norm. Thus, we obtain the uniform upper bound for the difference in the control signals

$$\|u_{\rm ref} - u\|_{\mathcal{L}_\infty} \leq \|C(s)\theta\|_{\mathcal{L}_1}\|x_{\rm ref} - x\|_{\mathcal{L}_\infty} + \left\|C(s)\frac{s + a_m}{b}\right\|_{\mathcal{L}_1} \frac{2\theta_{\max}}{\sqrt{\Gamma}}\,. \tag{27}$$

Notice that without the lowpass filter, that is, with $C(s) = 1$, the transfer function $C(s)(s+a_m)/b$ reduces to $(s+a_m)/b$, which is improper, and hence, in the absence of the filter $C(s)$, we cannot uniformly upper bound $|u_{\rm ref}(t) - u(t)|$ as we did in (27).

This analysis illustrates the role of $C(s)$ toward obtaining a uniform performance bound for the control signal of the $\mathcal{L}_1$ adaptive control architecture, as compared to its nonadaptive version. We further notice that this uniform bound is inverse proportional to the square root of the rate of adaptation, similar to the tracking error. Thus, both performance bounds can be systematically improved by increasing the rate of adaptation.

Performance and Robustness Analysis using a Simplified Scalar System

Because a large adaptation rate in case of MRAC leads to poor robustness characteristics, we conduct a preliminary robustness analysis of $\mathcal{L}_1$ controller using classical control tools. For that purpose we assume that $a_m = 1$ and $b = 1$ in (1), and we analyze the performance of

the closed–loop adaptive system in the presence of input disturbances and measurement noise. We notice that in this case both MRAC and $\mathcal{L}_1$ adaptive controller reduce to a linear model–following controller, the performance and robustness of which can be analyzed using tools from classical control. Namely, we use Nyquist criterion to analyze stability and robustness of this system. Thus, consider the scalar system

$$\dot{x}(t) = -x(t) + u(t) + \sigma(t)\,, \quad x(0) = x_0\,, \tag{28}$$

$$z(t) = x(t) + n(t)\,,$$

where $z(t) \in \mathbb{R}$ is the measurement of the system state $x(t) \in \mathbb{R}$, corrupted with noise $n(t) \in \mathbb{R}$; $\sigma(t) \in \mathbb{R}$ is the unknown signal to be rejected by the control input $u(t) \in \mathbb{R}$.

Model Reference Adaptive Control

Since we have shown that the state predictor parametrization of MRAC is equivalent to the MRAC, in this section we focus on robustness and performance analysis of the MRAC architecture described above in (6) and (8). For the system with input disturbance in (28), MRAC reduces to an integral controller

$$u(t) = -\hat{\sigma}(t) + r(t)\,, \tag{29}$$

where $\hat{\sigma}(t) \in \mathbb{R}$ is the estimate of $\sigma(t)$, given by

$$\dot{\hat{\sigma}}(t) = -\Gamma e(t) = -\Gamma(x_m(t) - z(t))\,, \quad \sigma(0) = \sigma_0\,, \tag{30}$$

$\Gamma \in (0,\ \infty)$, and $x_m(t) \in \mathbb{R}$ is the state of the ideal system in (5), which in this case becomes

$$\dot{x}_m(t) = -x_m(t) + r(t)\,, \quad x_m(0) = x_0\,. \tag{31}$$

The block diagram of the closed–loop system is shown in Figure 3.

From Figure 3 we can see that in the absence of input disturbance and measurement noise, the closed–loop system response is identical to the response of the ideal system in (31). Next, for the performance analysis we consider the transfer functions from the input disturbance and the measurement noise to the system control input and the output. From Figure 3 we obtain

$$H_{x\sigma}(s) = \frac{s}{s^2 + s + \Gamma}\,, \qquad H_{xn}(s) = -\frac{\Gamma}{s^2 + s + \Gamma}\,, \tag{32}$$

$$H_{u\sigma}(s) = -\frac{\Gamma}{s^2 + s + \Gamma}\,, \qquad H_{un}(s) = -\Gamma\frac{s+1}{s^2 + s + \Gamma}\,. \tag{33}$$

We notice that all the transfer functions have the same denominator, which gives a stable pair of closed–loop poles with the damping inverse proportional to the $\sqrt{\Gamma}$ and the natural frequency proportional to $\sqrt{\Gamma}$. Hence, in the presence of fast adaptation the MRAC scheme may develop high–frequency oscillations. Further analysis shows that increasing the adaptation gain, on one hand, reduces the gain of $H_{x\sigma}(s)$ at low–frequencies, which improves disturbance rejection, but on the other hand, larger adaptation gain shifts the pair of the closed–loop system poles to the right. This fact implies that $H_{un}(s)$ acts similarly to a differentiator and leads to undesired amplification of the measurement noise in the control channel. Thus we see that in MRAC the adaptation gain resolves the performance tradeoff between disturbance rejection and noise attenuation.

Next we investigate the robustness properties of MRAC. For this purpose we consider

the loop transfer function of this system with negative feedback

$$L_1(s) = \frac{\Gamma}{s(s+1)}\,, \tag{34}$$

which gives the two most commonly used stability margins, that is, the gain and the phase margins. Figure 5a shows that the Nyquist plot of $L_1(s)$ never crosses the negative part of the real line; therefore the closed–loop system has infinite gain margin $g_m = \infty$. The gain crossover frequency ω_{gc} can be computed from

$$|L_1(j\omega_{gc})| = \frac{\Gamma}{\omega_{gc}\sqrt{\omega_{gc}^2+1}} = 1\,,$$

which leads to the phase margin

$$\phi_m = \pi + \angle L_1(j\omega_{gc}) = \arctan\left(\frac{1}{\omega_{gc}}\right)\,.$$

Careful analysis indicates that increasing Γ leads to higher gain crossover frequency and consequently reduces the phase margin. The reduction of phase margin with large Γ can also be observed in Figure 5a. Thus, if increasing Γ improves the tracking performance for all $t \geq 0$, including the transient phase, then it hurts the robustness, which is also called relative stability, of the closed–loop system. Hence, the adaptation rate Γ is the key to the tradeoff between performance and robustness in the design of MRAC.

$\mathcal{L}_1$ Adaptive Control

The state predictor of the $\mathcal{L}_1$ adaptive controller given by (10) takes the form

$$\dot{\hat{x}}(t) = -\hat{x}(t) + u(t) + \hat{\sigma}(t)\,, \quad \hat{x}(0) = x_0\,.$$

The parametric estimate, given by (12), is thus replaced by

$$\dot{\hat{\sigma}}(t) = -\Gamma\tilde{x}(t)\,, \quad \sigma(0) = \sigma_0\,,$$

where $\tilde{x}(t) \triangleq \hat{x}(t) - z(t)$ and $\Gamma \in (0,\ \infty)$. Next, similar to (16), we use a lowpass filtered version of $\hat{\sigma}(t)$

$$u(s) = -C(s)\hat{\sigma}(s) + r(s)\,. \tag{35}$$

The block diagram of this system is given in Figure 4.

From Figure 4 we see that, similar to MRAC, in the absence of input disturbance and measurement noise, the closed–loop system recovers the ideal model in (31). From the block diagram we can also derive the transfer functions from the input disturbance and the measurement noise to the system input and the output

$$H_{x\sigma}(s) = \frac{1}{s+1}\left(1 - \frac{\Gamma C(s)}{s^2+s+\Gamma}\right)\,, \qquad H_{xn}(s) = -\frac{\Gamma}{s^2+s+\Gamma}C(s)\,, \tag{36}$$

$$H_{u\sigma}(s) = -\frac{\Gamma}{s^2+s+\Gamma}C(s)\,, \qquad H_{un}(s) = -\Gamma\frac{s+1}{s^2+s+\Gamma}C(s)\,. \tag{37}$$

Notice that these transfer functions have the same denominator. Moreover, in the absence of the filter, that is, $C(s) \equiv 1$, the controller in (35) reduces to the MRAC–type integral controller

introduced in (29), and the transfer functions in (36)–(37) reduce to (32)–(33). This fact implies that the $\mathcal{L}_1$ controller also results in a lightly damped closed–loop pole in the presence of fast adaptation. However, for $\mathcal{L}_1$ controller all the transfer functions containing this pole are followed by the lowpass filter. Hence, the effect of the lightly damped pole can be compensated or even canceled by appropriate choice of the filter, avoiding the undesired transient behavior, which is observed in MRAC. This compensation allows for safe increase of the adaptation rate without hurting the noise attenuation properties of the system and without causing high frequency oscillations in the control channel. Notice that the origin of the fast, lightly damped pole is in the estimation loop shown in Figure 4, which is implemented inside the controller block. Hence the compensation of this pole with the help of the filter occurs completely inside the controller and cannot be affected by the system uncertainties or unmodeled system dynamics. On the other hand, from Figure 3 we can see that for MRAC the lightly damped pole due to large adaptation gain is generated by the loop, which involves the plant. Therefore even small system uncertainties in the presence of fast adaptation may cause this pole to drift to the right hand side of the complex plain causing closed–loop system instability. This observation elucidates how the lowpass filter in $\mathcal{L}_1$ adaptive controller helps to decouple the estimation performance from the robustness of the adaptive controller, which consequently enables fast adaptation.

In the foregoing analysis, we further consider a first–order lowpass filter

$$C(s) = \frac{\omega_c}{s + \omega_c}\,, \tag{38}$$

although similar results can be obtained using more complex filters. The loop transfer function

of this system (with negative feedback) is

$$L_2(s) = \frac{\Gamma C(s)}{s(s+1) + \Gamma(1 - C(s))}\,. \tag{39}$$

Notice that in the absence of the filter, that is, with $C(s) = 1$, the loop transfer function in (39) reduces to (34), that is, $L_2(s) = L_1(s)$. Although (39) has a more complex structure as compared to (34), the Nyquist plot in Figure 5b shows that the phase and the gain margins of the $\mathcal{L}_1$ controller are not significantly affected by large values of Γ. The effect of the adaptive gain on the robustness margins of the two closed–loop systems is presented in Figure 6. The figure shows that, while the phase margin of the MRAC–type integral controller vanishes as the adaptation gain Γ is increased, the $\mathcal{L}_1$ adaptive controller has guaranteed bounded–away–from–zero phase and gain margins in the presence of fast adaptation.

Further, notice that, as $\Gamma \to \infty$, the expression in (39) leads to the limiting loop transfer function, given by

$$L_{2l}(s) = \frac{C(s)}{1 - C(s)} = \frac{\omega_c}{s}\,. \tag{40}$$

This loop transfer function represents the loop transfer function of the $\mathcal{L}_1$ reference system, which in this case reduces to

$$x_{\rm ref}(s) = \frac{1}{s+1}(u_{\rm ref}(s) + \sigma(s))\,, \tag{41}$$

$$u_{\rm ref}(s) = -C(s)\sigma(s) + r(s)\,. \tag{42}$$

This transfer function has an infinite gain margin, that is, $g_m = \infty$, and a phase margin of $\phi_m = \pi/2$. However, from Figure 6a, we notice that the gain margin of the $\mathcal{L}_1$ controller is

finite and converges to $g_m = 6.02$ dB with the increase of Γ. We note that the (high–frequency) dynamics of the adaptation loop do not appear in the limiting loop transfer function in (40). Then, since the phase crossover frequency tends to infinity as the adaptation gain Γ increases, this limiting loop transfer function cannot be used to analyze the gain margin of the closed–loop system with the $\mathcal{L}_1$ adaptive controller. However, the gain crossover frequency stays in the low–frequency range, where the limiting loop transfer function in (40) approximates the loop transfer function in (39). Consequently, the limiting loop transfer function can be used to analyze the phase margin of the closed–loop adaptive system.

Adaptive Control in the Presence of Unknown Input Gain

In this section we revisit the main adaptive architectures for a class of multidimensional systems with time varying uncertainties, disturbances and an unknown input gain. We consider direct and indirect MRAC architectures, as given in Figures 7a, 7b [57]. In the direct architecture, the controller parameters are directly updated, while in the indirect architecture the plant parameters are estimated and used in the feedback law. Notice that in the case of known system input gain these architectures are identical and therefore we do not distinguish them in the previous section as direct and indirect, but we refer to the difference due to the predictor. We present in this section the indirect architecture using the state predictor parametrization of MRAC, and — similar to the prior development — use this architecture as a basis for the development of the $\mathcal{L}_1$ adaptive controller.

Thus, consider the system dynamics given by

$$\dot{x}(t) = A_m x(t) + b\left(\omega u(t) + \theta^\top(t) x(t) + \sigma(t)\right), \quad x(0) = x_0, \tag{43}$$

$$y(t) = c^\top x(t), \tag{44}$$

where $x(t) \in \mathbb{R}^n$ is the measured state of the system; $A_m \in \mathbb{R}^{n\times n}$ is a known Hurwitz matrix that defines the desired dynamics for the closed–loop system; $b,\, c \in \mathbb{R}^n$ are known constant vectors; $u(t) \in \mathbb{R}$ is the control input; $y(t) \in \mathbb{R}$ is the regulated output; $\sigma(t) \in \mathbb{R}$ is the unknown disturbance, $\theta(t) \in \mathbb{R}^n$ is the vector of unknown time–varying parameters, and $\omega \in (0,\ \infty)$ is the unknown system input gain. The unknown quantities are subject to the bounds

$$\omega \in \Omega \triangleq [\omega_{\min},\ \omega_{\max}], \quad \theta(t) \in \Theta, \quad \sigma(t) \in \Delta \triangleq [-\sigma_b,\ \sigma_b], \tag{45}$$

$$\|\dot{\theta}(t)\| \leq d_\theta, \quad |\dot{\sigma}(t)| \leq d_\sigma, \tag{46}$$

for all $t \geq 0$, where Θ is a given convex compact set,

$$0 < \omega_{\min} < \omega_{\max} < \infty,$$

and σ_b, d_θ, d_σ are known lower and upper bounds. The control objective is to determine a state feedback controller $u(t)$ such that $y(t)$ follows a given uniformly bounded piecewise continuous input $r(t) \in \mathbb{R}$, $\|r\|_{\mathcal{L}_\infty} \leq \bar{r}$, with the desired specifications given according to the ideal system

$$\dot{x}_m(t) = A_m x_m(t) + b k_g r(t), \quad x_m(0) = x_0, \tag{47}$$

$$y_m(t) = c^\top x_m(t), \tag{48}$$

where $x_m(t) \in \mathbb{R}^n$ is the state, and

$$k_g \triangleq -\frac{1}{c^\top A_m^{-1} b}\,. \tag{49}$$

ensures that $y_m(t)$ tracks step reference inputs with zero steady–state error. We notice that this ideal model is obtained from the system in (43)–(44) by applying the nominal controller

$$u_{\rm nom}(t) = \frac{1}{\omega}\left(k_g r(t) - \theta^\top(t) x(t) - \sigma(t)\right)\,, \tag{50}$$

which, similar to (3), assumes complete cancelation of uncertainties in the system (43)–(44), irrespective of their nature or the origin.

Direct Model Reference Adaptive Control

The direct MRAC law uses the estimates of the unknown controller parameters in (50) and takes the form

$$u(t) = \hat{k}_r(t) r(t) - \hat{k}_x^\top(t) x(t) - \hat{d}(t)\,, \tag{51}$$

where $\hat{k}_x(t) \in \mathbb{R}^n$ is the estimate of $k_x(t) \triangleq \theta(t)/\omega$, $\hat{d}(t) \in \mathbb{R}$ is the estimate of $d(t) \triangleq \sigma(t)/\omega$, and $\hat{k}_r(t) \in \mathbb{R}$ is the estimate of $k_r \triangleq k_g/\omega$ in (50). Substituting (51) into (43) yields the closed–loop system dynamics

$$\begin{aligned}
\dot{x}(t) &= \left(A_m - \omega b \tilde{k}_x^\top(t)\right) x(t) - \omega b \tilde{d}(t) + \omega b \hat{k}_r(t) r(t)\,, \quad x(0) = x_0\,,\\
y(t) &= c^\top x(t)\,,
\end{aligned}$$

where $\tilde{k}_x(t) \triangleq \hat{k}_x(t) - k_x(t)$, and $\tilde{d}(t) \triangleq \hat{d}(t) - d(t)$ denote the parametric estimation error.

Let $e(t) \triangleq x_m(t) - x(t)$ be the tracking error signal. Then

$$\dot{e}(t) = A_m e(t) + \omega b \tilde{k}_x^\top(t) x(t) + \omega b \tilde{d}(t) - b\omega \tilde{k}_r(t) r(t)\,, \quad e(0) = 0\,, \tag{52}$$

where $\tilde{k}_r(t) \triangleq \hat{k}_r(t) - k_r$. In the case of time varying system parameters, the update laws for the parametric estimates use the projection operator, which ensures boundedness of the adaptive estimates by definition. The projection operator plays a crucial role in ensuring robustness and avoiding parameter drift. For more details see "Projection Operator". Thus, the adaptation laws are given by

$$\dot{\hat{k}}_x(t) = \Gamma \mathrm{Proj}\big(\hat{k}_x(t), -x(t)e^\top(t)Pb\big)\,, \quad \hat{k}_x(0) = k_{x0}\,, \tag{53}$$

$$\dot{\hat{d}}(t) = \Gamma \mathrm{Proj}\big(\hat{d}(t), -e^\top(t)Pb\big)\,, \quad \hat{d}(0) = d_0\,, \tag{54}$$

$$\dot{\hat{k}}_r(t) = \Gamma \mathrm{Proj}\big(\hat{k}_r(t), r(t)e^\top(t)Pb\big)\,, \quad \hat{k}_r(0) = k_{r0}\,, \tag{55}$$

where $\Gamma \in (0, \infty)$ is the adaptation gain, $\hat{k}_{x0}$, $\hat{d}_0$, $\hat{k}_{r0}$ represent the "best possible guess" of the ideal values of the unknown parameters, the projection bounds are set according to the available conservative bounds in (45), and $P = P^\top > 0$ solves the algebraic Lyapunov equation

$$A_m^\top P + P A_m = -Q$$

for arbitrary $Q = Q^\top > 0$.

Next we examine boundedness and asymptotic properties of the error dynamics in (52) by considering the Lyapunov function candidate

$$V(e(t), \tilde{k}_x(t), \tilde{d}(t), \tilde{k}_r(t)) = e^\top(t)Pe(t) + \frac{1}{\Gamma}\left(\tilde{k}_x^\top(t)\tilde{k}_x(t) + \tilde{d}^2(t) + \tilde{k}_r^2(t)\right)\omega\,. \tag{56}$$

Using the property of the projection operator in (S3), we obtain an upper bound on the time–derivative of the Lyapunov function along the system trajectories (52)–(55)

$$\dot{V}(t) \leq -e^{\top}(t)Qe(t) - \frac{2}{\Gamma}\left(\tilde{k}_x^{\top}(t)\dot{k}_x(t) + \tilde{d}(t)\dot{d}(t)\right)\omega\,.$$

Notice that $\dot{V}(t) \leq 0$, if

$$e^{\top}(t)Qe(t) \geq \frac{4\omega_{\max}}{\Gamma\omega_{\min}^2}\left(\theta_{\max}\|\theta\|d_\theta + \sigma_b d_\sigma\right)\,,$$

where

$$\theta_{\max} \triangleq \max_{\theta\in\theta}\|\theta\|\,. \tag{57}$$

Therefore, from (56) it follows that

$$\|e(t)\| \leq \sqrt{\frac{\omega_{\max}\theta_{md}}{\lambda_{\min}(P)\omega_{\min}^2\Gamma}}\,, \quad \text{for all} \;\; t \geq 0\,,$$

where $\lambda_{\min}(\cdot)$ and $\lambda_{\max}(\cdot)$ denote the minimum and the maximum eigenvalue of the matrix, and

$$\theta_{md} \triangleq \frac{4\lambda_{\max}(P)}{\lambda_{\min}(Q)}\left(\theta_{\max}d_\theta + \sigma_b d_\sigma\right) + 4\theta_{\max}^2 + 4\sigma_b^2 + k_g^2\frac{(\omega_{\max}-\omega_{\min})^2}{\omega_{\max}^2}\,.$$

Hence, the signals $e(t)$, $\tilde{k}_x(t)$, $\tilde{d}(t)$, $\tilde{k}_r(t)$ are uniformly bounded. Since $x(t) = x_m(t) - e(t)$, and $x_m(t)$ is the state of a stable ideal model, then $x(t)$ is uniformly bounded. We note that in the presence of time–varying system parameters or disturbances the asymptotic stability cannot be achieved.

Indirect Model Reference Adaptive Control

In an indirect MRAC scheme, given in Figure 7b, we estimate the plant parameters $\hat{\omega}(t) \in \mathbb{R}$, $\hat{\theta}(t) \in \mathbb{R}^n$, and $\hat{\sigma}(t) \in \mathbb{R}$, and not the controller parameters. To derive the adaptive laws we consider a reparametrization of the above architecture using a state predictor, given by

$$\dot{\hat{x}}(t) = A_m \hat{x}(t) + b(\hat{\omega}(t)u(t) + \hat{\theta}^\top(t)x(t) + \hat{\sigma}(t)) \,, \quad \hat{x}(0) = x_0 \,, \tag{58}$$

$$\hat{y}(t) = c^\top \hat{x}(t) \,, \tag{59}$$

where $\hat{x}(t) \in \mathbb{R}^n$ is the state of the predictor. The system in (58)–(59) replicates the system structure from (43)–(44), with the unknown parameters replaced by their estimates. The error in the indirect control scheme is the estimation error $\tilde{x}(t) \triangleq \hat{x}(t) - x(t)$, which is governed by

$$\dot{\tilde{x}}(t) = A_m \tilde{x}(t) + b\left(\tilde{\omega}(t)u(t) + \tilde{\theta}^\top(t)x(t) + \tilde{\sigma}(t)\right) \,, \quad \tilde{x}(0) = 0 \,, \tag{60}$$

where

$$\tilde{\omega}(t) \triangleq \hat{\omega}(t) - \omega \,, \quad \tilde{\theta}(t) \triangleq \hat{\theta}(t) - \theta(t) \,, \quad \tilde{\sigma}(t) \triangleq \hat{\sigma}(t) - \sigma(t) \,.$$

The indirect MRAC control law uses the estimates of the plant parameters to achieve the control objective. The control law is obtained by replacing the values of the unknown plant parameters in (50) by their estimates

$$u(t) = \frac{1}{\hat{\omega}(t)}\left(k_g r(t) - \hat{\theta}^\top(t)x(t) - \hat{\sigma}(t)\right) \,. \tag{61}$$

This definition of the control law requires the adaptation law to ensure that the estimate $\hat{\omega}(t)$ remains bounded away from zero. This property is achieved by the projection based adaptation

law, similar to (53)–(55)

$$\dot{\hat{\omega}}(t) = \Gamma \mathrm{Proj}(\hat{\omega}(t), -u(t)\tilde{x}^\top(t)Pb)\,, \quad \hat{\omega}(0) = \hat{\omega}_0\,, \tag{62}$$

$$\dot{\hat{\theta}}(t) = \Gamma \mathrm{Proj}(\hat{\theta}(t), -x(t)\tilde{x}^\top(t)Pb)\,, \quad \hat{\theta}(0) = \hat{\theta}_0\,, \tag{63}$$

$$\dot{\hat{\sigma}}(t) = \Gamma \mathrm{Proj}(\hat{\sigma}(t), -\tilde{x}^\top(t)Pb)\,, \quad \hat{\sigma}(0) = \hat{\sigma}_0\,, \tag{64}$$

where $\Gamma \in (0, \infty)$ is the adaptation gain, and $\hat{\omega}_0 > \omega_{\min}$, $\hat{\theta}_0$, $\hat{\sigma}_0$ are the initial conditions for the plant parameter estimates selected according to the conservative knowledge of their ideal values.

The choice of the Lyapunov function candidate

$$V(\tilde{x}(t), \tilde{\omega}(t), \tilde{\theta}(t), \tilde{\sigma}(t)) = \tilde{x}^\top(t)P\tilde{x}(t) + \frac{1}{\Gamma}\left(\tilde{\omega}^2(t) + \tilde{\theta}^\top(t)\tilde{\theta}(t) + \tilde{\sigma}^2(t)\right) \tag{65}$$

leads to

$$\dot{V}(t) \leq -\tilde{x}^\top(t)Q\tilde{x} - \frac{2}{\Gamma}\left(\tilde{\theta}^\top(t)\dot{\theta}(t) + \tilde{\sigma}(t)\dot{\sigma}(t)\right)\,. \tag{66}$$

Similar to direct MRAC, from this inequality we obtain the uniform upper bound

$$\|\tilde{x}(t)\| \leq \frac{\gamma_0}{\sqrt{\Gamma}}\,, \quad \text{for all} \;\; t \geq 0\,, \tag{67}$$

where

$$\gamma_0 \triangleq \sqrt{\frac{\theta_{mi}}{\lambda_{\min}(P)}}\,, \quad \theta_{mi} \triangleq 4\theta_{\max}^2 + 4\sigma_b^2 + (\omega_{\max} - \omega_{\min})^2 + 4\frac{\lambda_{\max}(P)}{\lambda_{\min}(Q)}\left(\theta_{\max}d_\theta + \sigma_b d_\sigma\right)\,, \tag{68}$$

and $\theta_{\max}$ is defined in (57). We notice that the Lyapunov function in (65) and its derivative in (66) are independent of the choice of the control signal. Hence, the uniform bound for $\tilde{x}(t)$ is independent of the control choice.

Notice that substitution of (61) into (58) leads to the same ideal model as in (47)

$$\dot{\hat{x}}(t) = A_m \hat{x}(t) + b k_g r(t)\,, \quad \hat{x}(0) = x_0.$$

Hence, the state predictor with the indirect control law given by (61) is equivalent to the ideal system in (47). Since $x(t) = \hat{x}(t) - \tilde{x}(t)$, and $\hat{x}(t) = x_m(t)$, where $x_m(t)$ is the state of a stable ideal model, then $x(t)$ is uniformly bounded. Finally, the bound in (67) implies that the tracking error can be arbitrarily reduced if we increase the adaptation gain Γ.

$\mathcal{L}_1$ Adaptive Control

The $\mathcal{L}_1$ adaptive control architecture for unknown system input gain is presented in Figure 7c [56]. Consider the system in (43), and assume that (45) holds. The $\mathcal{L}_1$ adaptive controller uses the same state predictor and the adaptation laws, as the indirect MRAC given by (58)–(59) and (62)–(64), respectively. Therefore the $\mathcal{L}_1$ controller has the same prediction error dynamics as the indirect MRAC in (60), and the uniform bound on the prediction error given in (67) also holds. The key difference between the indirect MRAC and the $\mathcal{L}_1$ adaptive controller lies in the definition of the control law. Recall that in the case of known system input gain, the $\mathcal{L}_1$ adaptive controller considers a lowpass filter in the definition of the control law. However, in the presence of unknown system input gain, the lowpass filter cannot be directly applied to the control signal. To show where the problem lies, consider the filtered version of the control signal in (61)

$$u_f(s) = C_f(s) u(s)\,,$$

where $u(s)$ is the Laplace transform of $u(t)$ in (61), and $C_f(s)$ is a lowpass filter. Let $c_f(t)$ be the impulse response of the transfer function $C_f(s)$. Then

$$u_f(t) = c_f(t) * u(t) = c_f(t) * \left(\frac{k_g r(t) - \hat{\theta}^\top(t) x(t) - \hat{\sigma}(t)}{\hat{\omega}(t)} \right) ,$$

where $*$ denotes the convolution operator. Substituting this expression in the state predictor (58), we obtain

$$\dot{\hat{x}}(t) = A_m \hat{x}(t) + b \left(\hat{\omega}(t) c_f(t) * \left(\frac{k_g r(t) - \hat{\theta}^\top(t) x(t) - \hat{\sigma}(t)}{\hat{\omega}(t)} \right) + \hat{\theta}^\top(t) x(t) + \hat{\sigma}(t) \right) . \quad (69)$$

Notice that the parameter estimate $\hat{\omega}(t)$ may change rapidly due to the fast adaptation, and because the convolution operator does not allow for cancelation of $\hat{\omega}(t)$ in this expression, it may lead to unpredictable consequences on the system's performance. The $\mathcal{L}_1$ adaptive controller instead generates the control $u(t)$ from

$$u(s) = kD(s)\hat{\eta}(s) , \quad (70)$$

where $\hat{\eta}(s)$ is the Laplace transform of

$$\hat{\eta}(t) \triangleq k_g r(t) - \hat{\omega}(t) u(t) - \hat{\theta}^\top(t) x(t) - \hat{\sigma}(t) ,$$

and $D(s)$ is an arbitrary strictly proper transfer function that for all values of $\omega \in [\omega_{\min},\ \omega_{\max}]$ leads to a stable strictly proper transfer function

$$C(s) = \frac{\omega k D(s)}{1 + \omega k D(s)} \quad (71)$$

with unit DC gain $C(0) = 1$ [56]. Notice that in (70) $\hat{\omega}(s)$ is not multiplying $kD(s)$. Therefore in this approach $\hat{\omega}(t)$ can be viewed as a time–varying gain of the filter in (70), which directly compensates for $\hat{\omega}(t)$ in (69).

For better understanding of the nature of this control law notice that the requirement on $C(0) = 1$ implies that $D(s)$ must contain an integrator. Hence, for the case of slowly varying parameters $\theta(t) \approx const$ and $\sigma(t) \approx const$, in steady state, when $u(t) \approx const$, the input to the filter must be $\hat{\eta}(t) \approx 0$. Therefore the control law (70) leads to

$$k_g r(t) - \hat{\omega}(t)u(t) - \hat{\theta}^\top(t)x(t) - \hat{\sigma}(t) \approx 0\,.$$

Comparing this equation to the indirect MRAC control law (61), we find that the $\mathcal{L}_1$ control law avoids the division by $\hat{\omega}(t)$. The filter in the $\mathcal{L}_1$ control law (70) solves the design equation dynamically by driving $\hat{\eta}(t)$ in (70) to zero [58].

$\mathcal{L}_1$ Reference System

Similar to the scalar case with known system input gain, the closed–loop system with the $\mathcal{L}_1$ adaptive controller does not follow the ideal system in (47)–(48), due to the limited bandwidth of the control channel enforced by $C(s)$. Instead, the closed–loop system is approximating the $\mathcal{L}_1$ reference system. To derive the dynamics of the reference system for the system in (43)–(44), consider the case when the system parameters are precisely known. Then the controller in (70) takes the form

$$u_{\rm ref}(s) = kD(s)(k_g r(s) - \eta_{\rm ref}(s) - \omega u_{\rm ref}(s))\,, \tag{72}$$

where $\eta_{\rm ref}(s)$ is the Laplace transform of

$$\eta_{\rm ref}(t) \triangleq \theta^\top(t) x_{\rm ref}(t) + \sigma(t)\,.$$

Thus, the reference control law can be rewritten as

$$u_{\rm ref}(s) = \frac{1}{\omega} C(s)(k_g r(s) - \eta_{\rm ref}(s))\,, \tag{73}$$

where $C(s)$ is defined in (71). Substituting the reference controller from (73) into the system dynamics in (43) leads to the $\mathcal{L}_1$ reference model

$$\dot{x}_{\rm ref}(t) = A_m x_{\rm ref}(t) + b\left(\omega u_{\rm ref}(t) + \theta^\top(t) x_{\rm ref}(t) + \sigma(t)\right)\,, \quad x_{\rm ref}(0) = x_0\,. \tag{74}$$

The lowpass filter $C(s)$ can thus be viewed as a means for resolving the ambiguity in (69) due to the convolution, which also deviates from the desired ideal system, by leading to the $\mathcal{L}_1$ reference system, given in (73)–(74). Having the bandwidth of $C(s)$ comparable with the control channel bandwidth, the reference system in (73)–(74) assumes partial compensation of uncertainties within the bandwidth of the control channel. For more details about the bandwidth of the control system refer to "Available Bandwidth of Control Systems".

The closed–loop $\mathcal{L}_1$ reference system can also be written in frequency domain as

$$x_{\rm ref}(s) = H(s)C(s)k_g r(s) + H(s)(1 - C(s))\eta_{\rm ref}(s) + x_{\rm in}(s)\,, \tag{75}$$

where $H(s) \triangleq (s\mathbb{I} - A_m)^{-1}b$, and

$$x_{\rm in}(s) \triangleq (s\mathbb{I} - A_m)^{-1}x_0$$

is the Laplace transform of the ideal system response due to the initial conditions. From (75) we obtain the upper bound

$$\|x_{\rm ref}\|_{\mathcal{L}_\infty} \leq \|H(s)C(s)\|_{\mathcal{L}_1} k_g \|r\|_{\mathcal{L}_\infty} + \|G(s)\|_{\mathcal{L}_1}(L\|x_{\rm ref}\|_{\mathcal{L}_\infty} + \sigma_b) + \|x_{\rm in}\|_{\mathcal{L}_\infty}\,,$$

where

$$L \triangleq \max_{\theta\in\Theta} \|\theta\|_1\,, \quad G(s) \triangleq H(s)(1-C(s))\,.$$

By rewriting this upper bound as

$$\|x_{\rm ref}\|_{\mathcal{L}_\infty} \leq \frac{\|H(s)C(s)\|_{\mathcal{L}_1} k_g \|r\|_{\mathcal{L}_\infty} + \|G(s)\|_{\mathcal{L}_1}\sigma_b + \|x_{\rm in}\|_{\mathcal{L}_\infty}}{1 - \|G(s)\|_{\mathcal{L}_1} L}\,,$$

we obtain the sufficient condition for stability of the $\mathcal{L}_1$ reference system using the $\mathcal{L}_1$–norm of the transfer function $G(s)$

$$\|G(s)\|_{\mathcal{L}_1} < \frac{1}{L}\,. \tag{76}$$

Notice that this condition is consistent with the stability condition obtained for the scalar case in (21), and can be satisfied for arbitrary $H(s)$ by choosing a $C(s)$ with sufficiently large bandwidth.

Notice that the reference control signal in (72) depends on the unknown parameters ω, $\theta(t)$, and the disturbance $\sigma(t)$. In "Reference Controller for Multidimensional Systems" an equivalent alternative form of this controller is given, which allows for the direct implementation of it.

Uniform Performance Bounds

To derive the performance bounds we follow the steps similar to the scalar case, described in (22)–(27) and obtain, [56]

$$\|x_{\rm ref} - x\|_{\mathcal{L}_\infty} \leq \frac{\gamma_1}{\sqrt{\Gamma}}\,, \quad \|u_{\rm ref} - u\|_{\mathcal{L}_\infty} \leq \frac{\gamma_2}{\sqrt{\Gamma}}\,, \tag{77}$$

where

$$\gamma_1 \triangleq \frac{\|C(s)\|_{\mathcal{L}_1}}{1 - \|G(s)\|_{\mathcal{L}_1} L}\gamma_0\,, \tag{78}$$

$$\gamma_2 \triangleq \frac{1}{\omega}\,\|C(s)\|_{\mathcal{L}_1}\, L\gamma_1 + \frac{1}{\omega}\left\|\frac{C(s)c_0^\top}{c_0^\top H(s)}\right\|_{\mathcal{L}_1}\gamma_0\,, \tag{79}$$

γ_0 is given by (68), and $c_0 \in \mathbb{R}^n$ is a vector, which makes $c_0^\top H(s)$ minimum–phase and relative degree one. For more details on the role of this vector see "Special Form of State–to–Input Stability". Notice that both performance bounds in (77) are inverse proportional to the adaptation rate $\sqrt{\Gamma}$. Increasing Γ is limited by the available CPU and high–frequency sensor noise. Recalling that $\mathcal{L}_1$ adaptive controller attempts to compensate for the uncertainties within only the bandwidth of the control channel, we conclude that the performance limitations of $\mathcal{L}_1$ adaptive controller are reduced to hardware limitations. Notice that these performance bounds are derived in the case when the initial conditions of the state predictor are equal to the initial conditions of the plant. However similar performance bounds can be derived also for the case of their mismatch. For details, see "Performance Bounds and Time–Delay Margin in the Presence of Nonzero Trajectory Initialization Errors".

Benchmark Problem: Rohrs's Example

In this section we analyze Rohrs's example from [21, 59], which is constructed with a particular objective of analyzing the robustness properties of MRAC architectures. The system under consideration in [59] is a first–order stable system with unknown time–constant and dc gain, and with two fast highly damped unmodeled poles

$$\begin{aligned} y(s) &= A(s)\mu(s)\,, \quad A(s) = \frac{2}{s+1}\,, \\ \mu(s) &= \Delta(s)u(s)\,, \quad \Delta(s) = \frac{229}{s^2+30s+229}\,. \end{aligned} \tag{80}$$

The system has a gain crossover frequency of $\omega_{gc} = 1.70\ \mathrm{rad/s}$ and a phase margin of $\phi_m = 107.67\ \mathrm{deg}$. Its phase crossover frequency and the gain margin are $\omega_{\phi c} = 16.09\ \mathrm{rad/s}$ and $g_m = 24.62\ \mathrm{dB}$, respectively. The control objective in [59] is given through the first–order stable reference model

$$y_m(s) = \frac{3}{s+3} r(s)\,.$$

Notice that the unmodeled dynamics has faster poles, which are separated from the system dynamics in their frequency range. The Bode plot given in Figure 8 illustrates this separation. We see that the unmodeled dynamics start affecting the system's Bode diagram in the region with less than -20 dB magnitude, where the input signals are attenuated. Usually a properly designed control system does not attempt to act in the frequency range beyond the plant dynamics, since on the one hand it may lead to high gain control and on the other the level of uncertainties in high–frequency region is usually high. Thus from a classical control point of view it is not difficult to handle the unmodeled dynamics given by (80).

Model Reference Adaptive Control. Parameter Drift

The MRAC controller for this system takes the form

$$u(t) = \hat{k}_y(t)y(t) + \hat{k}_r(t)r(t)\,,$$

$$\dot{\hat{k}}_y(t) = -e(t)y(t)\,, \quad \hat{k}_y(0) = \hat{k}_{y0}\,, \tag{81}$$

$$\dot{\hat{k}}_r(t) = -e(t)r(t)\,, \quad \hat{k}_r(0) = \hat{k}_{r0}\,, \tag{82}$$

where $e(t) = y(t) - y_m(t)$. The corresponding feedback loop of the MRAC architecture is shown in Figure 9.

For simulations we consider the same reference inputs as in [59]. The first reference input has the exact phase crossover frequency

$$r_1(t) = 0.3 + 1.85\sin(16.1t)\,,$$

while the second one is also a sinusoidal reference signal, but at a frequency that is, approximately half of the phase crossover frequency

$$r_2(t) = 0.3 + 2\sin(8t)\,.$$

We use the same initial conditions as in [59], namely, $y(0) = 0$, $\hat{k}_r(0) = 1.14$, and $\hat{k}_y(0) = -0.65$. The simulation results from [59] are reproduced in Figures 10 and 11. In Figure 10, we can see that, while tracking $r_1(t)$, the closed–loop system is unstable due to parameter drift. In Figure 11, bursting takes place in the response of the closed–loop adaptive system to the reference signal $r_2(t)$.

$\mathcal{L}_1$ Adaptive Controller

Next we apply $\mathcal{L}_1$ adaptive controller from "$\mathcal{L}_1$ Adaptive Controller for Systems with Unmodeled Actuator Dynamics" to Rohrs's example. For this purpose, we rewrite Rohrs's example in state–space form as

$$\dot{x}(t) = -3x(t) + 2\left(\mu(t) + x(t)\right) , \quad x(0) = x_0 ,$$

$$y(t) = x(t) ,$$

where

$$\mu(s) = \frac{229}{s^2 + 30s + 229} u(s) .$$

Then, the state predictor takes the form

$$\dot{\hat{x}}(t) = -3\hat{x}(t) + 2\left(\hat{\omega}(t)u(t) + \hat{\theta}(t)x(t) + \hat{\sigma}(t)\right) , \quad \hat{x}(0) = x_0 ,$$

$$\hat{y}(t) = \hat{x}(t) ,$$

with $\hat{\omega}(t)$, $\hat{\theta}(t)$ and $\hat{\sigma}(t)$ being governed by

$$\dot{\hat{\omega}}(t) = \Gamma \mathrm{Proj}\left(\hat{\omega}(t), -\tilde{x}(t)u(t)\right) , \quad \hat{\omega}(0) = \hat{\omega}_0 , \tag{83}$$

$$\dot{\hat{\theta}}(t) = \Gamma \mathrm{Proj}\left(\hat{\theta}(t), -x(t)\tilde{x}(t)\right) , \quad \hat{\theta}(0) = \hat{\theta}_0 , \tag{84}$$

$$\dot{\hat{\sigma}}(t) = \Gamma \mathrm{Proj}\left(\hat{\sigma}(t), -\tilde{x}(t)\right) , \quad \hat{\sigma}(0) = \hat{\sigma}_0 . \tag{85}$$

The $\mathcal{L}_1$ control law is given by

$$u(s) = -kD(s)(\hat{\eta}(s) - k_g r(s)) ,$$

where $\hat{\eta}(t) \triangleq \hat{\omega}(t)u(t) + \hat{\theta}(t)x(t) + \hat{\sigma}(t)$ and $k_g = \frac{3}{2}$. The block diagram of the $\mathcal{L}_1$ adaptive control system is given in Figure 12.

The simulation plots for the inputs $r_1(t)$ and $r_2(t)$, using the $\mathcal{L}_1$ adaptive controller with $k = 5$, $D(s) = 1/s$, and $\Gamma = 1000$, are given in Figures 13–15. The initial conditions are set to $x_0 = 0$, $\hat{\omega}_0 = 1.14$, $\hat{\theta}_0 = 0.65$, and $\hat{\sigma}_0 = 0$. The projection bounds are set to $\Theta = [-10,\ 10]$, $\Delta = 10$, and $\Omega = [0.55.5]$. We see from the plots that the $\mathcal{L}_1$ adaptive controller guarantees that both the system output and the parameters remain bounded, while achieving an expected level of performance.

For further insight into the $\mathcal{L}_1$ adaptive controller we analyze the implementation block diagram in Figure 12 from a classical control perspective. We note that, while the feedback gain $\hat{\theta}(t)$ plays a similar role as the feedback gain $\hat{k}_y(t)$ in MRAC, the adaptive parameter $\hat{\omega}(t)$ appears in the feedforward path as a feedback gain around the integrator $\frac{k}{s}$, and thus has the ability to adjust the bandwidth of the lowpass filter, the output of which is the feedback signal of the closed–loop adaptive system. Recall that in MRAC the feedforward gain $\hat{k}_r(t)$ does is not engaged in the stabilization process and scales only the reference input. Note that the various modifications of the adaptive laws, such as the σ–modification and the e–modification, are used only to ensure boundedness of the parameter estimates, and thus avoid the parameter drift, but by no means affect the phase in the system, as $\hat{\omega}(t)$ does in the $\mathcal{L}_1$ architecture. Instead, with the $\mathcal{L}_1$ adaptive controller, the open–loop system bandwidth changes as both $\hat{\omega}(t)$ and $\hat{\theta}(t)$ adapt, which leads to simultaneous adaptation on the loop gain and the phase of the closed–loop system.

Piecewise Constant Adaptation Laws for $\mathcal{L}_1$ Controller

In this section we present the $\mathcal{L}_1$ adaptive output feedback controller using the piecewise constant adaptive laws. For a brief review of this adaptive architecture, applicable to non–SPR reference systems, see "$\mathcal{L}_1$ Adaptive Output–Feedback Controller with Piecewise Constant Adaptation Law". We use a first–order system to elucidate the features of this adaptive law. This simplification allows for performing time–domain analysis of the transient behavior. Thus, let the system dynamics be given by

$$\dot{x}(t) = -ax(t) + b(u(t) + d(t))\,, \quad x(0) = x_0\,, \tag{86}$$

where $x(t) \in \mathbb{R}$ is the measured system state, $a \in \mathbb{R}$ is the unknown system parameter with known conservative bounds, $b \in \mathbb{R}^+$ is a known system parameter; $d(t) \in \mathbb{R}$ is the input disturbance. The adaptive controller must ensure that the system output $x(t)$ tracks a bounded reference signal $r(t)$ with the desired transient specifications given by the ideal system

$$\dot{x}_m(t) = -a_m x_m(t) + bk_g r(t)\,, \quad x_m(0) = x_0\,,$$

where $a_m \in \mathbb{R}^+$ is a known system parameter, $k_g = a_m/b$.

The system in (86) can be written as

$$\dot{x}(t) = -a_m x(t) + b(u(t) + \sigma(t))\,, \tag{87}$$

where

$$\sigma(t) \triangleq \frac{a_m - a}{b} x(t) + d(t)\,.$$

The state predictor for this example takes the form

$$\dot{\hat{x}}(t) = -a_m \hat{x}(t) + bu(t) + \hat{\sigma}(t)\,, \tag{88}$$

where $\hat{\sigma}(t)$ is the parameter estimate generated by the sampled update law

$$\hat{\sigma}(t) = -\Phi^{-1}(T_s)\mu(T_s)\tilde{x}(iT_s)\,, \quad t \in [iT_s,\ (i+1)T_s)\,, \tag{89}$$

with $T_s \in \mathbb{R}^+$ being the sampling period, $\tilde{x}(t) \triangleq \hat{x}(t) - x(t)$, while

$$\Phi(T_s) = \int_0^{T_s} \mathrm{e}^{-a_m(T_s-\tau)} d\tau = \left[\frac{1}{a_m}\mathrm{e}^{-a_m(T_s-\tau)}\right]\Bigg|_0^{T_s} = \frac{1}{a_m}\left(1 - \mathrm{e}^{-a_m T_s}\right)\,, \tag{90}$$

$$\mu(T_s) = \mathrm{e}^{-a_m T_s}\,. \tag{91}$$

The control signal is computed as the output of the lowpass filter $C(s)$ with unit dc gain $C(0) = 1$

$$u(s) = C(s)\left(k_r r(s) - \frac{1}{b}\hat{\sigma}(s)\right)\,,$$

where $r(s)$ and $\hat{\sigma}(s)$ are the Laplace transforms of $r(t)$ and $\hat{\sigma}(t)$ respectively.

To demonstrate the role of the sampling and the inversion of $\Phi(T_s)$ in the update law, we rewrite the system in (87) in frequency domain as

$$x(s) = \frac{b}{s + a_m}(u(s) + \sigma(s))\,, \tag{92}$$

where $\sigma(s)$ is the Laplace transform for $\sigma(t)$. The state predictor can be similarly rewritten as

$$\hat{x}(s) = \frac{b}{s + a_m}\left(u(s) + \frac{1}{b}\hat{\sigma}(s)\right)\,. \tag{93}$$

Subtracting (92) from (93), we obtain the prediction error dynamics

$$\tilde{x}(s) = \frac{b}{s+a_m}\left(u(s) + \frac{1}{b}\hat{\sigma}(s)\right) - \frac{b}{s+a_m}(u(s)+\sigma(s)) = \frac{b}{s+a_m}\left(\frac{1}{b}\hat{\sigma}(s) - \sigma(s)\right) . \quad (94)$$

Assume that during $t \in [0, t_0)$ for some $t_0 > 0$ the system is affected by the disturbance $\sigma(t)$, which resulted in $\tilde{x}(t_0) = \tilde{x}_0 \neq 0$. Next we check how the system reacts to the accumulated prediction error $\tilde{x}_0$. In order to see the control system response, which is not affected by the disturbance, we set the disturbance on the next time interval $t \in [t_0, t_0 + T_s]$ to zero. The solution to (94) on the time interval $t \in [t_0, t_0 + T_s]$ for $\sigma(t) = 0$ is given by

$$\tilde{x}(t) = \tilde{x}_0 \mathrm{e}^{-a_m(t-t_0)} + \frac{1}{a_m}\hat{\sigma}(t_0)\left(1 - \mathrm{e}^{-a_m(t-t_0)}\right) .$$

At the end of the sampling interval we have

$$\tilde{x}(t_0 + T_s) = \tilde{x}_0 \mathrm{e}^{-a_m T_s} + \frac{1}{a_m}\hat{\sigma}(t_0)\left(1 - \mathrm{e}^{-a_m T_s}\right) .$$

Substituting the value of the estimate given by (89) yields

$$\begin{aligned}\tilde{x}(t_0 + T_s) &= \tilde{x}_0 \mathrm{e}^{-a_m T_s} - \frac{1}{a_m}\hat{\Phi}^{-1}(T_s)\mu(T_s)\tilde{x}(t_0)\left(1 - \mathrm{e}^{-a_m T_s}\right) \\ &= \tilde{x}_0 \mathrm{e}^{-a_m T_s} - \mathrm{e}^{-a_m T_s}\tilde{x}(t_0) = 0 . \end{aligned} \quad (95)$$

Thus, we observe that the update law on each sampling time generates an estimate, which completely compensates for the prediction error accumulated on the previous sampling period. However, in reality, the disturbance $\sigma(t)$ is not zero during $t \in [t_0, t_0 + T_s]$. Therefore the value of $\tilde{x}(t_0 + T_s)$ usually is not zero since the error dynamics are also affected by the additive disturbance (see (94)). Setting the sampling time T_s small enough the value of $\tilde{x}(t)$ can be kept

small and arbitrary performance improvement can be achieved in the presence of disturbances. The proof of this result is given in [60].

To clarify deeper the nature of this compensation consider the definition of $\Phi(T_s)$ in (90). We notice that $\Phi(T_s)$ is equal to the system state at the time T_s for a constant unit control signal, zero initial conditions, and in the absence of the disturbance, that is,

$$\Phi(T_s) = x(T_s)\,, \quad u(t) \equiv 1\,, \quad \sigma \equiv 0\,, \quad x(0) = 0\,.$$

From (95) we see that $\Phi^{-1}(T_s)$ inverts the error dynamics discretely. Namely, $\Phi^{-1}(T_s)$ cancels the effect of the system dynamics at fixed sampling times iT_s, $i = 1,\ 2,\ 3,\ \ldots$, making the system response equal to

$$\tilde{x}((i+1)T_s) = \tilde{x}(iT_s)\mathrm{e}^{-a_m T_s} - \mu(T_s)\tilde{x}(iT_s)\,.$$

The role of $\mu(T_s)\tilde{x}(iT_s)$ is to compensate for the prediction error accumulated since the previous sample period. Further notice that for every number $T_s > 0$ the quantity $\Phi(T_s)$ in (90) is bounded away from zero. This fact implies that the inverse of $\Phi(T_s)$ exists for every $T_s > 0$, and the sampled update law can be applied to an arbitrary system. The same holds also for systems of arbitrary dimension, including non–strictly positive real systems, as proved in [60, 61], where $\Phi(T_s)$ is a non–singular matrix of a more general structure. However, because $\Phi(T_s)$ approaches zero as $T_s \to 0$, this adaption law cannot be written for the case of continuous–time systems. Despite that, the control signal is continuous, since it is defined as an output of a lowpass filter.

Illustrative Example

To demonstrate the interpretation of the $\mathcal{L}_1$ adaptive controller with piecewise constant adaptation laws given in the previous section we consider the first–order system in (86). Let the system parameters be given by $a = a_m = b = 1$. We set the sampling time $T_s = 0.01$ s, which results in

$$\Phi(T_s) = \frac{1}{a_m}\left(1 - \mathrm{e}^{-a_m T_s}\right) = 0.01\,,$$

and

$$\mu(T_s) = \mathrm{e}^{-a_m T_s} = 0.99\,.$$

For the control design we choose the first–order lowpass filter

$$C(s) = \frac{1}{0.1s + 1}\,.$$

Let the disturbance be given by

$$\begin{aligned} d(t) = {} & 100\big(\mathfrak{u}(t - 0.01) - \mathfrak{u}(t - 0.02)\big) \\ & + \big(300 + 500\sin(500t)\big)\big(\mathfrak{u}(t - 0.04) - \mathfrak{u}(t - 0.05)\big) \\ & + \big(500\sin(1000t) - 500\big)\big(\mathfrak{u}(t - 0.07) - \mathfrak{u}(t - 0.08)\big)\,, \end{aligned} \tag{96}$$

where $\mathfrak{u}(t)$ denotes a step function. This function is zero everywhere except for three intervals of the length T_s. The distance between these intervals is $2T_s$. On the first interval the disturbance is constant, while on the second and the third intervals (96) contains sine waves with different frequencies and bias. This shape allows for separation of the system response to the error produced by the disturbance from the intervals, where the system is affected by the disturbance.

This separation occurs because the length and the starting time of the disturbance intervals coincide with the sampling period and the time of samples of the system. In particular, this fact means that during the first disturbance interval the sampled update law generates zero estimate. The update law responds to the effect of the disturbance in only the second sample period, when the disturbance is zero. Thus, can observe the system transient resulting from the disturbance and the system response to the resulting error separately.

Figure 16 shows the simulation results for the system without the plant uncertainties and the disturbance $d(t)$. The plot of the prediction error given by Figure 16c along with the plot for the parameter estimates given by Figure 16d show that the $\mathcal{L}_1$ controller does not respond to the disturbance during the sampling period, when the disturbance occurs. However, at the beginning of the following sampling period, the controller generates a parameter estimate, which cancels the prediction error, accumulated during this sampling period. During other sampling periods both the prediction error and the parameter estimate remain zero.

The perfect cancellation of the error caused by the disturbance $d(t)$ in one sample step as observed in Figure 16c, is possible, if the plant pole is the same as the pole of the desired dynamics, that is, $a = a_m$. Otherwise, if $a \neq a_m$, the ideal plant dynamics used by the inversion–based update law are different from the real plant dynamics, which results in additional prediction error. This error is treated by the $\mathcal{L}_1$ controller the same way as the error resulting from the disturbance.

Figure 17 shows the simulation results for the unstable plant with the parameters $a = -0.5$, $b = 0.5$ and the same $\mathcal{L}_1$ controller. Notice that while the controller tends to cancel the prediction error, it cannot compensate for it completely due to the uncertain plant dynamics.

However, a small value of the sampling time, namely, $T_s = 0.01$ s makes this error small, as predicted in [60, 61].

Benchmark Problem: Two Carts

The two–cart mass–spring–damper (MSD) example is a benchmark problem for robust control design. In [62], a slightly modified version of the original two–cart system is used to illustrate the design methodology and performance of the robust multiple model adaptive control. Next, we revisit the two–cart example with the $\mathcal{L}_1$ output feedback adaptive controller presented in "$\mathcal{L}_1$ Adaptive Output–Feedback Controller with Piecewise Constant Adaptation Law". Additional explanations and simulations can be found in [63].

The two–cart system is shown in Figure 18. The states $x_1(t)$ and $x_2(t)$ represent the absolute position of the two carts, whose masses are m_1 and m_2 respectively. Only $x_2(t)$ is available for measurement. The signal $d(t)$ is a random colored disturbance force acting on the mass m_2, and $u(t)$ is the control force, which acts upon the mass m_1. The disturbance force $d(t)$ is modeled as a first–order (colored) stochastic process generated by driving a lowpass filter with continuous–time white noise $\xi(s)$, with zero–mean and unit intensity, that is, $\Xi = 1$, and

$$d(s) = \frac{\alpha}{s+\alpha}\xi(s)\,, \quad \alpha > 0\,.$$

The state–space representation is given by

$$\dot{x}(t) = Ax(t) + Bu(t) + L\xi(t)\,,$$

$$y(t) = Cx(t) + \theta(t)\,,$$

where the state vector is

$$x^\top(t) \;=\; \left[\begin{array}{ccccc} x_1(t) & x_2(t) & \dot{x}_1(t) & \dot{x}_2(t) & d(t) \end{array}\right]^\top,$$

and

$$A = \left[\begin{array}{ccccc} 0 & 0 & 1 & 0 & 0 \\ 0 & 0 & 0 & 1 & 0 \\ -\frac{k_1}{m_1} & \frac{k_1}{m_1} & -\frac{b_1}{m_1} & \frac{b_1}{m_1} & 0 \\ \frac{k_1}{m_2} & -\frac{k_1+k_2}{m_2} & \frac{b_2}{m_2} & -\frac{b_1+b_2}{m_2} & \frac{1}{m_2} \\ 0 & 0 & 0 & 0 & -\alpha \end{array}\right], \tag{97}$$

$$B^\top = \left[\begin{array}{ccccc} 0 & 0 & \frac{1}{m_1} & 0 & 0 \end{array}\right], \quad L^\top = \left[\begin{array}{ccccc} 0 & 0 & 0 & 0 & \alpha \end{array}\right], \tag{98}$$

$$C = \left[\begin{array}{ccccc} 0 & 1 & 0 & 0 & 0 \end{array}\right], \tag{99}$$

while $\theta(t)$ is an additive sensor noise affecting the single measurement, and it is modeled as white noise, independent of $\xi(t)$, defined by

$$\mathrm{E}\{\theta(t)\} = 0\,, \quad \mathrm{E}\{\theta(t)\theta(\tau)\} = 10^{-6}\delta(t-\tau)\,.$$

The parameters in (97)–(99) are fixed and known

$$m_1 = m_2 = 1\,,\ k_2 = 0.15\,,\ b_1 = b_2 = 0.1\,,\ \alpha = 0.1\,,$$

while the spring constant k_1 is unknown with known upper and lower bounds

$$0.25 \leq k_1 \leq 1.75\,.$$

The control objective is to design a control law $u(t)$ so that the mass m_2 tracks a reference step signal $r(t)$ following a desired model, while minimizing the effects of the disturbance $d(t)$ and the sensor noise $\theta(t)$.

The control problem is challenging because the control signal $u(t)$ is applied through the uncertain spring, which makes the amount of force exerted through the spring to the mass m_2 uncertain. Taking into account the fact that only x_2 is measurable we have a non–collocated actuator problem [62]. Moreover the model contains unknown time delay τ in the control channel, whose maximum possible value is 0.05 s.

For application of the $\mathcal{L}_1$ adaptive output feedback controller to the two–cart example, the design procedure described in [64] leads to

$$\begin{aligned} M(s) &= \frac{1}{s^3 + 1.4s^2 + 0.17s + 0.052} \\ C(s) &= \frac{0.18s + 0.19}{s^5 + 2.8s^4 + 3.3s^2 + 2.0s^2 + 0.66s + 0.19}\,, \end{aligned}$$

while the sample–time for adaptation is set to $T_s = 1$ ms.

Figures 19 to 20 show the response of the closed–loop system with the $\mathcal{L}_1$ adaptive output

feedback controller to step reference inputs of different amplitudes and for different values of the unknown parameters k_1 and τ. As we can see, the $\mathcal{L}_1$ adaptive controller drives the mass m_2 to the desired position in about 15 s for arbitrary values of the unknown parameters within given bounds, while minimizing the effects of both the disturbance and the sensor noise present in the system.

Safety–Critical Flight Control Application

Under the NASA's Aviation Safety Program in 2007–2010, the Integrated Resilient Aircraft Control Project had an objective of maturation of the adaptive flight control technology into a tool that would help to mitigate and recover from faults, failures and upsets that might lead to loss of control. An $\mathcal{L}_1$ all–adaptive control law was flown in a series of remotely piloted flight tests on the NASA Airborne Subscale Transport Aircraft Research (AirSTAR) Generic Transport Model (GTM) aircraft. For details on the program and the GTM arcraft see "NASA's Airborne Subscale Transport Aircraft Research". In this section we provide an overview of the results from these flight tests; for additional details see [55] and [65].

The research control law developed for the GTM aircraft has as its primary objective achieving tracking for a variety of tasks with guaranteed stability and robustness in the presence of uncertain dynamics, such as changes due to rapidly varying flight conditions during standard maneuvers and unexpected failures. All of these requirements must be achieved while providing Level 1 [66, 67] handling qualities under nominal flight conditions with graceful degradation under significant adversity. For more information on handling qualities see "Aircraft Handling Qualities and Their Specifications". In particular, one essential objective for safe flight under

adverse conditions is for the aircraft never to leave the extended flight envelope, since no guarantees for recovery can be made once outside the boundary and in uncontrollable space as illustrated in Figure 1. Consequently, the adaptive controller is expected to learn fast enough to keep the aircraft within the extended flight envelope. This requirement implies that the control law action in the initial 2–3 seconds after initiation of an adverse condition is the key to safe flight.

An $\mathcal{L}_1$ control system used for this application is a three axes angle of attack α, roll rate p, sideslip angle β command augmentation system, and is based on the theory presented in "$\mathcal{L}_1$ Adaptive Controller for Systems with Unmatched Uncertainties". For inner–loop flight control system (FCS) design, the effects of slow outer–loop variables, such as airspeed, pitch and bank angles, may appear as unmatched uncertainties in the dynamics of the inner–loop variables we are trying to control, such as angle of attack, sideslip angle, roll rate. More detailed discussion of aircraft flight dynamics can be found in [68]. Also, unmodeled nonlinearities, cross–coupling between axes and dynamic asymmetries may lead to unmatched uncertainties in the inner–loop system dynamics. If the design of the inner–loop FCS does not account for these uncertainties, then their effect in the inner–loop dynamics requires continuous compensation by the pilot, thereby increasing the pilot's workload. Therefore, automatic compensation for the undesirable effects of these unmatched uncertainties on the output of the system is essential to achieve desired performance, reduce pilot's workload and improve the aircraft's handling qualities.

Notice that an $\mathcal{L}_1$ adaptive flight control system provides a systematic framework for adaptive controller design that allows for explicit enforcement of MIL–Standard requirements [67] and reduces the tuning effort required to achieve desired closed–loop performance, which in turn

reduces the design cycle time and development costs. In particular, the design of an $\mathcal{L}_1$ adaptive flight control system for the GTM is based on the linearized dynamics of the aircraft at a nominal flight condition corresponding to an equivalent airspeed of 80 knots and an altitude of 1000 ft. These linear dynamics are further simplified to include only short–period dynamics in the longitudinal axis and roll rate p, sideslip angle β, yaw rate r in the lateral–directional dynamics, neglecting bank angle ϕ. Moreover, the phugoid dynamics, with velocity and pitch attitude as the primarily states, are treated as unmatched uncertainty. Since the airplane is Level I at this flight condition, the nominal desired dynamics of the linear state predictor are chosen to be similar to those of the airplane. However some additional damping is added to longitudinal and directional dynamics of the state predictor, while the lateral dynamics are set to be slightly faster than the original ones in order to satisfy performance specifications. The state predictor is scheduled to specify different performance requirements at special flight regimes such high speed above the allowable research envelope and post–stall high angle of attack. In order to improve the handling qualities of the airplane, a linear prefilter $K_g(s)$ is added to the adaptive FCS so as to ensure desired decoupling properties as well as desired command tracking performance. Overdamped second–order lowpass filters with unity dc gain are used in all control channels, while their bandwidths are set to ensure minimum total time–delay margin of 0.130 s and a gain margin of 6 dB. Finally, the adaptation sampling time is set to $T_s = 1/600$ s, which corresponds to the execution speed of the AirSTAR flight control computer. We notice that the same control parameters for the prefilter, the lowpass filters, and the adaptation rate are used across the entire flight envelope with no scheduling or reconfiguration. Further details about the design of the $\mathcal{L}_1$ adaptive controller for the GTM can be found in [69].

Flight Control Law Evaluation

The material presented in this section are the results of a flight tests of an $\mathcal{L}_1$ all–adaptive controller flown on a twin turbine–powered, dynamically scaled GTM AirSTAR aircraft with tail number T2 conducted on 4 June 2010 and 10 September 2010 at Ft. Pickett, VA. Recall that an $\mathcal{L}_1$ adaptive α, p–β command response control laws are designed for a nominal aircraft at a single flight condition for $V = 80$ KEAS. The flight test procedures are outlined in the flight test plan [70] and the test cards [71], relevant sections of which are summarized here to provide the necessary background to put the presented results in the appropriate context.

The flight tests consist of the stability and robustness evaluations. The first is done by increasing latency in the system until instability occurs, and the second is done by simultaneously degrading longitudinal and lateral stability while reducing pitch control authority by 50%. The stability degradation is designed to gradually decrease stability, 50%, 75%, 100% (neutrally stable aircraft), 125% (highly unstable aircraft), until the tested flight controller is no longer able to maintain stable flight. In addition to stability and robustness evaluation, an $\mathcal{L}_1$ all–adaptive control law is tested in the high angle of attack, post–stall section of the flight envelope. $\mathcal{L}_1$ is the only control law to date that flew in the high angle of attack, post–stall regime on the GTM aircraft. Further control law evaluation performed during the September deployment involves offset landing task. This task is characterized by an offset from the center line of the runway on final approach — 100 ft to the left of the centerline, 100 ft above the runway, 1800 ft downrange from desired touchdown spot. This task is considered very challenging for a pilot under nominal conditions. For flight test the task is made even more difficult by adding offset landings with 100% stability degradation, neutrally stable aircraft, and 125% stability degradation, unstable, in

longitudinal and lateral axes simultaneously while reducing pitch control authority by 50%. The research pilot evaluates the controller performance during the task with a Cooper–Harper rating (CHR) for handling qualities. A brief set of representative flight test results are provided in this section, while more details and data analysis can be found in [55] and [65].

Moreover, based on the performance of an $\mathcal{L}_1$ all–adaptive controller in comparison to the open loop in the post–stall regime, an $\mathcal{L}_1$ flight controller is asked to provide, for the September 2010 deployment, precise acquisition and tracking of high angle of attack in support of nonlinear aerodynamic modeling, in other words the GTM serves as a flying wind tunnel. In order to provide the requested support and improve precision tracking, small modifications are added to an $\mathcal{L}_1$ control law. The primary modification involves trading off performance and robustness by increasing the bandwidth of a filter in the angle of attack matched uncertainty channel. The result demonstrated in flight is a more precise tracking in post–stall regime. However, the penalty as predicted by theory is the reduction of latency robustness.

Stability and Robustness Evaluation Summary

In summary, the June 2010 flight test evaluation can be summarized as follows. An $\mathcal{L}_1$ all–adaptive control law is robust to an additional 0.125–s latency added to the system and with a nominal 0.022–s delay present the total latency robustness is 0.147 s. Furthermore, an $\mathcal{L}_1$ controller can tolerate the 100% degradation in longitudinal and lateral stability, for which the aircraft is neutrally stable, while experiencing 50% degradation in longitudinal control effectiveness. The aircraft $\mathcal{L}_1$ adaptive controller system is considered to be well performing combination with solid Level 1 handling qualities rating from the research pilot.

The nominal flight in the race track pattern and the responses to the pitch and roll axis wave trains, angle of attack (WT29) and roll rate (WT30) commands respectively, form the basis for comparison with aircraft under various degree of stability degradation. This task also presents an opportunity to illustrate typical aircraft response for a given research flight control law.

Figure 21 shows 70 s of flight that includes both wave trains, one complete turn and part of another turn. The lack of pilot input during the wave train injection, manifested as a precise straight line doublet, can be observed in Figure 21a and Figure 21b. Moreover, note sideslip angle error β maintained within ± 0.8 deg by an $\mathcal{L}_1$ all–adaptive control law and the nonzero command that comes from vane calibration bias as shown in Figure 21c. The surface commands during this flight segment are illustrated in Figure 21d. One item of note, since the rudder is very powerful and can add significant load for small deflections, especially at higher speed, small amplitude for the rudder is highly desired.

Another item of interest is how well the control law isolates the commanded response to the appropriate axis and minimizes cross–coupling. The plots in Figure 22a–22d show pitch axis wave train and corresponding lateral–directional response and in Figure 22e–22i roll axis wave train and corresponding longitudinal–directional responses. Consider angle of attack wave train tracking in Figure 22a and the smooth elevator command/response in Figure 22c. The cross–coupling response in the lateral–directional axes is minimal with the roll and yaw rates never exceeding ± 5 deg/s, which is considered within the turbulence/noise level especially for the roll rate. The roll rate command doublet achieves 30–deg bank angle as per design with a reasonable aileron command as shown in Figures 22e and 22g. The pitch axis cross–coupling is minimal by design since the angle of attack is commanded to a constant value necessary to

maintain nose up during the bank to bank maneuver. In the directional axis, sideslip angle is within ± 1 deg, and yaw rate is within ± 10 deg/s as shown in Figure 22f. Hence, based on the responses in Figures 22e–22i, an $\mathcal{L}_1$ all–adaptive control law generates minimal cross–coupling between the axes.

While looking at the angle of attack response to a commanded doublet in Figure 22a, we consider the speed of the response in the context of a piloted aircraft. The original tuning of this control law is done in a batch simulation, with minimal attention to Mil–Standards, with the goal of tracking a doublet command as fast and as precise as possible. The initial comment from the pilot flying a control law thus tuned is "too sensitive in pitch". This comment is consistent among different pilots and different control laws tuned with the same goal in mind. After this initial evaluation, the control law is retuned using Mil–Standards as a guide to achieve Level 1 flying qualities. During the control law development process, it is observed that even if the Mil–Standards for a fighter aircraft category are employed to tune the control law, it is typically not sufficient to provide satisfactory pitch response. We speculate that the issue arises with the speed of GTM short period dynamics that are at least 3 times faster than those of an F–16 for example. The performance of the aircraft whose responses are shown in Figure 21 and Figure 22 is judged to be Level 1. Pilot comment at the post flight 23 debrief is "a nice Level 1 flying airplane for light turbulence conditions". Consequently, angle of attack response to a commanded doublet appears much slower than typical batch simulation examples.

Recall that stability degradation is turned on simultaneously in longitudinal and lateral axes while degrading longitudinal controllability by 50%. The longitudinal degradation is static stability decrease and lateral axis is roll damping decrease. The first case is a 50% stability

degradation. The longitudinal axis response is essentially the same as the nominal aircraft. Despite slightly increased response to turbulence by roll rate, the pilot notes that he did not detect a perceptible difference from flying the nominal aircraft. For 75% degradation in stability, which is considered severe, there is some degradation in tracking performance and increased excitation by turbulence of the roll axis. The next case of interest we illustrate is the graceful degradation of an $\mathcal{L}_1$ all–adaptive controller performance when it is unable to maintain prescribed performance. This case refers to 100% stability degradation case.

Plots in Figures 23a–23b show pitch and roll axis response with marks of 100% fault and wave trains engagement. Figures 23c–23d shows the angular rates and actuator commands respectively through the entire segment of flight. The dynamic response, especially in roll rate, shows oscillatory behavior with overshoots as well as increased actuator amplitudes in an attempt to compensate, which compared to that of the nominal aircraft indicate the deterioration in response.

The segments containing the 100% stability degradation fault and wave trains are isolated in Figure 24. The engagement of fault, pitch axis wave train and associated state and actuator responses of interest are shown in Figures 24a–24d. The overall pitch axis closed loop damping is decreased as evidenced by an overshoot in angle of attack response and larger magnitude pitch rate response. The inboard elevator segment in Figure 24b, scheduled with angle of attack independent of the control law, has relatively large deflections to produce 100% reduction in longitudinal stability as compared to the deflections in the case of the nominal airplane. In the lateral–directional axes shown in Figure 24c, there is more excitation of the roll rate by turbulence, since roll damping is also 100% degraded, and potentially more cross–coupling in

the roll axis. The yaw rate response looks similar to the nominal case shown in Figure 22b and remains within ± 5 deg/s. The pilot comment is that he observed roll ratcheting during the pitch axis wave train.

The roll axis wave train and the associated variables are illustrated in Figures 24e–24i. For a 100% stability degradation fault, roll rate is more oscillatory, excited by turbulence and stick inputs as shown in Figure 24e and the ailerons respond, shown in Figure 24g, to try to damp out overshoot and turbulence induced oscillations. However, at the tail end of the wave train, there are two ± 20 deg/s oscillations that the controller is slow in damping out. Perhaps at this stage the controller is reaching the limit of its ability to provide robust performance in the roll axis. The rudder response in this case also has a more distinctive shape but remains small amplitude as it tries to help control roll rate without exciting yaw rate and sideslip, which is commanded to 0 deg and 0 deg/s respectively at all times. The directional axis cross–coupling is once again minimal, ± 10 deg/s as shown by Figure 24f. The pitch axis cross–coupling shown in Figure 24h is once again very similar to the nominal case shown in Figure 22h and the elevator response once again shows inboard elevator destabilizing longitudinal axis and not responding to control law commands illustrated Figure 24i. The pilot observes that there is no observable roll ratcheting during the roll rate doublet unlike what he sees during the pitch axis doublet. An $\mathcal{L}_1$ all–adaptive controller with tuning parameters set for June 2010 deployment is unable to handle highly unstable aircraft characterized by 125% stability degradation. Nevertheless, we note that once the destabilizing fault is turned off, the controller immediately brings the airplane to nominal flight performance. Based on the performance in flight test and its predictability, the pilot had the confidence to take the GTM in the post–stall high angle of attack regime.

High Angle of Attack Capture

Interest in post–stall high angle of attack conditions during June 2010 flight test were two fold. First, there is an interest in exploiting the AirSTAR capability as a flying wind tunnel to model unsteady nonlinear aerodynamics encountered at high angles of attack post–stall flight regimes. The second impetus comes from trying to stress the $\mathcal{L}_1$ all–adaptive flight control law and further explore its performance under flight conditions far removed from the original design point and characterized by rapidly changing nonlinear dynamics. The primary challenge associated with post–stall high angle of attack is roll off due to asymmetric wing stall. Roll asymmetry with strong roll off tendency is expected to occur at about 13–deg angle of attack. Also, roll damping characteristics are expected to rapidly change from stable to slightly unstable in the 10–deg to 12–deg angle of attack range. At angles of attack above stall, roll damping is expected to improve and aerodynamic asymmetry is expected to reduce. The defining stall characteristic is expected to be an unstable pitch break occurring at 13–deg angle of attack. Low static and dynamic longitudinal stability is expected at 15–deg angle of attack.

The high angle of attack capture with an $\mathcal{L}_1$ all–adaptive control law is performed as the last set of maneuvers on flight 23. During the flight Pilot acquires $\alpha = 18$ deg twice in a very repeatable manner. His comment is that the aircraft appears to want to go to $\alpha = 18$ deg and stay there. In addition, the aircraft is very well behaved in roll during the entire acquisition maneuver. Moreover, the control law is very predictable. Two flights later on the same morning, during flight 25, the same high angle of attack acquisition maneuver is attempted using stick to surface control, nominal control for the aircraft, as described in angle of attack buildup above. As a point of reference, the GTM is open loop Level 1 FQ aircraft in its normal flight envelope.

The pilot makes 3 attempts to capture 18–deg angle of attack without exceeding 45 deg of bank angle, none of these attempts are successful. Figures 25 to 27 show several variables of interest for post–stall angle of attack maneuvers and provide side–by–side look at the performance of an $\mathcal{L}_1$ all–adaptive control law and stick–to–surface control. Figure 25 shows the angle of attack, roll rate, and bank angle as functions of time for the first attempt to capture $\alpha = 18$ deg. The largest roll rate with an $\mathcal{L}_1$ controller occurs between 13 and 14 deg and is within ± 20, which translates to roughly 12–deg bank angle. The bank–angle excursion lasts for less than 2 s before returning to a fairly constant 5–deg offset. The pilot captures and maintains 18–deg angle of attack for over 7 s. Moreover, the combination of power setting and pilot command saturates all segments of the elevator from 849 to 854 s without observable ill effect on the control system or aircraft dynamics as can be seen in Figure 25c. At 854 s, the pilot initiates recovery, recovers by 856 s and initiates a turn by 858 s.

More dramatic differences in performance are observed in the variables that are explicitly affected by high angle of attack aerodynamics. In particular the roll rate that translates into bank angle. Figure 26 shows the $\alpha - p$ envelope and the performance of stick to surface and $\mathcal{L}_1$ adaptive controller respectively. Note that an $\mathcal{L}_1$ controller roll rate never exceeds 20 deg/s while in state to surface configuration roll rate exceeds 40 deg/s in the best–case scenario, acquisition attempt 3. Persistently high roll rate necessarily translates into large bank angles as shown by $\alpha - \phi$ plot in Figure 27. Under admittedly conservative rules for allowable bank angle for this maneuver, all three stick to surface attempts are abandoned since each exceeds 45–deg bank angle. Bank angle under $\mathcal{L}_1$ all–adaptive control law, however, never exceeds 15 deg. Thus an $\mathcal{L}_1$ all–adaptive controller improves pilot's ability to fly the aircraft at high angles of attack. The controller, designed at a single flight condition for $V = 80$ KEAS, $\alpha \approx 4.5$ deg, provides some increase

in pitch damping and significant increase in roll rate damping through stall and post–stall pitch break and roll off. Moreover, an $\mathcal{L}_1$ all–adaptive controller demonstrates robustness to persistently saturated actuators at high angle of attack. A detailed analysis of the stability and performance of the $\mathcal{L}_1$ adaptive controller in the presence of control input saturation can be found in [72].

Based on the flight test results of June 2010, it was decided to use the $\mathcal{L}_1$ adaptive control law to support the unsteady aerodynamic modeling work at post–stall, high angle of attack during the September 2010 deployment. The control law task in support of modeling work is to attain stable flight at $\alpha = 18$ deg, once the desired angle of attack is reached, follow a predetermined input wave train while the pilot stays out of the loop, especially in the longitudinal axis. In an attempt to achieve more precise tracking performance at high angles of attack, the bandwidth of the filter for matched adaptive estimates of the α channel is set higher than the one from June deployment. As predicted by theory, the tradeoff for increased performance is decrease in latency robustness. The measured decrease was from 0.125–s additional latency tolerance to 0.095 s. The tracking precision provided by an $\mathcal{L}_1$ all–adaptive controller at post–stall high α is illustrated in Figure 28. The GTM response to the prescribed inputs — step commands 18 deg to 15 deg, 15 deg to 20 deg, 20 deg to 15 deg; Schroeder sweep — is shown in Figure 28. In summary, in this and in other supporting roles [65], an $\mathcal{L}_1$ adaptive controller facilitates precision tracking and decreased workload, thus, enhancing the experimental capability of the GTM aircraft.

Lastly we show the flight test results of an $\mathcal{L}_1$ all–adaptive control law during an offset landing maneuvers from flight 41 on 10 September 2010. Typically, this task is considered a high workload task where the pilot is just trying to put the aircraft down in the middle of the runway. During the flight test the task demands more precision with requirements set on

aircraft attitude and position on the runway. The offset landing task is also performed with 100% stability degradation, neutrally stable, and 50% reduction in pitch control authority as well as 125% stability degradation, highly unstable, and 50% pitch control authority reduction. More detailed discussion can be found in [65] and [71]. Under nominal aircraft stability, an $\mathcal{L}_1$ control law is rated CHR 3, Level 1 handling qualities. Neutrally stable aircraft with an $\mathcal{L}_1$ controller experiences some handling qualities degradation and is rated CHR 5, Level 2; highly unstable aircraft also achieves a safe landing with CHR 7, Level 3 handling qualities, aircraft barely misses the adequate performance box on the runway. Of all the controllers tested, $\mathcal{L}_1$ provides the highest handling qualities rating for each offset landing stability case. Notice two interesting items. While the GTM is very stable Level 1 aircraft in open loop, stick–to–surface configuration and rated as CHR 3, Level 1 for offset landing for nominal stability, the same task is abandoned by the pilot for the neutral stability case with resulting rating of CHR 10, uncontrollable aircraft with catastrophic landing likely to imminent. The second item to note is that the level of aircraft induced instability during flight 41 for the neutrally stable case is higher than prescribed by the task due to perceptible level of turbulence and the architecture of artificial destabilization. In other words, during flight 41 the GTM was unstable to some degree.

In summary, the series of flight tests on the GTM remotely piloted aircraft conducted with an $\mathcal{L}_1$ all–adaptive control law provided a challenging, real world environment that stressed the control law to its limits, exposed its behavior at the limits and verified the theoretical prediction of its behavior. The results show that the $\mathcal{L}_1$ based control law provides predictable behavior in the neighborhood of the design point as well as dynamically far removed, the fast adaptation is a feature that facilitates predictable behavior for the pilot even as significant changes in aircraft dynamics happen unexpectedly, and the controller behavior at the limits of uncertainty and time

delay tolerance is a graceful degradation and not an abrupt cliff.

Conclusions

This article presents the development of $\mathcal{L}_1$ adaptive control theory and its application to safety critical flight control system development. Several architectures of the theory and benchmark examples are analyzed. The key feature of $\mathcal{L}_1$ adaptive control architectures is the decoupling of estimation and control, which enables the use of arbitrary fast estimation rates without sacrificing robustness. Rohrs example and two–cart system are used as benchmark problems for illustration. NASA's flight tests on subscale commercial jet verify the theoretical claims in a set of safety–critical test flights.

References

[1] S. A. Jacklin, "Closing certification gaps in adaptive flight control software", in: *AIAA Guidance, Navigation and Control Conference*, AIAA-2008-6988, Honolulu, HI, 2008.

[2] C. Cao and N. Hovakimyan, "Stability margins of $\mathcal{L}_1$ adaptive control architecture", *IEEE Transactions on Automatic Control*, vol. 55, no. 2 2010.

[3] P. C. Gregory, "Air research and development command plans and programs", in: *Proc. self adaptive flight control symposium*, ed. by P. C. Gregory, Wright-Patterson Air Force Base, Ohio, 1959, pp. 8–15.

[4] E. Mishkin and L. Braun, *Adaptive Control Systems*, New York, NY: McGraw-Hill, 1961.

[5] K. J. Åström, "Adaptive control around 1960", in: *Proc. 34th IEEE conference on decision and control*, New Orleans, Louisiana, 1995, pp. 2784–2789.

[6] L. W. Taylor Jr. and E. J. Adkins, "Adaptive control and the X-15", in: *Princeton University Conference on Aircraft Flying Qualities*, Princeton, NJ, 1965.

[7] L. Ljung, *System Identification—Theory for the User*, Englewood Cliffs, New Jersey: Prentice Hall, 1987.

[8] R. Kalman, "Design of self-optimizing control systems", *ASME Transactions*, vol. 80, pp. 468–478, 1958.

[9] K. J. Åström and B. Wittenmark, "On self-tuning regulators", *Automatica*, vol. 9, no. 2, pp. 185–199, 1973.

[10] B. Egardt, *Stability of Adaptive Controllers*, New York, NY: Springer-Verlag New York, Inc., 1979.

[11] G. C. Goodwin and K. S. Sin, *Adaptive Filtering Prediction and Control*, Englewookd Cliffs, New Jersey: Prentice Hall, 1984.

[12] S. Sastry and M. Bodson, *Adaptive Control: Stability, Convergence and Robustness*, Englewookd Cliffs, New Jersey: Prentice Hall, 1989.

[13] S. Sastry, *Nonlinear Systems: Analysis, Stability, and Control*, Interdisciplinary Applied Mathematics, New York, NY: Springer-Verlag New York, Inc., 1999.

[14] J.-J. E. Slotine and W. Li, *Applied Nonlinear Control*, Englewood Cliffs, NJ: Prentice Hall, 1991.

[15] P. R. Kumar and P. P. Varaiya, *Stochastic systems: estimation, identification, and adaptive control*, Englewookd Cliffs, New Jersey: Prentice Hall, 1986.

[16] K. J. Åström and B. Wittenmark, *Adaptive Control*, 2nd, Originally published by Addison Wesley, 1995, New York: Dover, 2008.

[17] R. E. Bellman, *Adaptive Control Processes—A Guided Tour*, Princeton, NJ: Princeton University Press, 1961.

[18] Y. D. Landau, *Adaptive Control: the Model Reference Approach*, Control & Systems Theory, New York, NY: Marcel Dekker, Inc., 1979.

[19] A. S. Morse, "Global stability of parameter-adaptive control systems", *IEEE Transactions on Automatic Control*, vol. 25, no. 3, pp. 433–439, 1980.

[20] K. S. Narendra, Y.-H. Lin, and L. S. Valavani, "Stable adaptive controller design, part II: proof of stability", *IEEE Transactions on Automatic Control*, vol. 25, no. 3, pp. 440–448, 1980.

[21] C. E. Rohrs, L. S. Valavani, M. Athans, and G. Stein, “Robustness of continuous-time adaptive control algorithms in the presence of unmodeled dynamics”, *IEEE Transactions on Automatic Control*, vol. 30, no. 9, pp. 881–889, 1985.

[22] K. J. Åström, “Interactions between excitation and unmodeled dynamics in adaptive control”, in: *IEEE Conference on Decision and Control*, Las Vegas, NV, 1984, pp. 1276–1281.

[23] B. D. O. Anderson, “Failures of adaptive control theory and their resolution”, *Communications in information and systems*, vol. 5, no. 1, pp. 1–20, 2005.

[24] P. A. Ioannou and P. V. Kokotović, “An asymptotic error analysis of identifiers and adaptive observers in the presence of parasitics”, *IEEE Transactions on Automatic Control*, vol. 27, no. 4, pp. 921–927, 1982.

[25] P. A. Ioannou and P. V. Kokotović, *Adaptive Systems with Reduced Models*, Secaunus, NJ: Springer-Verlag New York, Inc., 1983.

[26] P. A. Ioannou and P. V. Kokotović, “Robust redesign of adaptive control”, *IEEE Transactions on Automatic Control*, vol. 29, no. 3, pp. 202–211, 1984.

[27] B. B. Peterson and K. S. Narendra, “Bounded error adaptive control”, *IEEE Transactions on Automatic Control*, vol. 27, no. 6, pp. 1161–1168, 1982.

[28] G. Kresselmeier and K. S. Narendra, “Stable model reference adaptive control in the presence of bounded disturbances”, *IEEE Transactions on Automatic Control*, vol. 27, no. 6, pp. 1169–1175, 1982.

[29] K. S. Narendra and A. M. Annaswamy, “A new adaptive law for robust adaptation without persistent excitation”, *IEEE Transactions on Automatic Control*, vol. 32, no. 2, pp. 134–145, 1987.

[30] P. A. Ioannou and J. Sun, *Robust Adaptive Control*, Upper Saddle River, NJ: Prentice Hall, 1996.

[31] K. S. Tsakalis, "Performance limitations of adaptive parameter estimation and system identification algorithms in the absence of excitation", *Automatica*, vol. 32, no. 4, pp. 549–560, 1996.

[32] K. A. Wise, E. Lavretsky, J. Zimmerman, J. Francis, D. Dixon, and B. Whitehead, "Adaptive flight control of a sensor guided munition", in: *AIAA Guidance, Navigation and Control Conference*, AIAA-2005-6385, San Francisco, CA, 2005.

[33] K. A. Wise, E. Lavretsky, and N. Hovakimyan, "Adaptive control in flight: theory, application, and open problems", in: *American Control Conference*, Minneapolis, MN, 2006, pp. 5966–5971.

[34] R. W. Beard, N. B. Knoebel, C. Cao, N. Hovakimyan, and J. S. Matthews, "An $\mathcal{L}_1$ adaptive pitch controller for miniature air vehicles", in: *AIAA Guidance, Navigation and Control Conference*, AIAA-2006-6777, Keystone, CO, 2006.

[35] C. Cao, N. Hovakimyan, I. Kaminer, V. V. Patel, and V. Dobrokhodov, "Stabilization of cascaded systems via $\mathcal{L}_1$ adaptive controller with application to a UAV path following problem and flight test results", in: *American Control Conference*, New York, NY, 2007, pp. 1787–1792.

[36] C. Cao, N. Hovakimyan, and E. Lavretsky, "Application of $\mathcal{L}_1$ adaptive controller to wing rock", in: *AIAA Guidance, Navigation and Control Conference*, AIAA-2006-6426, Keystone, CO, 2006.

[37] V. V. Patel, C. Cao, N. Hovakimyan, K. A. Wise, and E. Lavretsky, "$\mathcal{L}_1$ adaptive controller for tailless unstable aircraft", in: *American Control Conference*, New York, NY, 2007, pp. 5272–5277.

[38] V. V. Patel, C. Cao, N. Hovakimyan, K. A. Wise, and E. Lavretsky, "$\mathcal{L}_1$ adaptive controller for tailless unstable aircraft in the presence of unknown actuator failures", in: *AIAA Guidance, Navigation and Control Conference*, AIAA-2006-6314, Hilton Head, SC, 2007.

[39] J. Wang, C. Cao, V. V. Patel, N. Hovakimyan, and E. Lavretsky, "$\mathcal{L}_1$ adaptive neural network controller for autonomous aerial refueling with guaranteed transient performance", in: *AIAA Guidance, Navigation and Control Conference*, AIAA-2006-6206, Keystone, CO, 2006.

[40] J. Wang, V. V. Patel, C. Cao, N. Hovakimyan, and E. Lavretsky, "$\mathcal{L}_1$ adaptive neural network controller for autonomous aerial refueling in the presence of unknown actuator failures", in: *AIAA Guidance, Navigation and Control Conference*, AIAA-2006-6313, Hilton Head, SC, 2007.

[41] I. M. Gregory, C. Cao, V. V. Patel, and N. Hovakimyan, "Adaptive control laws for flexible semi-span wind tunnel model of high-aspect ratio flying wing", in: *AIAA Guidance, Navigation and Control Conference*, AIAA-2007-6525, Hilton Head, SC, 2007.

[42] R. Hindman, C. Cao, and N. Hovakimyan, "Designing a high performance, stable $\mathcal{L}_1$ adaptive output feedback controller", in: *AIAA Guidance, Navigation and Control Conference*, AIAA-2007-6644, Hilton Head, SC, 2007.

[43] I. Kaminer, O. A. Yakimenko, V. Dobrokhodov, A. M. Pascoal, N. Hovakimyan, V. V. Patel, C. Cao, and A. Young, "Coordinated path following for time-critical missions of multiple UAVs via $\mathcal{L}_1$ adaptive output feedback controllers", in: *AIAA Guidance, Navigation and Control Conference*, AIAA-2007-6409, Hilton Head, SC, 2007.

[44] Y. Lei, C. Cao, E. M. Cliff, N. Hovakimyan, and A. J. Kurdila, "Design of an $\mathcal{L}_1$ adaptive controller for air-breathing hypersonic vehicle model in the presence of unmodeled dynamics", in: *AIAA Guidance, Navigation and Control Conference*, AIAA-2006-6527, Hilton Head, SC, 2007.

[45] E. Kharisov, I. M. Gregory, C. Cao, and N. Hovakimyan, "$\mathcal{L}_1$ adaptive control for flexible space launch vehicle and proposed plan for flight validation", in: *AIAA Guidance, Navigation and Control Conference*, AIAA-2008-7128, Honolulu, HI, 2008.

[46] V. Dobrokhodov, I. Kitsios, I. Kaminer, K. D. Jones, E. Xargay, N. Hovakimyan, C. Cao, M. I. Lizárraga, and I. M. Gregory, "Flight validation of metrics driven $\mathcal{L}_1$ adaptive control", in: *AIAA Guidance, Navigation and Control Conference*, AIAA-2008-6987, Honolulu, HI, 2008.

[47] I. Kitsios, V. Dobrokhodov, I. Kaminer, K. D. Jones, E. Xargay, N. Hovakimyan, C. Cao, M. I. Lizárraga, I. M. Gregory, N. T. Nguyen, and K. S. Krishnakumar, "Experimental validation of a metrics driven $\mathcal{L}_1$ adaptive control in the presence of generalized unmodeled dynamics", in: *AIAA Guidance, Navigation and Control Conference*, AIAA-2009-6188, Chicago, IL, 2009.

[48] I. M. Gregory, C. Cao, E. Xargay, N. Hovakimyan, and X. Zou, "$\mathcal{L}_1$ adaptive control design for NASA AirSTAR flight test vehicle", in: *AIAA Guidance, Navigation and Control Conference*, AIAA-2009-5738, Chicago, IL, 2009.

[49] T. Leman, E. Xargay, G. Dullerud, and N. Hovakimyan, "$\mathcal{L}_1$ adaptive control augmentation system for the X-48B aircraft", in: *AIAA Guidance, Navigation and Control Conference,* AIAA-2009-5619, Chicago, IL, 2009.

[50] Z. Li, V. Dobrokhodov, E. Xargay, N. Hovakimyan, and I. Kaminer, "Development and implementation of $\mathcal{L}_1$ gimbal tracking loop onboard of small UAV", in: *AIAA Guidance, Navigation and Control Conference,* AIAA-2009-5681, Chicago, IL, 2009.

[51] Y. Lei, C. Cao, E. M. Cliff, N. Hovakimyan, A. J. Kurdila, and K. A. Wise, "$\mathcal{L}_1$ adaptive controller for air-breathing hypersonic vehicle with flexible body dynamics", in: *American Control Conference*, St. Louis, MO, 2009, pp. 3166–3171.

[52] B. Michini and J. How, "$\mathcal{L}_1$ adaptive control for indoor autonomous vehicles: design process and flight testing", in: *AIAA Guidance, Navigation and Control Conference*, AIAA-2009-5754, Chicago, IL, 2009.

[53] I. Kaminer, A. Pascoal, E. Xargay, N. Hovakimyan, C. Cao, and V. Dobrokhodov, "Path following for unmanned aerial vehicles using $\mathcal{L}_1$ adaptive augmentation of commercial autopilots", *Journal of Guidance, Control and Dynamics*, vol. 33, no. 2, pp. 550–564, 2010.

[54] X. Fan and R. C. Smith, "Model-based $\mathcal{L}_1$ adaptive control of hysteresis in smart materials", in: *IEEE Conference on Decision and Control*, Cancun, Mexico, 2008, pp. 3251–3256.

[55] I. M. Gregory, E. Xargay, C. Cao, and N. Hovakimyan, "Flight test of $\mathcal{L}_1$ adaptive controller on the NASA AirSTAR flight test vehicle", in: *AIAA Guidance, Navigation and Control Conference,* AIAA-2010-8015, Toronto, Canada, 2010.

[56] C. Cao and N. Hovakimyan, "Design and analysis of a novel $\mathcal{L}_1$ adaptive control architecture with guaranteed transient performance", *IEEE Transactions on Automatic Control*, vol. 53, no. 2, pp. 586–591, 2008.

[57] K. J. Åström and B. Wittenmark, *Adaptive control*, Boston, MA: Addison-Wesley Longman Publishing Co., Inc., 1994.

[58] E. Kharisov, N. Hovakimyan, and K. J. Åström, "Comparison of several adaptive controllers according to their robustness metrics", in: *AIAA Guidance, Navigation and Control Conference*, Accepted for publication., Toronto, Canada, 2010.

[59] C. E. Rohrs, L. S. Valavani, M. Athans, and G. Stein, "Robustness of adaptive control algorithms in the presence of unmodeled dynamics", in: *IEEE Conference on Decision and Control*, vol. 1, Orlando, FL, 1982, pp. 3–11.

[60] C. Cao and N. Hovakimyan, "$\mathcal{L}_1$ adaptive output-feedback controller for non-stricly-positive-real reference systems: missile longitudinal autopilot design", *AIAA Journal of Guidance, Control, and Dynamics*, vol. 32, no. 3, pp. 717–726, 2009.

[61] E. Xargay, N. Hovakimyan, and C. Cao, "$\mathcal{L}_1$ adaptive controller for multi-input multi-output systems in the presence of nonlinear unmatched uncertainties", in: *American Control Conference*, Baltimore, MD, 2010, pp. 874–879.

[62] S. Fekri, M. Athans, and A. M. Pascoal, "Issues, progress and new results in robust adaptive control", *International Journal of Adaptive Control and Signal Processing*, vol. 20, no. 10, pp. 519–579, 2006.

[63] E. Xargay, N. Hovakimyan, and C. Cao, "Benchmark problems of adaptive control revisited by $\mathcal{L}_1$ adaptive control", in: *Mediterranean Conference on Control and Automation*, Thessaloniki, Greece, 2009, pp. 31–36.

[64] J. Wang, C. Cao, N. Hovakimyan, R. Hindman, and D. B. Ridgely, "$\mathcal{L}_1$ adaptive controller for a missile longitudinal autopilot design", in: *AIAA Guidance, Navigation and Control Conference*, AIAA-2008-6282, Honolulu, HI, 2008.

[65] I. M. Gregory, E. Xargay, C. Cao, and N. Hovakimyan, "Flight test of an $\mathcal{L}_1$ adaptive controller at high angle of attack and sideslip", in: *AIAA Guidance, Navigation and Control Conference*, Portland, OR, 2011.

[66] G. E. Cooper and R. P. Harper Jr., *The use of pilot rating in the evaluation of aircraft handling qualities*, Technical Note D–5153, NASA, 1969.

[67] *MIL-STD-1797B. Flying qualities of piloted aircraft*, Interface Standard, (Limited circulation), US Department of Defense Military Specification, 2006.

[68] B. L. Stevens and F. L. Lewis, *Aircraft Control and Simulation*, New York, NY: John Wiley & Sons, 1992.

[69] E. Xargay, V. Dobrokhodov, I. Kaminer, N. Hovakimyan, C. Cao, I. M. Gregory, and R. B. Statnikov, "$\mathcal{L}_1$ adaptive flight control system: systematic design and V&V of control metrics", in: *AIAA Guidance, Navigation and Control Conference*, Submitted., Toronto, Canada, 2010.

[70] K. Cunningham, *AirSTAR flight test plan: 5.5 % dynamically scaled GTM tail number T2. deployment: 2010.02.* Tech. rep. GTMP–6326 2010.02, V 2.00, 2010.

[71] K. Cunningham, *AirSTAR flight test cards, v3.12*, tech. rep. GTMP–6325 2010.03, V 3.12, 2010.

[72] D. Li, N. Hovakimyan, and C. Cao, "Positive invariance set of $\mathcal{L}_1$ adaptive controller in the presence of input saturation", in: *AIAA Guidance, Navigation and Control Conference*, Toronto, Canada, 2010.

[73] T. L. Jordan, W. M. Langford, and J. S. Hill, “Airborne Subscale Transport Aircraft Research testbed-aircraft model development”, in: *AIAA Guidance, Navigation and Control Conference*, AIAA-2005-6432, San Francisco, CA, 2005.

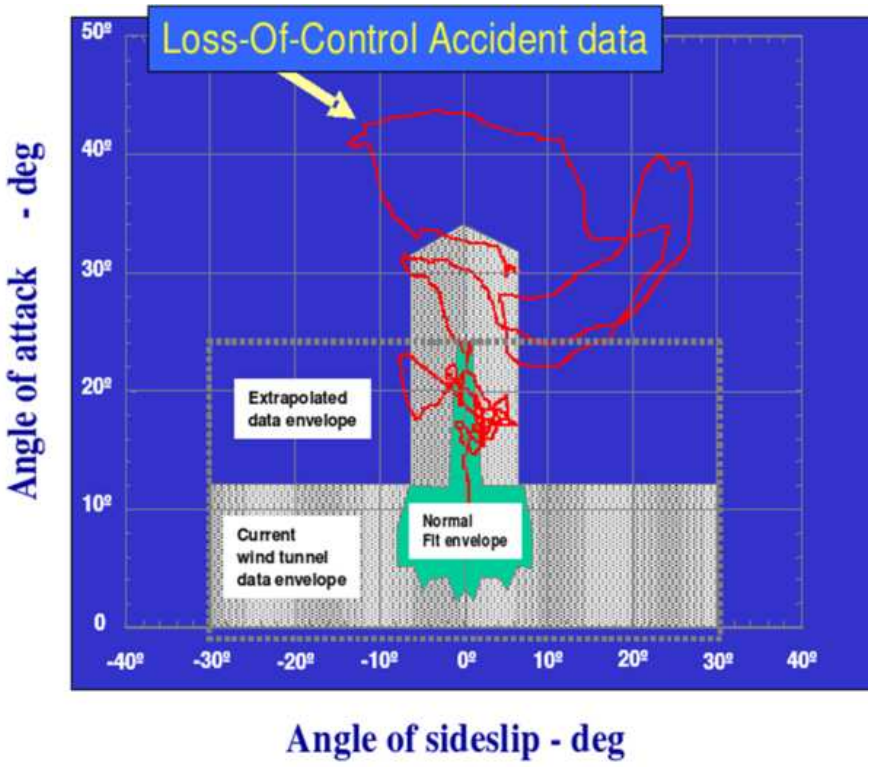

Figure 1: Loss of control accident data relative to angle of attack α and angle of sideslip β (from [73]). Angle of attack α and angle of sideslip β are two of the main state variables, describing aircraft dynamics. The green area is the combination of these variables associated with the normal flight envelope. The grey area corresponds to configurations, for which there are sufficiently adequate models based on wind–tunnel data. The blue area corresponds to configurations, for which the aerodynamic data are extrapolated from the grey area and are highly uncertain. Also, the pilots are not trained to fly the airplane in those $\alpha - \beta$ conditions and can potentially cause dangerous oscillations, known as pilot–induced oscillations (PIO) in aerospace industry.

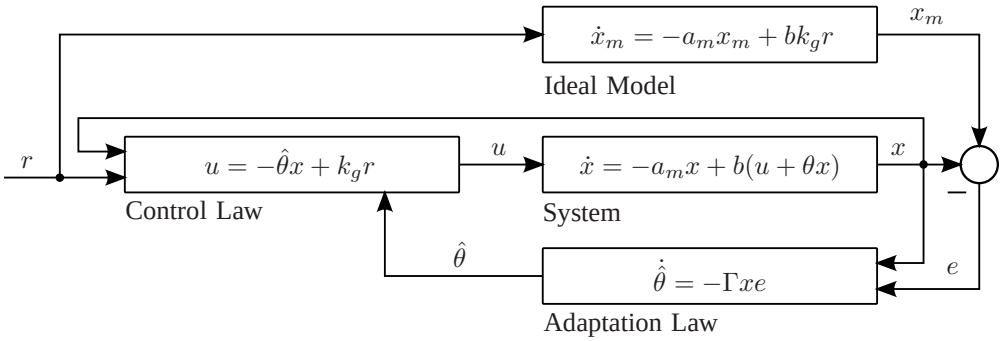

(a) MRAC

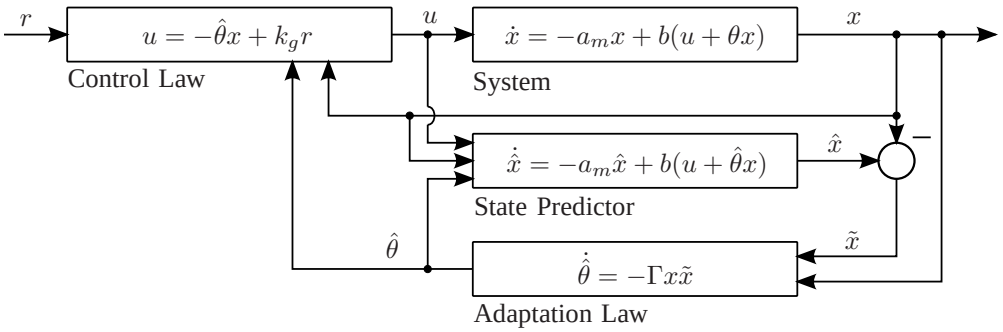

(b) MRAC with state predictor

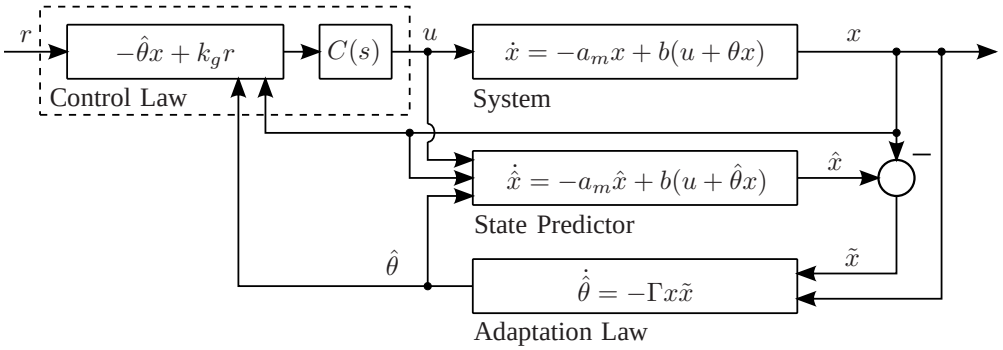

(c) $\mathcal{L}_1$ adaptive controller

Figure 2: Adaptive control architectures for the scalar case. The MRAC with state predictor is equivalent to the MRAC architecture. The $\mathcal{L}_1$ architecture is based on the MRAC with state predictor, but has a lowpass filter $C(s)$ in the control channel.

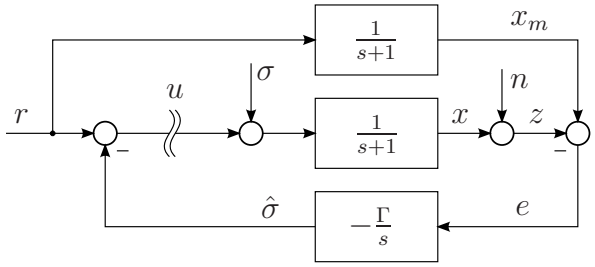

Figure 3: Closed–loop system with MRAC–type integral controller. The adaptation gain Γ is located in the feedback loop of the control system. Hence, the loop gain and the bandwidth of the closed–loop system are determined by Γ.

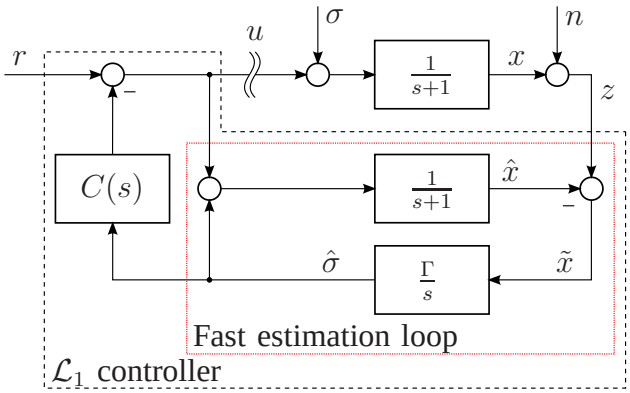

Figure 4: Closed–loop system with $\mathcal{L}_1$ adaptive controller. The adaptation gain Γ is affecting only fast estimation loop (red), while the bandwidth of the control loop is determined by the lowpass filter $C(s)$.

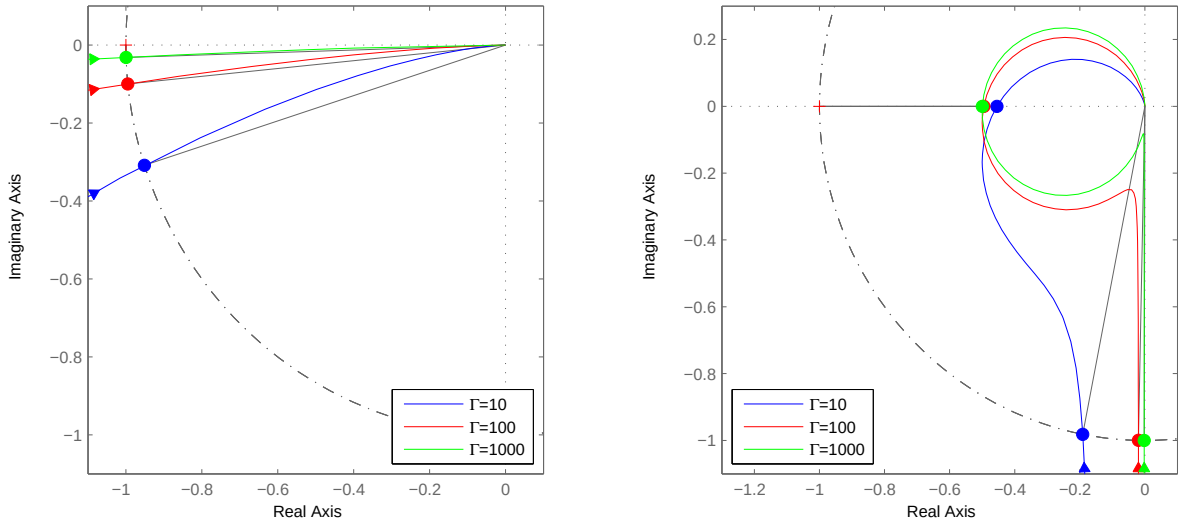

(a) integral controller

(b) $\mathcal{L}_1$ controller

Figure 5: Nyquist plots for the loop transfer functions. The plot (a) shows that the phase margin of the MRAC–type integral controller vanishes as the adaptation gain Γ is increases. On the other hand, the plot (b) shows that the phase margin of the $\mathcal{L}_1$ adaptive controller approaches $\pi/2$ as the adaptation gain is increased.

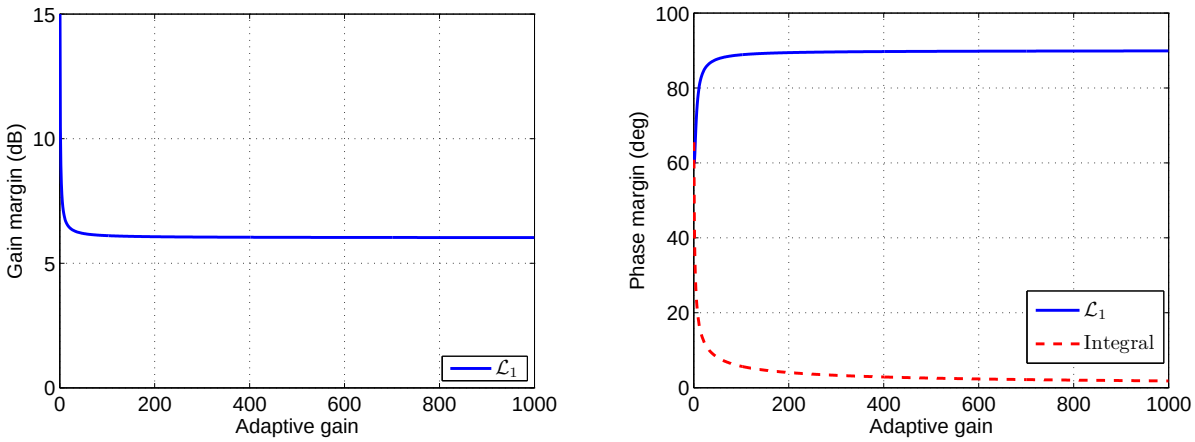

(a) gain margin (b) phase margin

Figure 6: Effect of high adaptation gain on the stability margins. The $\mathcal{L}_1$ adaptive controller has bounded–away–from–zero gain and phase margins. The MRAC integral type controller has infinite gain margin and diminishing with increasing adaptation gain phase margin. The results are consistent with Figure 5.

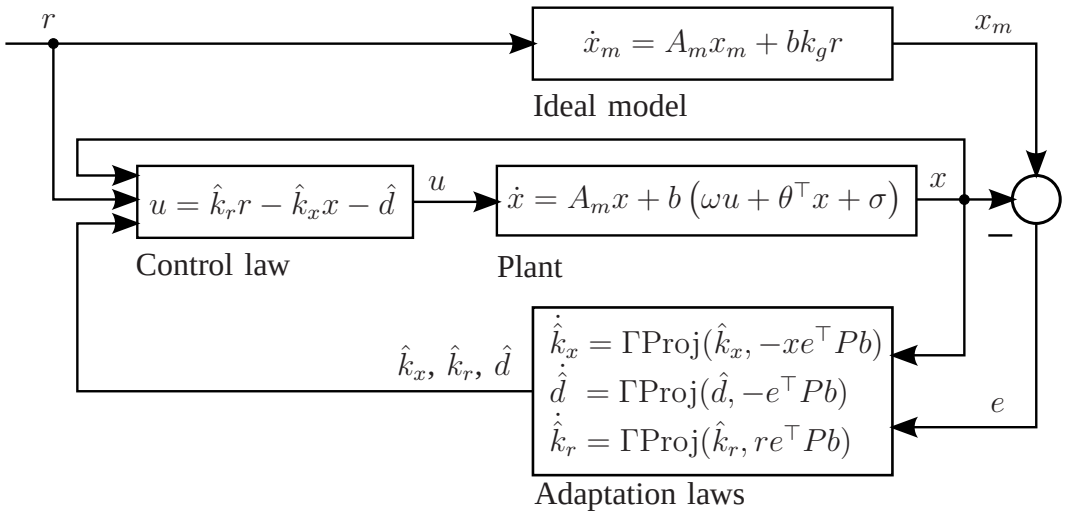

(a) Direct MRAC

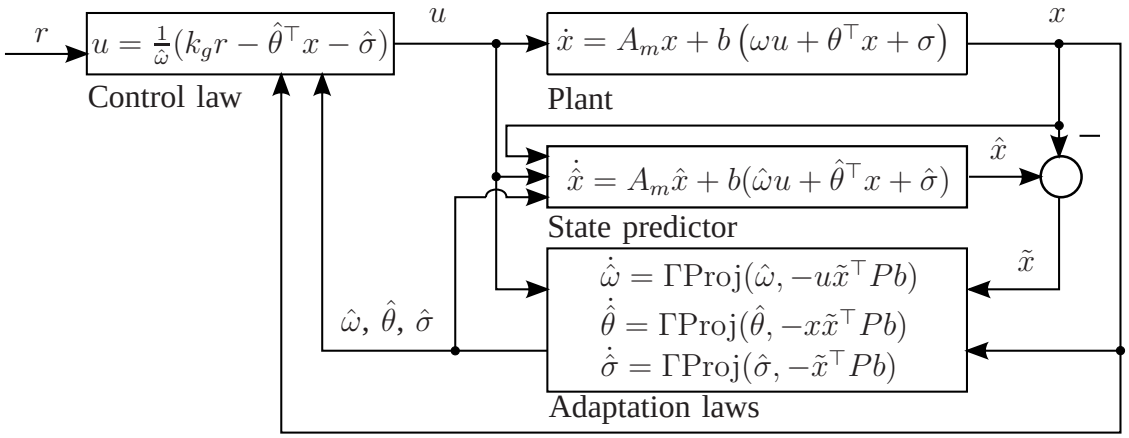

(b) Indirect MRAC

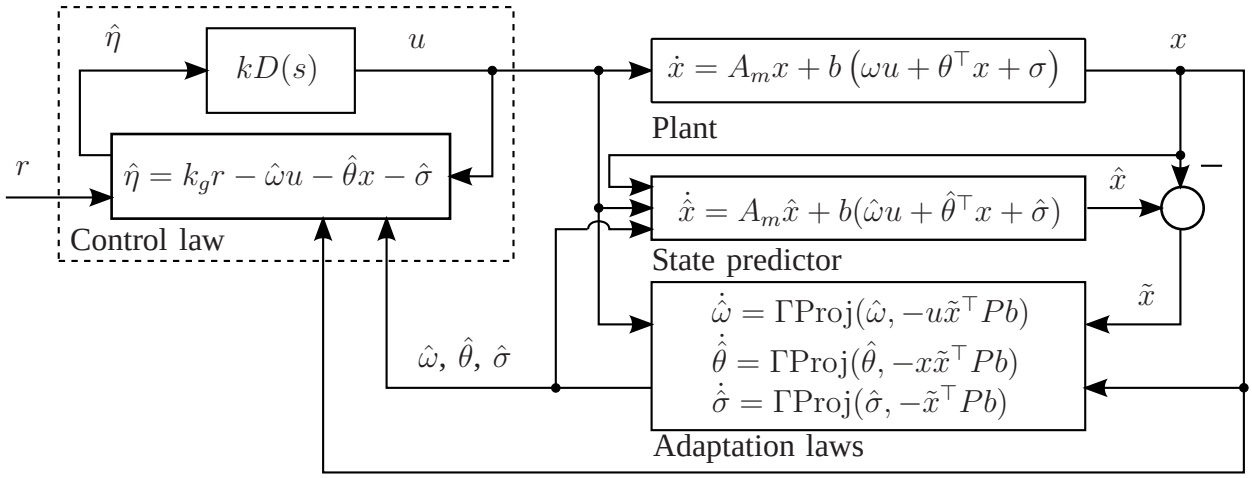

(c) $\mathcal{L}_1$ adaptive controller

Figure 7: Block diagrams of the adaptive control architectures. The indirect MRAC is based on state predictor. The $\mathcal{L}_1$ adaptive control architecture has the same state predictor and the adaptation laws as the indirect MRAC, but different control law.

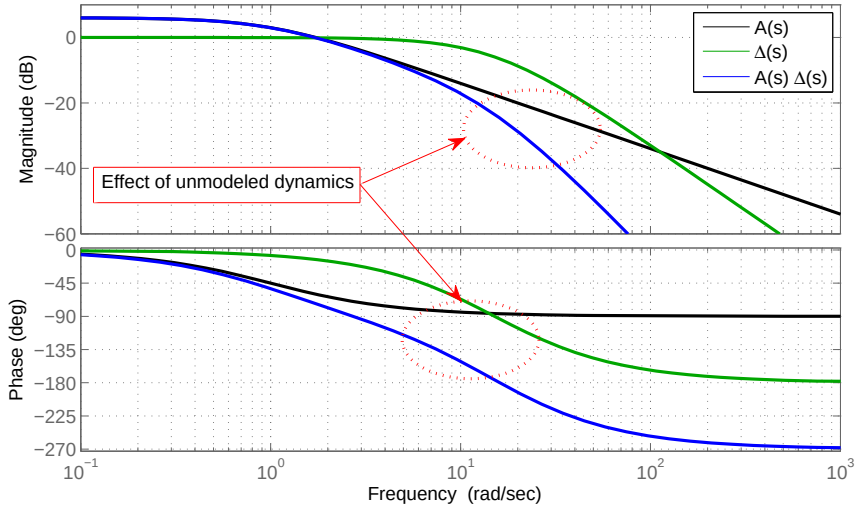

Figure 8: Impact of the unmodeled dynamics. The poles of the unmodeled dynamics are located far right from the pole of the system. Therefore unmodeled dynamics starts significantly affecting the system's Bode diagram in the region with less than -20 dB magnitude.

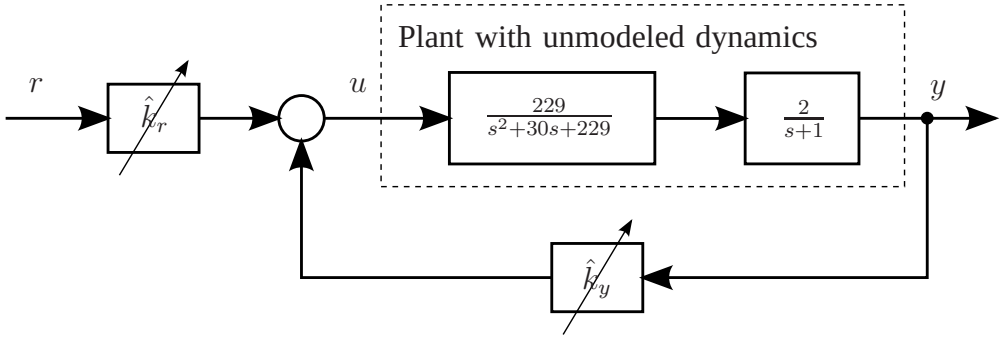

Figure 9: Rohrs' Example. Closed–loop MRAC system with fast and overdamped unmodeled dynamics. The estimates $\hat{k}_r$ and $\hat{k}_y$ are driven by the adaptive laws in (81)–(82).

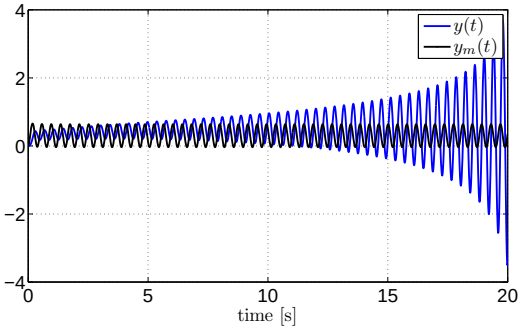

(a) System output $y(t)$, $y_m(t)$

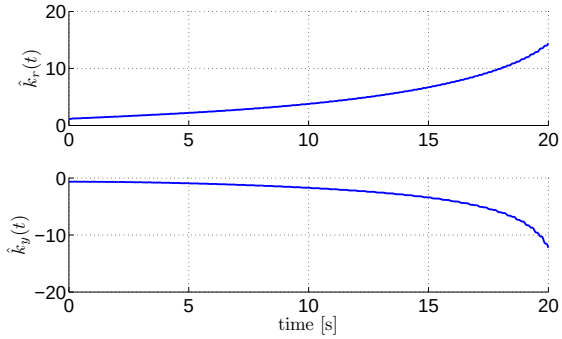

(b) Controller parameters $\hat{k}_r(t)$, $\hat{k}_y(t)$

Figure 10: Closed–loop MRAC response to $r_1(t)$. The adaptive estimates in (b) experience parameter drift, which leads to instability and unbounded growth of the system output in (a)

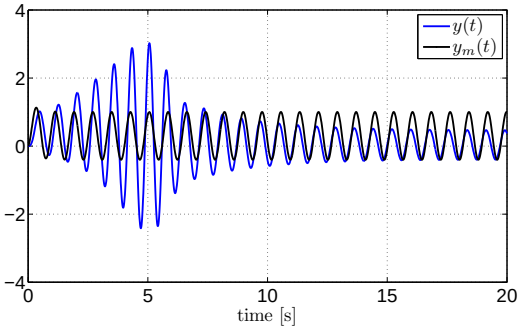

(a) System output $y(t)$, $y_m(t)$

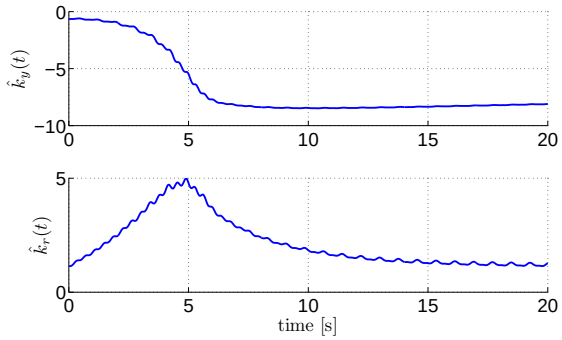

(b) Controller parameters $\hat{k}_r(t)$, $\hat{k}_y(t)$

Figure 11: Closed–loop MRAC response to $r_2(t)$. The parameter estimates for a short period of time move to the set for which the controller with frozen parameters is unstable. This behavior of the estimates results in temporarily instability of the closed–loop MRAC and causes bursting.

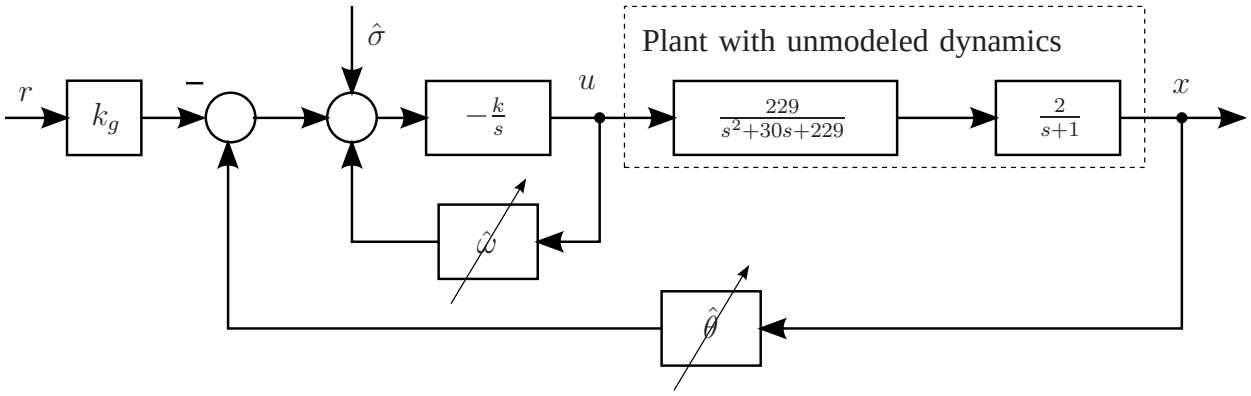

Figure 12: Rohrs' Example. Closed–loop $\mathcal{L}_1$ control system with fast and overdamped unmodeled dynamics. The estimates $\hat{\omega}$, $\hat{\theta}$ and $\hat{\sigma}$ are driven by the adaptive laws in (83)–(85).

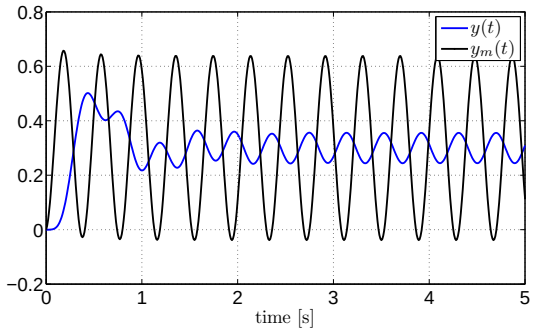

(a) System output $y(t)$, $y_m(t)$

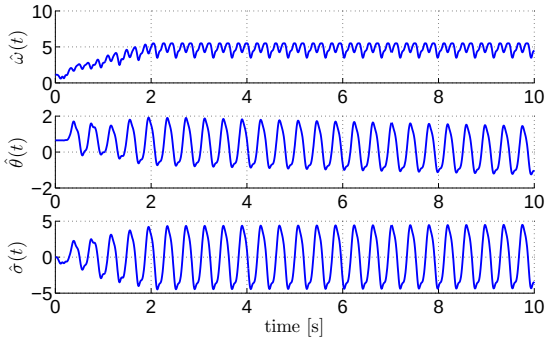

(b) Controller parameters $\hat{\omega}(t)$, $\hat{\theta}(t)$, $\hat{\sigma}(t)$

Figure 13: Closed–loop response of the $\mathcal{L}_1$ adaptive control system to $r_1(t)$. Projection operator helps to avoid the parameter drift. Therefore the system output and the parameter estimates remain bounded.

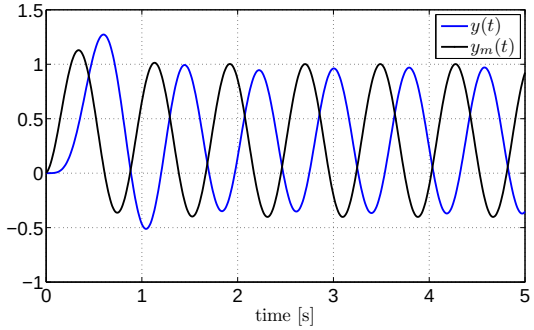

(a) System output $y(t)$, $y_m(t)$

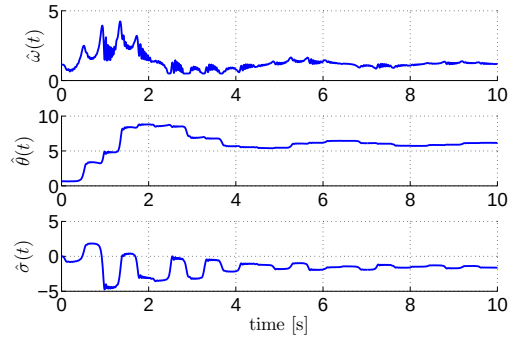

(b) Controller parameters $\hat{\omega}(t)$, $\hat{\theta}(t)$, $\hat{\sigma}(t)$

Figure 14: Closed–loop response of the $\mathcal{L}_1$ adaptive control system to $r_2(t)$. We see that the parameter estimates remain bounded, and the control system does not experience the bursting phenomenon.

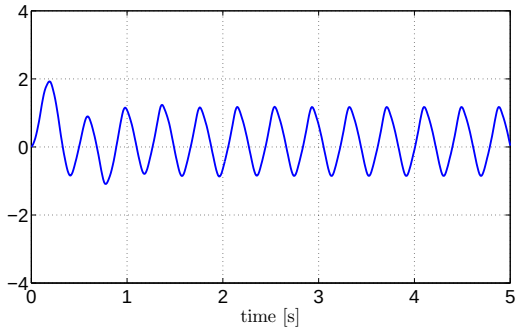

(a) $u(t)$ for $r_1(t)$

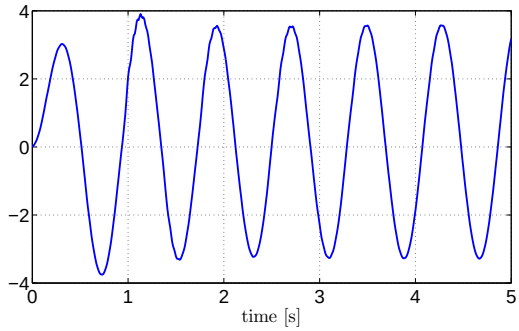

(b) $u(t)$ for $r_2(t)$

Figure 15: Control signal time–history for $\mathcal{L}_1$ adaptive control system. The control signal remains bounded and does not contain high–frequency content.

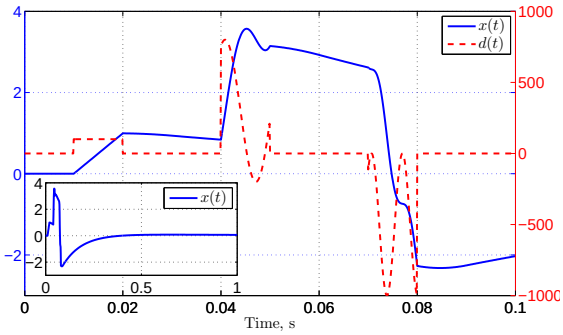

(a) State transient $x(t)$

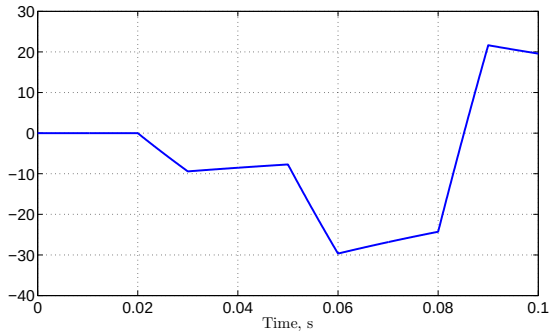

(b) Control history $u(t)$

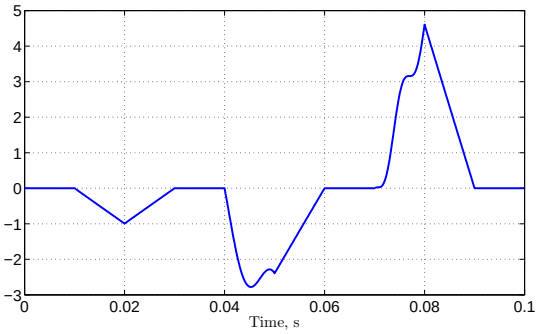

(c) Prediction error $\tilde{x}(t)$

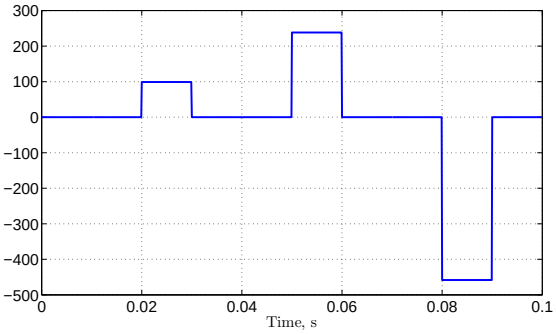

(d) Parameter estimate $\hat{\sigma}(t)$

Figure 16: System response to the disturbance $d(t)$. The plots show that at the beginning of the sampling period the $\mathcal{L}_1$ adaptive controller generates a parameter estimate, which completely cancels the prediction error, accumulated during the previous sampling period. Further, the controller does not respond to the disturbance during the sampling period, when the disturbance occurs. In the absence of the prediction error the controller generates zero control input.

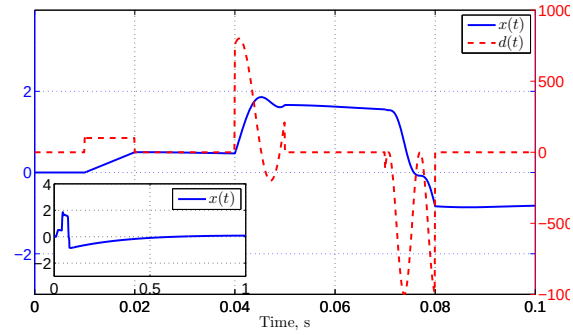

(a) State transient $x(t)$

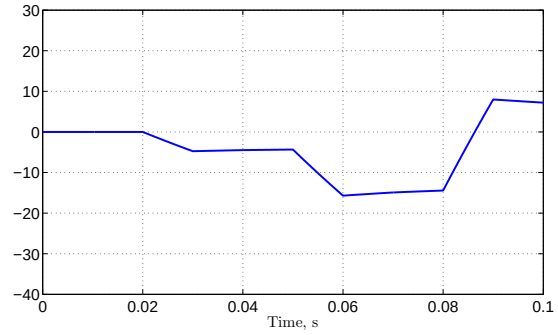

(b) Control history $u(t)$

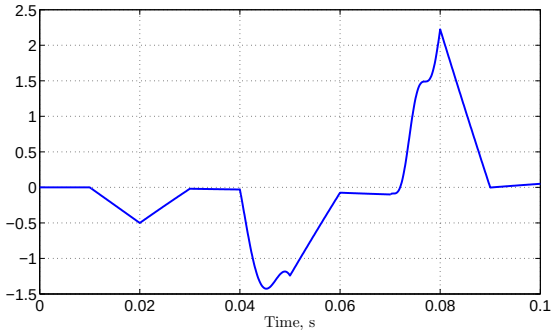

(c) Prediction error $\tilde{x}(t)$

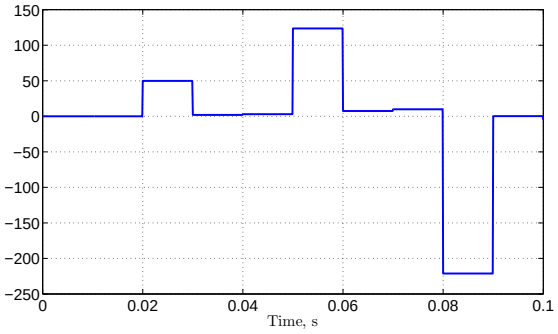

(d) Parameter estimate $\hat{\sigma}(t)$

Figure 17: System response to the disturbance $d(t)$. We observe that the system uncertainties do not allow for complete compensation of the prediction error during each sampling period. However, choosing the sampling period T_s smaller helps to keep the prediction error small.

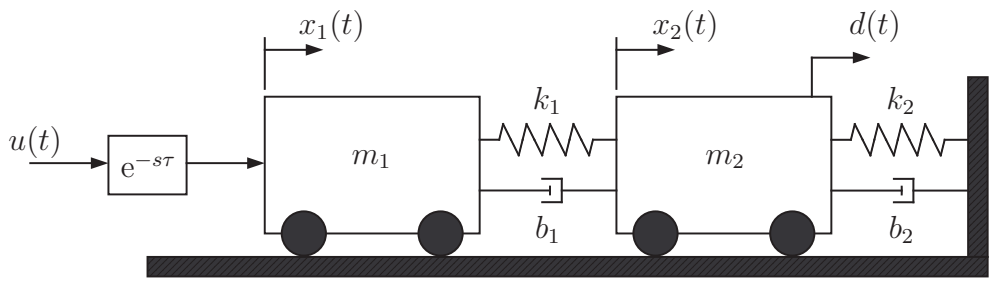

Figure 18: The two–cart MSD system. The states $x_1(t)$ and $x_2(t)$ represent the absolute positions of the two carts, whose masses are m_1 and m_2 respectively. Only $x_2(t)$ is measurable. The carts are mechanically connected between each other and the rigid surface by means of spring–damper couples k_1–b_1 and k_2–b_2 respectively. The signal $d(t)$ is a random colored disturbance force, and $u(t)$ is the control force, and the block with $\mathrm{e}^{-s\tau}$ represents the input time delay.

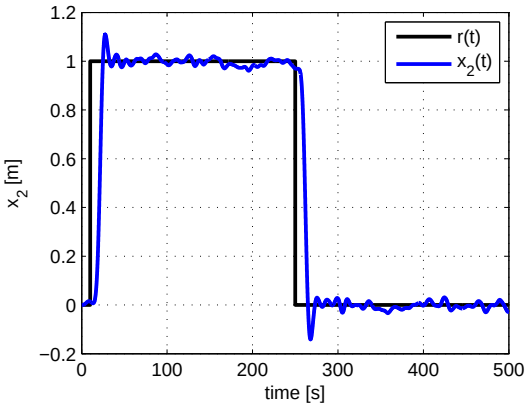

(a) system output $x_2(t)$

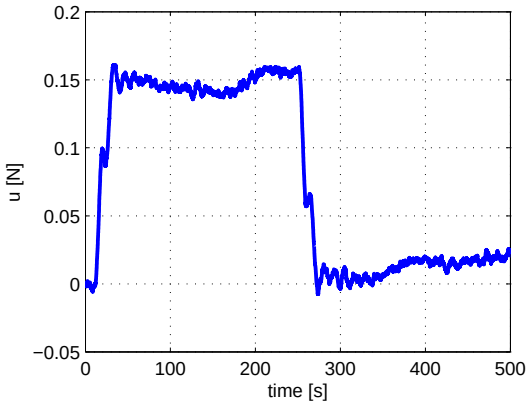

(b) control signal $u(t)$

Figure 19: Closed–loop response to a step input of 1 m with $k_1 = 0.25$ and $\tau = 0.05$ s. The system output is tracking the reference commands with the desired control specifications. The control signal remains bounded and does not exhibit high–frequency oscillations.

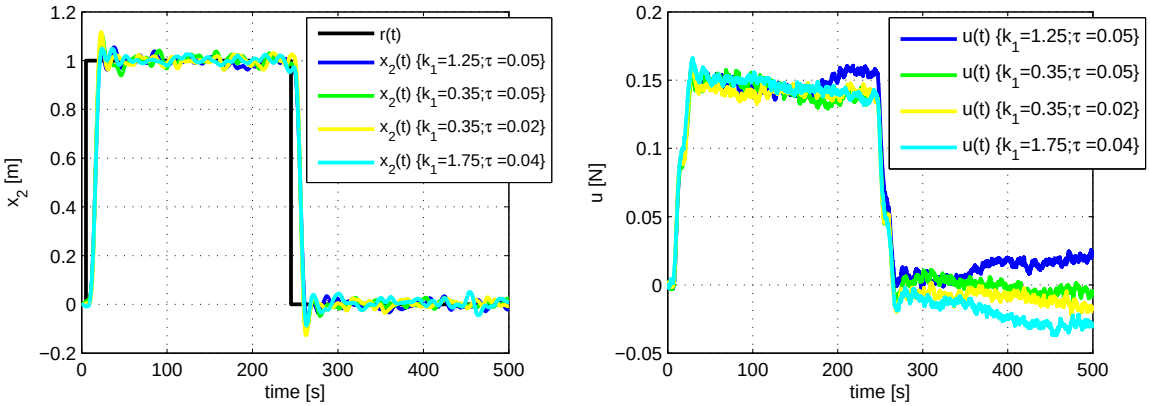

(a) system output $x_2(t)$ (b) control signal $u(t)$

Figure 20: Closed–loop response to a step input of 1 m for different values of the unknowns k_1 and τ. For all cases of unknown parameters the closed–loop system has similar response according to the expectations. The control signal changes with different values of the parameters, however it remains bounded and does not exhibit high–frequency oscillations.

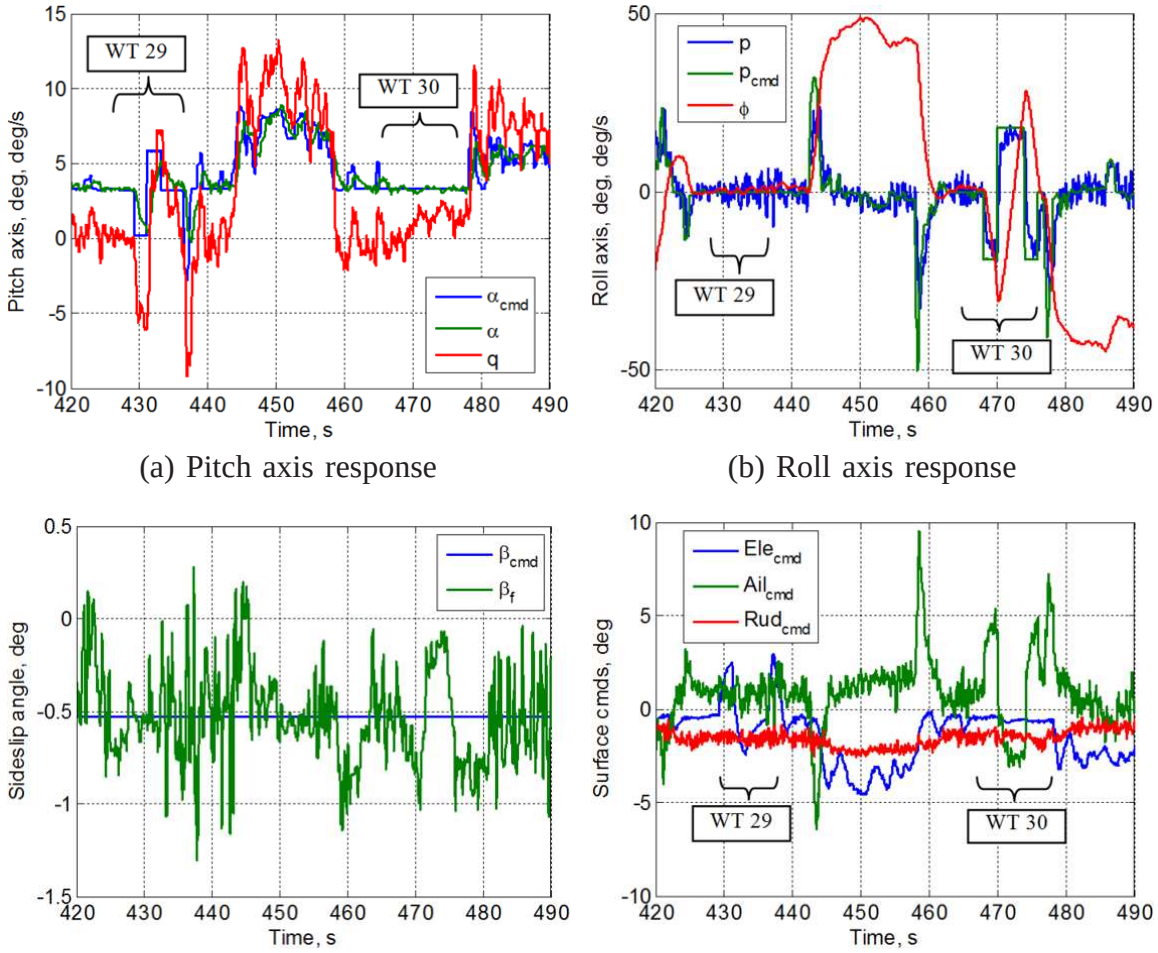

(a) Pitch axis response

(b) Roll axis response

(c) Directional axis response

(d) Actuator commands

Figure 21: The figure shows 70 s of flight that includes angle of attack and roll rate wave trains, one complete turn and part of another turn. The lack of pilot input during the wave train injection, manifests as a precise straight line doublet, can be observed in (a) and (b). Note very small sideslip angle β maintained by an $\mathcal{L}_1$ all–adaptive control law and the nonzero command that comes from vane calibration bias as shown in (c). The surface commands during this flight segment are illustrated in (d).

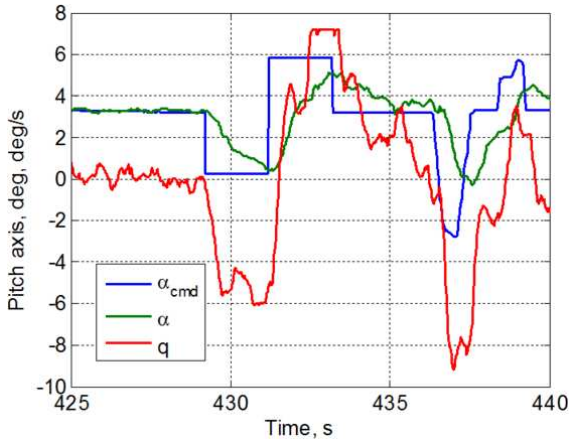

(a) Pitch axis wave train

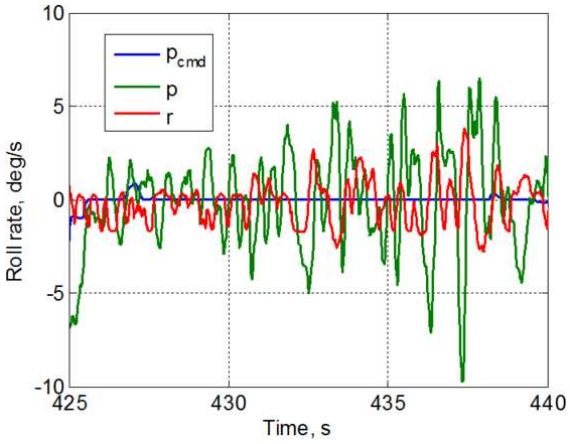

(b) Lateral–directional cross–coupling

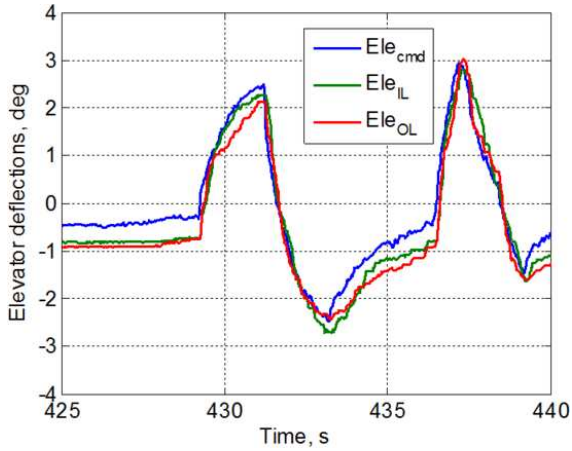

(c) Pitch axis actuators

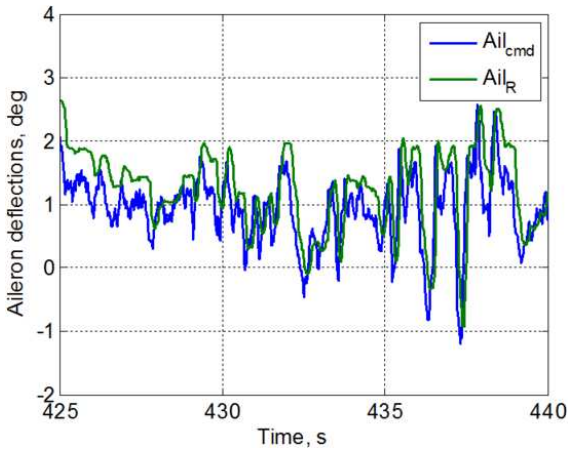

(d) Lateral–directional cross–coupling actuators

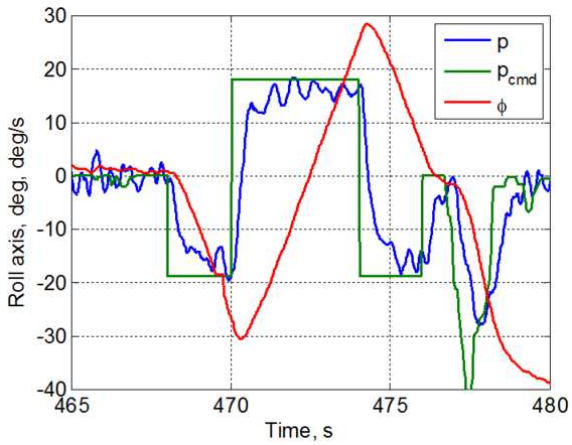

(e) Roll axis wave train

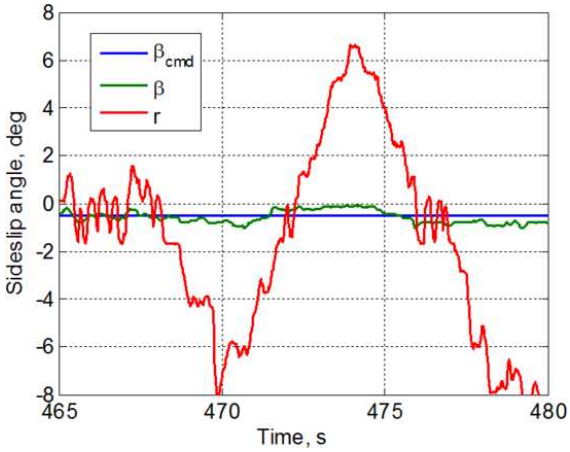

(f) Directional cross–coupling

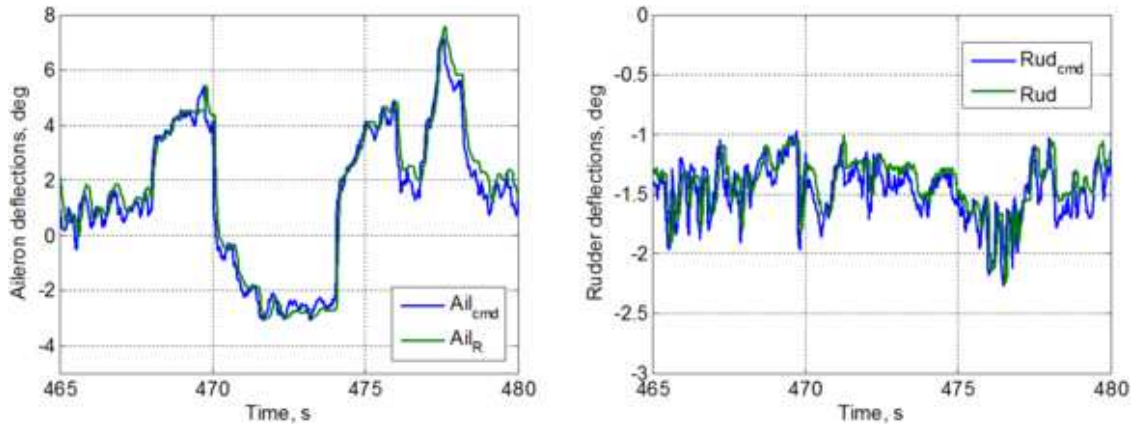

(g) Lateral–directional axes actuators

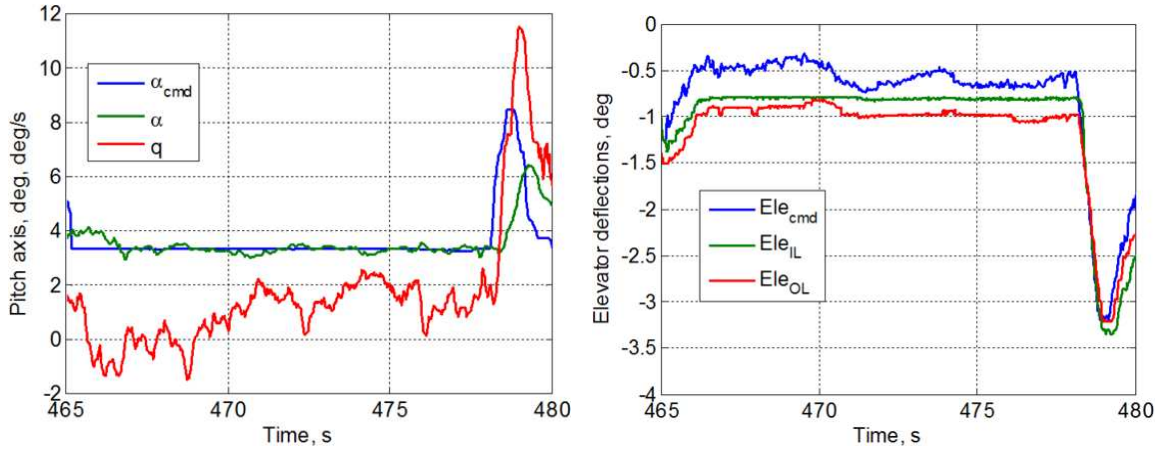

(h) Longitudinal cross–coupling

(i) Longitudinal axis actuators

Figure 22: The isolated wave train responses for the nominal aircraft. Angle of attack tracking the wave train is illustrated in (a), the corresponding elevator response is shown in (b) and the cross–coupling dynamics between the axis and the corresponding aileron response to suppress it are shown in (b) and (d) respectively. Note the angle of attack tracking in (a) corresponds to Level 1 handling qualities response. The lateral axis response to the wave train is in (e) the associated directional axis is in (f), the commanded aileron and rudder are in (g), while the longitudinal axis cross–coupling and the suppressing elevator response are in (h) and (i).

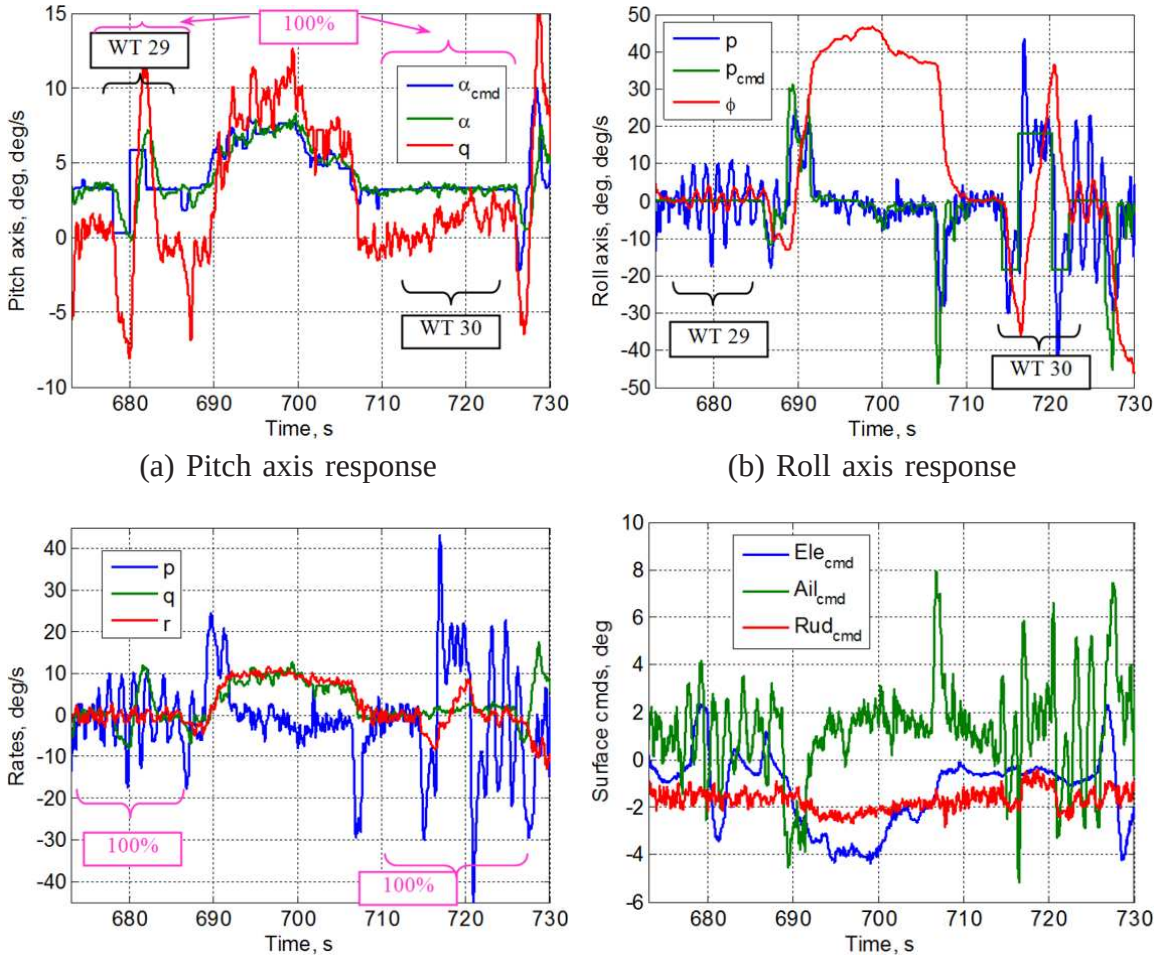

(a) Pitch axis response

(b) Roll axis response

(c) Aircraft rates

(d) Actuator commands

Figure 23: This set of maneuvers is performed with a neutrally stable aircraft and 50% degradation in pitch control power that is, 100% degradation in pitch stability and roll damping. Plots in (a)–(b) show pitch and roll axes response as well as mark where the 100% fault and wave trains are engaged. Figures (c)–(d) shows the angular rates and actuator commands respectively through the entire segment of flight. The dynamic response, especially in roll rate, shows oscillatory behavior with overshoots as well as increased actuator amplitudes in an attempt to compensate, which compared to that of the nominal aircraft indicate the deterioration in response.

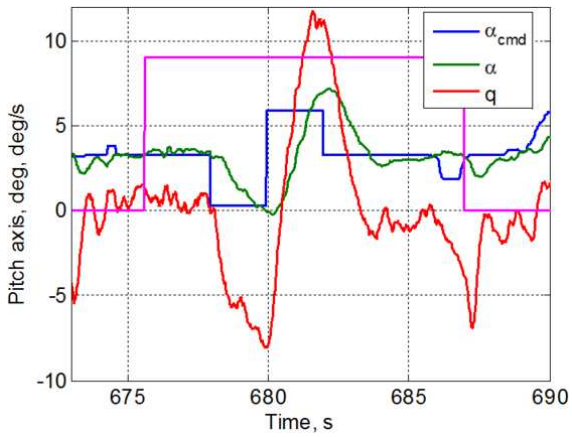

(a) Pitch axis wave train

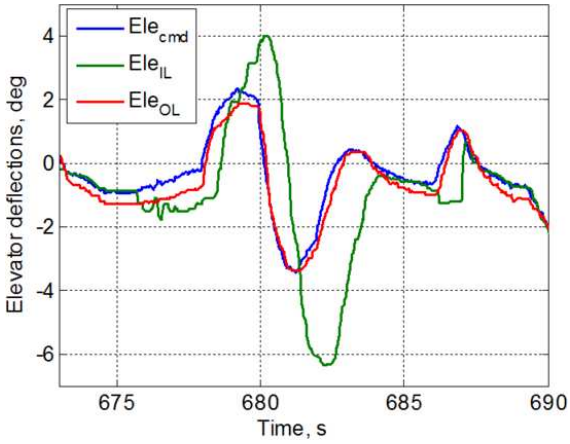

(b) Actuator deflections

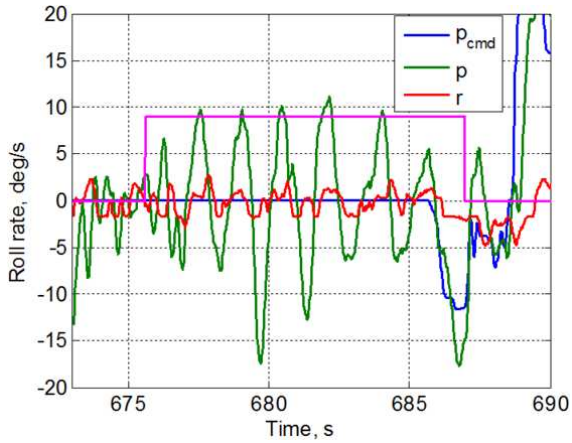

(c) Lateral–directional cross–coupling

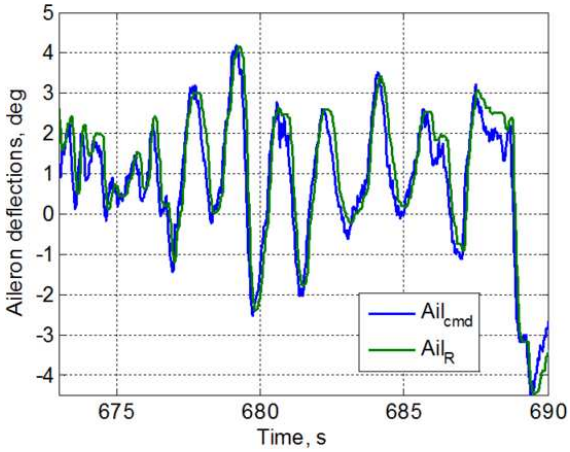

(d) Actuator deflections

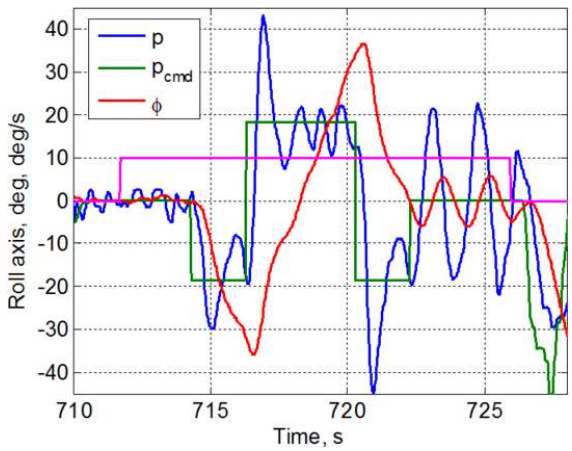

(e) Roll axis wave train

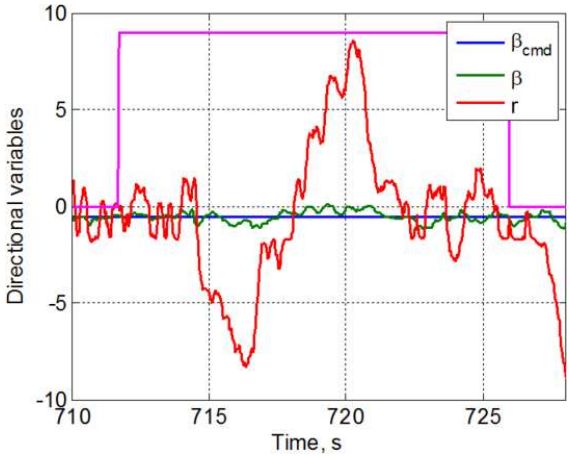

(f) Directional cross–coupling

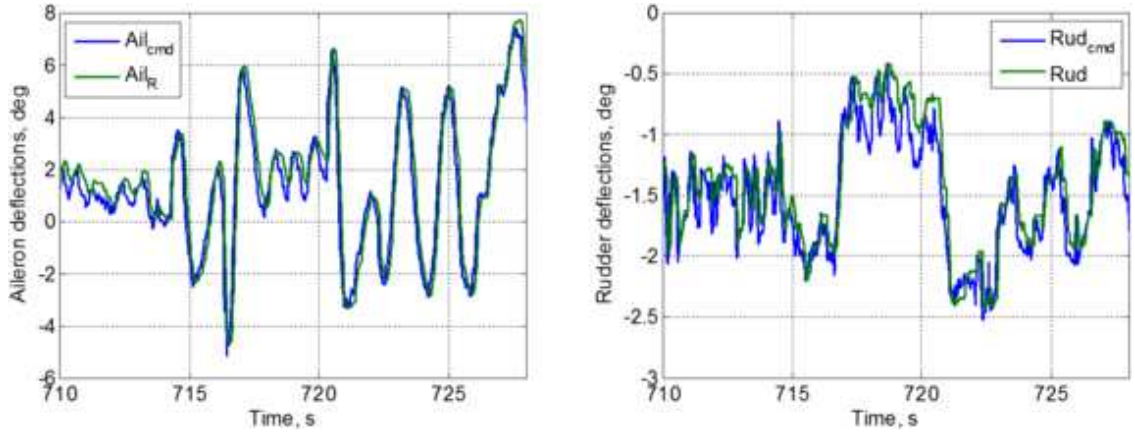

(g) Lateral–directional axes actuators

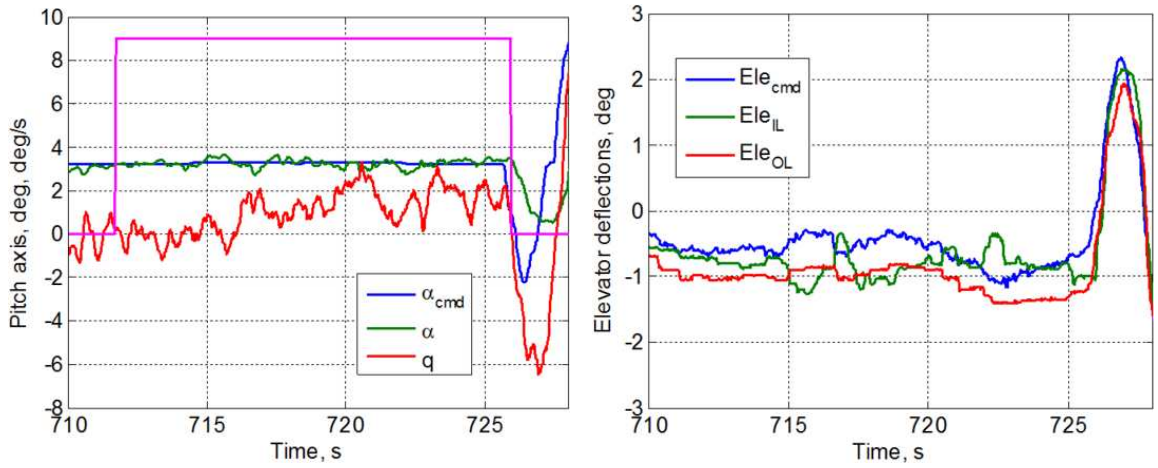

(h) Longitudinal cross–coupling

(i) Actuator deflections

Figure 24: The time when the fault is engaged is shown on the plots as a magenta finite time step. The engagement of fault, pitch axis wave train and associated state and actuator responses of interest are shown in (a)–(d). Note the inner left elevator segment $\mathrm{Ele_{IL}}$ acting independently of command in destabilizing the pitch axis. The overall pitch axis closed–loop damping decreases with fault as evidenced by an overshoot in angle of attack response and larger magnitude pitch rate response. In the lateral–directional axes in (c), there is more excitation of the roll rate by turbulence, since roll damping is also 100% degraded, and potentially more cross–coupling in the roll axis. Roll rate is more oscillatory, (e) excited by turbulence and stick inputs and the ailerons respond (g) to try to damp out the overshoot and turbulence induced oscillations. However, at the tail end of the wave train, there are two ± 20 deg/s oscillations that the controller is slow in damping out.

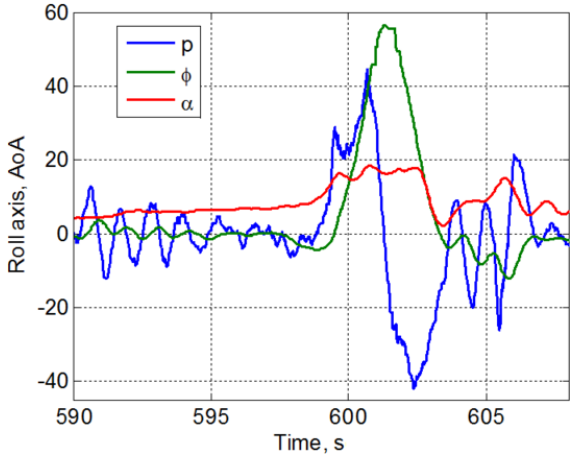

(a) Stick–to–surface

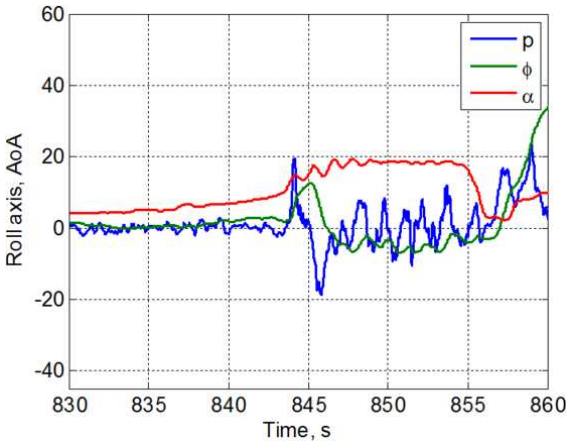

(b) $\mathcal{L}_1$ all–adaptive controller

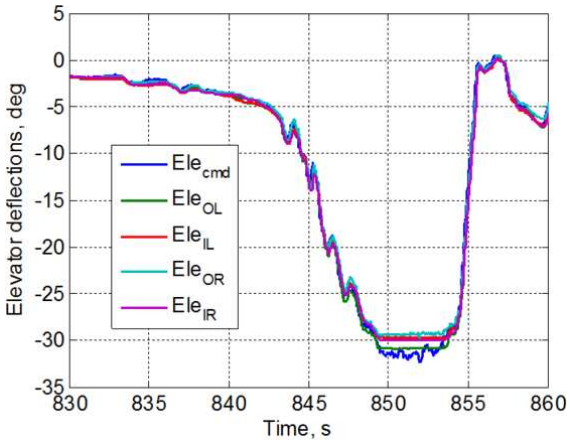

(c) Elevator surface response
for $\mathcal{L}_1$ all–adaptive controller

Figure 25: Post stall angle of attack capture maneuver defining variables — angle of attack α, roll rate p and bank angle ϕ — are shown as a function of time as the pilot makes his first attempt to capture $\alpha = 18$ deg. The largest roll rate with an $\mathcal{L}_1$ controller encountered between 13 and 14 degrees is less than ± 20, which translates to roughly 12 degrees bank angle. The bank–angle excursion lasts for less than 2 s before returning to a fairly constant 5–deg offset. The pilot captures and maintains 18–deg angle of attack for over 7 s. Moreover, the combination of power setting and pilot command saturates the all segments of the elevator from 849 to 854 s without observable ill effect on the control system or aircraft dynamics, (c). The responses for stick to surface are self–explanatory in (a).

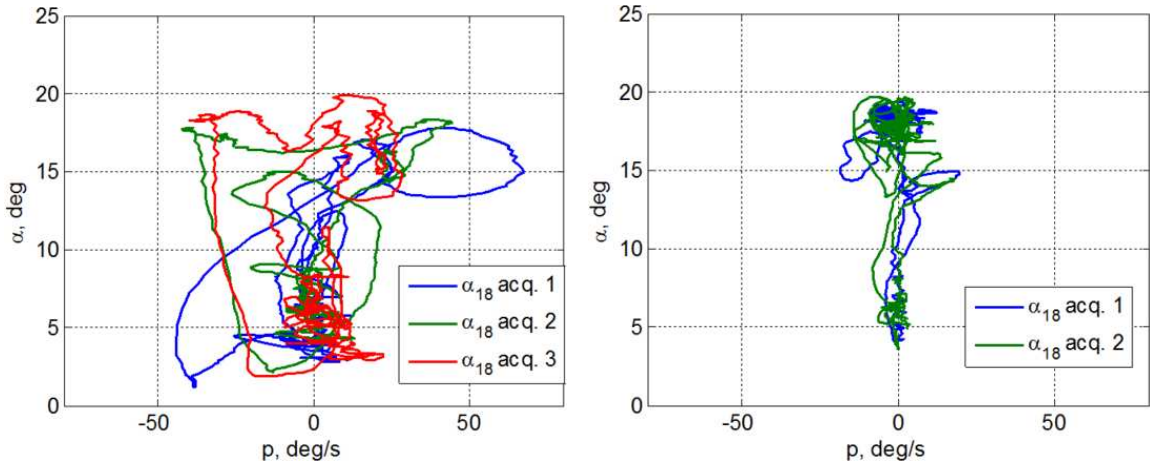

(a) Stick–to–surface (b) $\mathcal{L}_1$ all–adaptive controller

Figure 26: Post–stall angle of attack capture shows the $\alpha - p$ envelope and the performance of stick to surface and $\mathcal{L}_1$ adaptive controller respectively. Note that an $\mathcal{L}_1$ controller roll rate never exceeds 20 deg/s (b) while in state to surface configuration roll rate exceeds 40 deg/s in the best case scenario, acquisition attempt 3 (a).

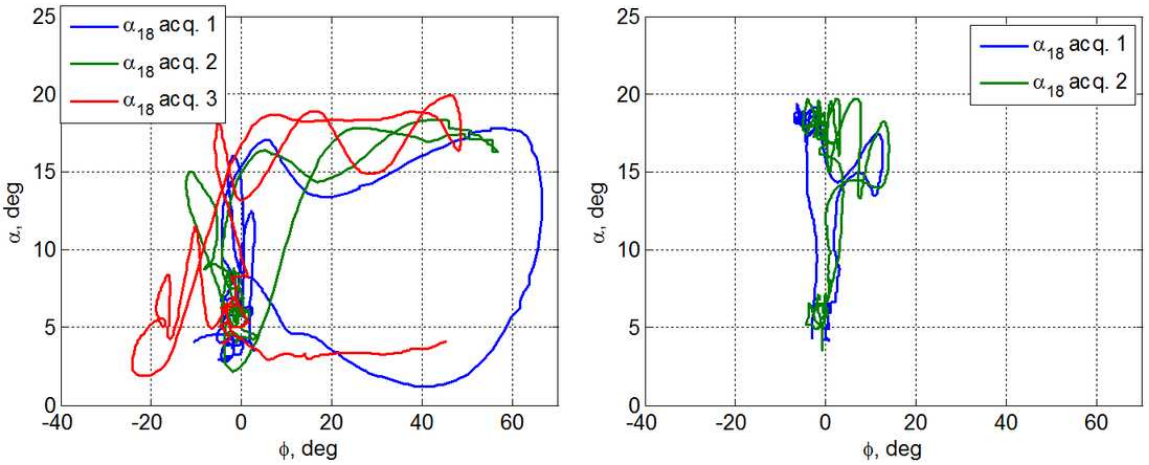

(a) Stick–to–surface (b) $\mathcal{L}_1$ all–adaptive controller

Figure 27: Post–stall angle of attack capture — angle of attack α / bank angle ϕ envelope. Persistently high roll rate necessarily translates into large bank angles as is shown in (a). Under admittedly conservative rules for allowable bank angle for this maneuver, all three stick to surface attempts have to be abandoned since each exceeded 45–deg bank angle. Bank angle under $\mathcal{L}_1$ all–adaptive control law, however, never exceeded 15 deg (b).

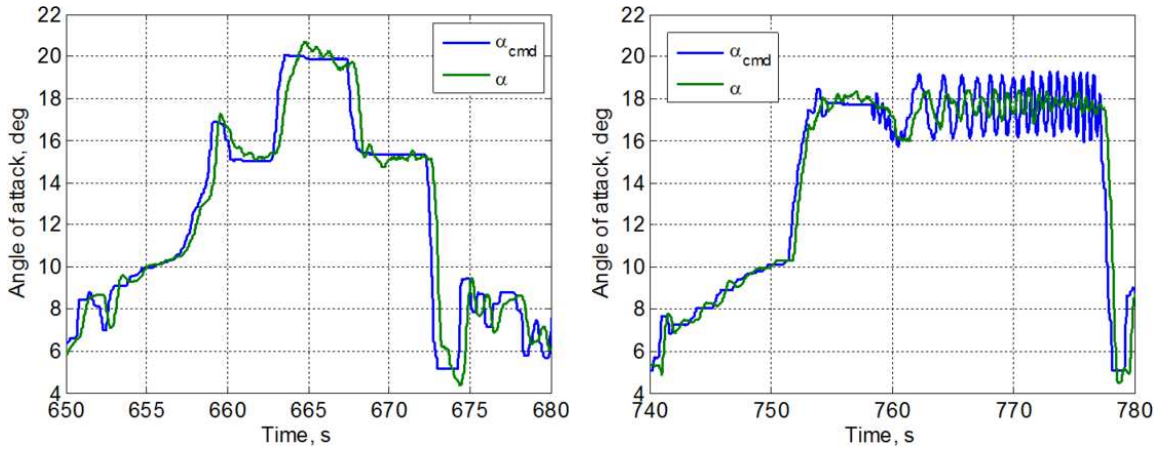

(a) Step input (b) Schroeder sweep

Figure 28: Post–stall angle of attack command following. The control law task to support the modeling work is to attain stable flight at $\alpha = 18$ deg, once the desired angle of attack is reached, follow a predetermined input wave train while the pilot stays out of the loop, especially in the longitudinal axis. The controller response to the prescribed inputs are shown — step command of 18 deg to 15 deg, 15 deg to 20 deg, 20 deg to 15 deg (a) and Schroeder sweep (b).

Sidebar 1. $\mathcal{L}_1$–Norm of a System

The $\mathcal{L}_1$–norm of a system sets the relation between the peak values of the system's input and output. Sometimes the $\mathcal{L}_1$–norm is also called as peak–to–peak gain of a system.

Let $G(s)$ be a strictly proper and stable system. For a given bounded input $u(t)$, its output $y(t)$ can be written as

$$y(t) = g(t) * u(t) = \int_0^t g(t-\tau)u(\tau)d\tau\,,$$

where "$*$" stands for the convolution operator, and $g(t)$ is the impulse response of $G(s)$. Letting

$$\|y\|_{\mathcal{L}_\infty} = \sup_{t\geq 0} |y(t)|\,,$$

we obtain the upper bound

$$|y(t)| = \left|\int_0^t g(\tau)u(t-\tau)d\tau\right| \leq \int_0^t |g(\tau)||u(t-\tau)|d\tau \leq \int_0^\infty |g(\tau)|d\tau\ \|u\|_{\mathcal{L}_\infty}\,.$$

The $\mathcal{L}_1$–norm of $G(s)$ is defined as

$$\|G(s)\|_{\mathcal{L}_1} = \int_0^\infty |g(\tau)|d\tau\,,$$

which leads to the following expression of the upper bound

$$\|y\|_{\mathcal{L}_\infty} \leq \|G(s)\|_{\mathcal{L}_1}\|u\|_{\mathcal{L}_\infty}\,.$$

Notice that this upper bound holds if and only if the system $G(s)$ is stable [S1]. For unstable systems the $\mathcal{L}_1$–norm does not exist, as the impulse response is unbounded. For m–input l–output

system the definition of the $\mathcal{L}_1$–norm is given by

$$\|G(s)\|_{\mathcal{L}_1} = \max_{i=1,\ \ldots,\ l} \left(\sum_{j=1}^{m} \int_0^{\infty} |g_{ij}(\tau)| d\tau \right) ,$$

where $g_{ij}(t)$ is the $\{ij\}^{\text{th}}$ entry of the impulse response matrix of the system $G(s)$. If $G_1(s)$ and $G_2(s)$ are stable proper systems, then

$$\|G(s)\|_{\mathcal{L}_1} \leq \|G_2(s)\|_{\mathcal{L}_1} \|G_1(s)\|_{\mathcal{L}_1} ,$$

where $G(s) = G_2(s)G_1(s)$ [S1].

References

[S1] N. Hovakimyan and C. Cao, $\mathcal{L}_1$ *Adaptive Control Theory*, Philadelphia, PA: Society for Industrial and Applied Mathematics, 2010.

Sidebar 2. Barbalat's lemma

For a continuous function $f : \mathbb{R} \to \mathbb{R}$ the convergence of the integral

$$\int_0^t f(\tau)d\tau$$

to a finite limit as $t \to \infty$ does not imply that the function $f(t) \to 0$ as $t \to \infty$. Barbalat's lemma states that, under an additional assumption on $f(t)$, the convergence to the limit can be proven.

Lemma 1 *Let $f : \mathbb{R} \to \mathbb{R}$ be a uniformly continuous function on $[0, \infty)$. Assume that*

$$\lim_{t\to\infty} \int_0^t f(\tau)d\tau$$

exists. Then

$$\lim_{t\to\infty} f(t) = 0\,.$$

Sidebar 3. Bridging Adaptive and Robust Control

Consider the system in (1). In frequency domain we rewrite it as

$$x(s) = H(s)(u(s) + \theta x(s)) + x_{\text{in}}(s)\,. \tag{S1}$$

For simplicity of explanation we consider zero initial conditions, which yields $x_{\text{in}}(s) \equiv 0$. Taking this assumption into account and multiplying (S1) by $C(s)$ and then dividing by $H(s)$, we obtain

$$C(s)\theta x(s) = \frac{C(s)}{H(s)}x(s) - C(s)u(s)\,.$$

Substituting this expression into the equation for the reference control signal in (17) and isolating $u(s)$, we obtain the following representation for the reference controller

$$u_{\text{ref}}(s) = \frac{C(s)}{1 - C(s)}k_g r(s) - \frac{1}{1 - C(s)}\frac{C(s)}{H(s)}x_{\text{ref}}(s)\,. \tag{S2}$$

Notice that $\frac{1}{1-C(s)}\frac{C(s)}{H(s)}$ is proper for all strictly proper $C(s)$. The block diagram of the closed–loop $\mathcal{L}_1$ reference system is shown in Figure S1. Notice that all elements of the controller implementation in Figure S1 are proper and stable. This representation of the $\mathcal{L}_1$ reference system is structurally similar to the DOB architecture, analyzed in [S2–S4]. DOB control design is based on the internal model principle, which assumes that the control system encapsulates either implicitly or explicitly a model of the system to be controlled. The $\mathcal{L}_1$ reference controller, similar to DOB, aims for compensation of the mismatch between the ideal model and the real system within the frequency range specified by the bandwidth of the lowpass filter. This structural similarity of the architectures allows for application of the robust control design methods, developed in DOB literature and robust control to the design of the filter $C(s)$ of the $\mathcal{L}_1$ adaptive

controller [S5].

References

[S2] K. Ohnishi, “A new servo method in mechatronics”, *Trans. of japanese society of electrical engineers*, vol. 107-D, pp. 83–86, 1987.

[S3] T. Umeno and Y. Hori, “Robust servo system design with two degrees of freedom and its application to novel motion control of robust manipulators”, *IEEE trans. industrial electronics*, vol. 40, no. 5, pp. 473–485, 1993.

[S4] W. C. Yang and M. Tomizuka, “Disturbance rejection through an external model for non-minimum phase systems”, *ASME j. of dynamic systems, measurement and control*, vol. 116, no. 1, pp. 39–44, 1994.

[S5] K. K. K. Kim, E. Kharisov, and N. Hovakimyan, “Filter design for $\mathcal{L}_1$ adaptive output–feedback controller”, in: *American Control Conference*, Submitted, San Francisco, CA, 2011.

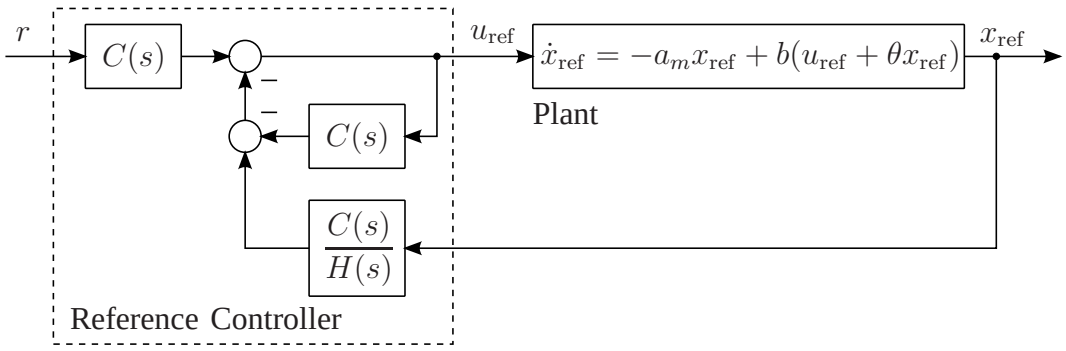

Figure S1: Reference controller of $\mathcal{L}_1$ architecture. The $\mathcal{L}_1$ reference system can be equivalently represented in this form. This representation is structurally similar to the DOB architecture, considered in [S2–S4]

Sidebar 4. Verifying the $\mathcal{L}_1$–Norm Bound

The stability of the $\mathcal{L}_1$ reference system is reduced to verification of the $\mathcal{L}_1$–norm condition in (21). For simplicity, let

$$C(s) = \frac{\omega_c}{s + \omega_c}\,,$$

where $\omega_c \in (0,\ \infty)$ is the filter bandwidth. From (20) it follows that

$$G(s) = (1 - C(s))H(s) = \frac{sH(s)}{s + \omega_c}\,.$$

Therefore

$$\|G(s)\theta\|_{\mathcal{L}_1} = \|(1 - C(s))H(s)\theta\|_{\mathcal{L}_1} \leq \left\|\frac{1}{s + \omega_c}\right\|_{\mathcal{L}_1} \|sH(s)\theta\|_{\mathcal{L}_1} = \frac{1}{\omega_c}\|sH(s)\theta\|_{\mathcal{L}_1}\,.$$

From the fact that $H(s)$ is strictly proper and stable it follows that $sH(s)$ is proper and stable, and therefore $\|sH(s)\theta\|_{\mathcal{L}_1}$ exists and is bounded. Therefore

$$\lim_{\omega_c \to \infty} \|G(s)\theta\|_{\mathcal{L}_1} \leq \lim_{\omega_c \to \infty} \frac{1}{\omega_c}\|sH(s)\theta\|_{\mathcal{L}_1} = 0\,,$$

and hence the $\mathcal{L}_1$–norm condition can be satisfied for arbitrary system in (1) by choosing the filter $C(s)$ with sufficiently large bandwidth.

Sidebar 5. Projection Operator

Projection–based adaptation laws are introduced in [S6]. The projection operator ensures boundedness of the parametric estimates by definition. Definition of the projection operator proceeds by considering a compact convex set with its smooth boundary given by

$$\Omega_c \triangleq \{\theta \in \mathbb{R}^n \mid f(\theta) \leq c\}\,, \quad 0 \leq c \leq 1\,,$$

where $f : \mathbb{R}^n \to \mathbb{R}$ is th smooth convex function

$$f(\theta) \triangleq \frac{(\epsilon_\theta + 1)\theta^\top \theta - \theta_{\max}^2}{\epsilon_\theta \theta_{\max}^2}\,,$$

with $\theta_{\max}$ being the norm bound imposed on the vector θ, and $\epsilon_\theta > 0$ is the projection tolerance bound of the choice. The projection operator is defined as

$$\mathrm{Proj}(\theta, y) \triangleq \begin{cases} y & \text{if } f(\theta) < 0\,, \\ y & \text{if } f(\theta) \geq 0 \text{ and } \nabla f^\top y \leq 0\,, \\ y - \frac{\nabla f}{\|\nabla f\|} \left\langle \frac{\nabla f}{\|\nabla\| f}, \ y \right\rangle f(\theta) & \text{if } f(\theta) \geq 0 \text{ and } \nabla f^\top y > 0\,. \end{cases}$$

The illustration of projection operator is shown in Figure S2. Notice that the projection operator $\mathrm{Proj}(\theta, y)$ does not alter y, if θ belongs to the set $\Omega_0 \triangleq \{\theta \in \mathbb{R}^n \mid f(\theta) \leq 0\}$. In the set $\{\theta \in \mathbb{R}^n \mid 0 \leq f(\theta) \leq 1\}$, if $\nabla f^\top y > 0$, the $\mathrm{Proj}(\theta, y)$ operator subtracts a vector normal to the boundary $\bar{\Omega}_{f(\theta)} = \{\bar{\theta} \in \mathbb{R}^n \mid f(\bar{\theta}) = f(\theta)\}$, so that we obtain a smooth transformation from the original vector field y to an inward or tangent vector field for Ω_1. As a result of this

transformation, the projection operator verifies the property

$$(\theta - \theta^*)^\top \big(\mathrm{Proj}(\theta, y) - y\big) \leq 0\,, \tag{S3}$$

for given vectors $y \in \mathbb{R}^n$, $\theta^* \in \Omega_0 \subset \Omega_1 \subset \mathbb{R}^n$ and $\theta \in \Omega_1$ [S6]. The proofs on ultimate boundedness of the adaptive errors strongly rely on this property of the projection operator.

References

[S6] J.-B. Pomet and L. Praly, “Adaptive nonlinear regulation: estimation from the Lyapunov equation”, *IEEE Transactions on Automatic Control*, vol. 37, no. 6, pp. 729–740, 1992.

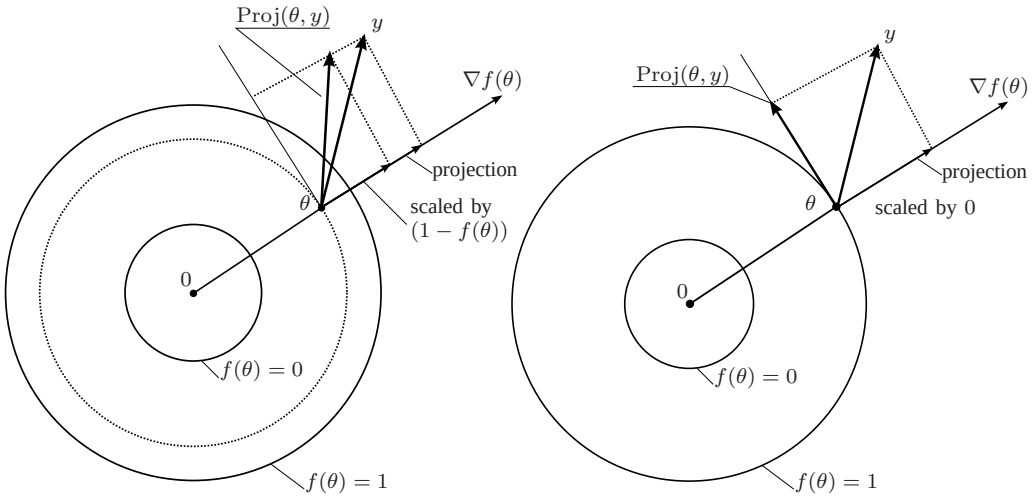

Figure S2: Illustration of the projection operator. Inside the set bounded by $f(\theta) = 0$ the projection operator does not modify the vector. In the set between $f(\theta) = 0$ and $f(\theta) = 1$ the projection operator scales down the normal component of the vector as it is shown in the left plot. On the boundary $f(\theta) = 1$ the normal component of the vector is completely canceled. The scaling factor changes continuously for all values of θ

Sidebar 6. Available Bandwidth of Control Systems

In classical control the *bandwidth* of system is defined as the frequency range $[0,\ \omega_b]$, where ω_b is the frequency at which the magnitude of the frequency response is 3 dB less than the value of the magnitude at zero frequency. The frequency ω_b is also called *cutoff frequency*. The bandwidth indicates the frequency range where the system is able to track input sinusoids, while it attenuates all signals with frequencies outside of its bandwidth. One of the key characteristics of the control systems is the *available bandwidth*, which is defined as the frequency range over which the unstructured multiplicative perturbations are less than unity. Note that the available bandwidth is not a function of the compensator or of the control design process. Rather, it is an a priori constraint imposed by the physical hardware we use in the control loop. Most importantly, the available bandwidth is finite [S7].

References

[S7] G. Stein, “Respect the unstable”, *IEEE Control Systems Magazine*, pp. 12–25, 2003.

Sidebar 7. Reference Controller for Multidimensional Systems

We note that the ideas discussed in "Bridging Adaptive and Robust Control" for the scalar case can be extended to the multidimensional case. To this end, we consider the reference system in (74) for zero initial conditions. In frequency domain it can be written as

$$x_{\mathrm{ref}}(s) = H(s)(\omega u_{\mathrm{ref}}(s) + \eta_{\mathrm{ref}}(s))\,. \tag{S4}$$

We choose a constant vector $c_0^\top$ satisfying the conditions of Lemma 2, which ensures that the transfer function $c_0^\top H(s)$ is minimum–phase and relative degree one. Therefore the transfer function $kD(s)c_0^\top/(c_0^\top H(s))$ is proper. Hence, multiplying (S4) by this transfer function, we obtain

$$\frac{kD(s)c_0^\top}{c_0^\top H(s)} x_{\mathrm{ref}}(s) = kD(s)(\omega u_{\mathrm{ref}}(s) + \eta_{\mathrm{ref}}(s))\,.$$

Substituting this expression into the equation for the reference control signal in (72) and isolating $u(s)$, we obtain the representation for the reference controller

$$u_{\mathrm{ref}}(s) = kD(s)k_g r(s) - \frac{kD(s)c_0^\top}{c_0^\top H(s)} x_{\mathrm{ref}}(s)\,,$$

which further can be rewritten as

$$u_{\mathrm{ref}}(s) = \frac{kD(s)}{c_0^\top H(s)} \left(c_0^\top H(s) k_g r(s) - c_0^\top x_{\mathrm{ref}}(s)\right)\,. \tag{S5}$$

This control law produces the same control signal as (72), however as compared to (72), it does not depend on the unknown system parameters and the disturbance.

Sidebar 8. Special Form of State–to–Input Stability

Consider the system dynamics

$$\dot{x}(t) = A_m x(t) + bu(t)\,, \quad x(0) = 0\,, \tag{S6}$$

where $x(t) \in \mathbb{R}^n$ is the system state vector, $u(t) \in \mathbb{R}$ is the control input (bounded and piecewise–continuous), $A_m \in \mathbb{R}^{n\times n}$, and $b \in \mathbb{R}^n$. Let $H(s) \triangleq (s\mathbb{I} - A_m)^{-1}b$, so that

$$x(s) = H(s)u(s)\,.$$

The norm of the system state can be upper bounded as

$$\|x_\tau\|_{\mathcal{L}_\infty} \leq \|H(s)\|_{\mathcal{L}_1}\|u_\tau\|_{\mathcal{L}_\infty}\,, \quad \text{for all} \;\; \tau \geq 0\,.$$

It follows that for a stable proper linear system it is possible to upperbound the norm of the output by a function of the norm of the input. The opposite question can also be asked; namely, whether it is possible to find an upper bound on the system input in terms of its output, without invoking the derivatives of the output. While for the system in (S6) the answer to this question is negative [S8], we show that a similar upper bound can be derived for the lowpass filtered input signal. For that purpose let

$$H(s) = \frac{N(s)}{D(s)}\,, \tag{S7}$$

where $D(s) = \det(s\mathbb{I} - A)$, and $N(s)$ is a $n \times 1$ vector with its i^{th} element being a polynomial function

$$N_i(s) = \sum_{j=1}^{n} N_{ij}s^{j-1}\,. \tag{S8}$$

Lemma 2 *If the pair* $(A_m,\ b)$ *in* (S6) *is controllable, then there exists* $c_o \in \mathbb{R}^n$ *such that* $c_o^\top N(s)/D(s)$ *has relative degree one, that is,* $\deg(D(s)) - \deg(c_o^\top N(s)) = 1$*, and* $N(s)$ *has all its zeros in the left half plane.*

Proof. It follows from (S7) that for arbitrary vector $c_o \in \mathbb{R}^n$

$$c_o^\top H(s) = \frac{c_o^\top N[s^{n-1}\ \cdots\ 1]^\top}{D(s)}\,,$$

where $N \in \mathbb{R}^{n\times n}$ is the matrix with its i^{th} row j^{th} column entry N_{ij} introduced in (S8).

Controllability of (A_m, b) implies that N is a full rank. Indeed, if the system is controllable, then for a given initial condition $x(0) = 0$ and arbitrary t_1 and x_{t_1}, there exists $u(\tau)$, $\tau \in [0,\ t_1]$ such that $x(t_1) = x_{t_1}$. If N is not full rank, then there exists a $\mu \in \mathbb{R}^n$, $\mu \neq 0$ such that $\mu^\top N(s) = 0$. Thus, for $x(0) = 0$ we have

$$\mu^\top x(s) = \mu^\top \frac{N(s)}{D(s)} u(s) = 0\,, \quad \text{for all}\ \ u(s)\,,$$

which implies that, in particular, $x(t) \neq \mu$ for all t. This conclusion contradicts the fact that $x(t_1) = x_{t_1}$ can be arbitrary point in $\mathbb{R}^n$. Thus, N must be full rank.

Consider an arbitrary vector $\bar{c} \in \mathbb{R}^n$ such that $\bar{c}^\top[s^{n-1}\ \cdots\ 1]^\top$ is a stable $n-1$ order polynomial, and let $c_o = (N^{-1})^\top \bar{c}$. Then

$$c_o^\top (s\mathbb{I} - A)^{-1} b = \frac{\bar{c}^\top[s^{n-1}\ \cdots\ 1]^\top}{D(s)}$$

has relative degree one with all its zeros in the left half plane. □

Next, consider an arbitrary strictly proper stable transfer function $C(s)$. From Lemma 2,

it follows that there exists $c_o \in \mathbb{R}^n$ such that $c_o^\top H(s)$ has relative degree one, and $c_o^\top H(s)$ has all its zeros in the left half plane. Hence, we can write

$$C(s)u(s) = \frac{C(s)}{c_o^\top H(s)} c_o^\top H(s)u(s) = H_1(s)x(s)\,,$$

where

$$H_1(s) \triangleq \frac{C(s)}{c_o^\top H(s)} c_o^\top$$

is proper and stable. Next, letting $\nu(s) \triangleq C(s)u(s)$, we have the upper bound

$$\|\nu_\tau\|_{\mathcal{L}_\infty} \leq \|H_1(s)\|_{\mathcal{L}_1} \|x_\tau\|_{\mathcal{L}_\infty}\,.$$

Thus we see that the filtered input signal $\nu(t)$ can be bounded in terms of the $\mathcal{L}_\infty$–norm of the system output.

References

[S8] D. Liberzon, A. S. Morse, and E. D. Sontag, “Output-input stability and minimum-phase nonlinear systems”, *IEEE Transactions on Automatic Control*, vol. 47, no. 3, pp. 422–436, 2002.

Sidebar 9. Performance Bounds and Time-Delay Margin in the Presence of Nonzero Trajectory Initialization Errors

In the design of state feedback $\mathcal{L}_1$ controllers, the state predictor is initialized identical to the plant. Next, we analyze the degradation of the performance bounds due to nonzero initialization errors.

For simplicity consider the system in (43)–(44) with constant uncertain parameters $\theta(t) = \theta = const$, while retaining the time–varying disturbance $\sigma(t)$. We consider the state predictor in (58)–(59) with the initial conditions different from the initial conditions of the plant $\hat{x}(0) = \hat{x}_0 \neq x_0$. This control system results in the prediction dynamics given in (60), but with nonzero initial condition, given by $\tilde{x}(0) = \hat{x}_0 - x_0$. Next, we consider the same adaptation laws as in (62)–(64) and the $\mathcal{L}_1$ control law given by (70). To derive the performance bounds for the closed–loop adaptive system with the $\mathcal{L}_1$ adaptive controller, we start with the following notation. For an m–input n–output stable proper transfer function $F(s)$ with impulse response matrix $f(t)$, let

$$\Psi_F(t) \triangleq \max_{i=1,\ldots,n} \sqrt{\sum_{j=1}^{m} f_{ij}^2(t)}\,,$$

where $f_{ij}(t)$ is the ij^{th} element of the impulse response matrix $f(t)$. Then for the prediction error dynamics in (60) with nonzero initial conditions $\tilde{x}(0) \neq 0$, the upper bound in (67) becomes

$$\|\tilde{x}(t)\| \leq \rho(t)\,, \quad \text{for all} \quad t \geq 0\,, \tag{S9}$$

where

$$\rho(t) \triangleq \sqrt{\frac{\left(V(0) - \frac{\theta_n}{\Gamma}\right) \mathrm{e}^{-\alpha t}}{\lambda_{\min}(P)} + \frac{\theta_n}{\lambda_{\min}(P)\Gamma}}\,, \quad \alpha \triangleq \frac{\lambda_{\min}(Q)}{\lambda_{\max}(P)}\,,$$
$$\theta_n \triangleq 4\theta_{\max}^2 + 4\sigma_b^2 + (\omega_{\max} - \omega_{\min})^2 + \frac{4\sigma_b d_\sigma}{\alpha}\,,$$

with $V(t)$ being the Lyapunov function in (65) [S1, Lemma 2.2.5]. Notice that this bound contains an exponentially decaying term and a constant component. In the limiting case, when the exponential term diminishes, this upper bound reduces to the one in (67), that is,

$$\lim_{t\to\infty} \rho(t) = \frac{\gamma_0}{\sqrt{\Gamma}}\,.$$

Using the bound on the prediction error in (S9), we obtain the performance bounds in the presence of nonzero initialization error, which hold for all $t \geq 0$ [S1, Theorem 2.2.3]

$$\|x_{\mathrm{ref}}(t) - x(t)\|_\infty \leq \gamma_3(t)\,,$$
$$\|u_{\mathrm{ref}}(t) - u(t)\|_\infty \leq \frac{1}{\omega}\Psi_{H_1}(t) * (\rho(t) + \|\tilde{x}_{\mathrm{in}}(t)\|) + \Psi_{H_3}(t) * \gamma_3(t)\,,$$

where

$$\gamma_3(t) \triangleq \Psi_{H_2}(t) * (\rho(t) + \|\tilde{x}_{\mathrm{in}}(t)\|)\,,$$
$$H_1(s) = \frac{C(s)c_0^\top}{c_0^\top H(s)}\,, \quad H_2(s) = (\mathbb{I} - G(s)\theta^\top)^{-1}C(s)\,, \quad H_3(s) = -\frac{C(s)\theta^\top}{\omega}\,,$$

and $\tilde{x}_{\mathrm{in}}(t)$ is the inverse Laplace transform of $\tilde{x}_{\mathrm{in}}(s) \triangleq (s\mathbb{I} - A_m)^{-1}(\hat{x}_0 - x_0)$.

The conclusion is that for open–loop LTI systems arbitrary nonzero trajectory initialization errors lead to exponentially decaying transient errors in the input and output signals of the

system.

The next theorem quantifies the time–delay margin at the system input.

Theorem 1 *Consider the system in* (43)–(44) *with constant uncertain parameters* $\theta(t) = \theta = const$*, subject to the bounds in* (45)–(46) *on the system uncertainties. Further, consider the state predictor in* (58)–(59) *with the initial conditions different from the initial conditions of the plant, that is,* $\hat{x}(0) = \hat{x}_0 \neq x_0$*, and the adaptation laws in* (62)–(64)*. Let the adaptive controller be defined according to* (70) *with* $D(s) = 1/s$*. If the* $\mathcal{L}_1$ *norm condition in* (76) *holds, and the projection bound* σ_b *and the adaptation gain* Γ *are set sufficiently large, then the closed–loop system remains stable for arbitrary input time–delay*

$$\tau < \mathcal{T}\,,$$

where $\mathcal{T}$ *is the time–delay margin of the linear time invariant system*

$$L_o(s) = \frac{C(s)}{1 - C(s)}(1 + \theta^\top \bar{H}(s))\,,$$

and

$$\bar{H}(s) \triangleq (s\mathbb{I} - A_m - b\theta^\top)^{-1} b\,.$$

This result is semiglobal in a sense that larger x_0 requires larger Δ for the projection bounds to ensure the same time–delay margin.

References

[S1] N. Hovakimyan and C. Cao, $\mathcal{L}_1$ *Adaptive Control Theory*, Philadelphia, PA: Society for Industrial and Applied Mathematics, 2010.

Sidebar 10. $\mathcal{L}_1$ Adaptive Controller for Systems with Unmodeled Actuator Dynamics

Consider the class of systems with multiplicative unmodeled dynamics located at the system input, [S9]

$$\dot{x}(t) = A_m x(t) + b\big(\mu(t) + \theta^\top(t)x(t) + \sigma_0(t)\big)\,, \quad x(0) = x_0\,, \tag{S10}$$
$$y(t) = c^\top x(t)\,,$$

where $x(t) \in \mathbb{R}^n$ is the system state vector (measured); $y(t) \in \mathbb{R}$ is the system regulated output; $A_m \in \mathbb{R}^{n\times n}$ is a known Hurwitz matrix specifying the desired closed–loop dynamics; $b,\ c \in \mathbb{R}^n$ are known constant vectors; $\theta(t) \in \mathbb{R}^n$ is a vector of time–varying unknown parameters; $\sigma_0(t) \in \mathbb{R}$ is a time–varying disturbance; and $\mu(t) \in \mathbb{R}$ is the output of the system

$$\mu(s) = F(s)u(s)\,,$$

where $u(t) \in \mathbb{R}$ is the control input, and $F(s)$ is an unknown stable transfer function with known sign of its DC gain.

Let $\theta(t)$ and $\sigma_0(t)$ satisfy

$$\theta(t) \in \Theta\,, \quad \sigma_0(t) \in \Delta = [-\sigma_b,\ \sigma_b]\,, \quad \text{for all} \ \ t \geq 0\,,$$
$$\|\dot{\theta}(t)\| \leq d_\theta < \infty\,, \quad |\dot{\sigma}_0(t)| \leq d_\sigma < \infty\,, \quad \text{for all} \ \ t \geq 0\,,$$

where Θ is a known convex compact set, and $\sigma_b,\ d_\theta,\ d_\sigma \in (0,\ \infty)$ are known conservative bounds. Also assume that there exists $L_F > 0$ verifying $\|F(s)\|_{\mathcal{L}_1} \leq L_F$, and known constants

$\omega_l,\ \omega_u \in \mathbb{R}$ satisfying

$$0 < \omega_l \leq F(0) \leq \omega_u \,,$$

where, without loss of generality, we assume $F(0) > 0$. Finally, for design purposes, we assume that we know a set $\mathbb{F}_\Delta$ of all admissible actuator dynamics.

The design of the $\mathcal{L}_1$ adaptive controller proceeds by considering a positive feedback gain $k > 0$ and a strictly proper stable transfer function $D(s)$, which imply that

$$C(s) \triangleq \frac{kF(s)D(s)}{1 + kF(s)D(s)} \tag{S11}$$

is strictly proper stable transfer function with dc gain $C(0) = 1$ for all $F(s) \in \mathbb{F}_\Delta$.

Next we present the elements for the $\mathcal{L}_1$ adaptive control architecture for the class of systems with unmodeled dynamics at the system input. The state predictor is given by

$$\dot{\hat{x}}(t) = A_m\hat{x}(t) + b\left(\hat{\omega}(t)u(t) + \hat{\theta}^\top(t)x(t) + \hat{\sigma}(t)\right) \,, \quad \hat{x}(0) = x_0 \,, \tag{S12}$$

$$\hat{y}(t) = c^\top\hat{x}(t) \,,$$

where $\hat{x}(t) \in \mathbb{R}^n$ is the predictor state, while $\hat{\omega}(t), \hat{\sigma}(t) \in \mathbb{R}$ and $\hat{\theta}(t) \in \mathbb{R}^n$ are the adaptive estimates driven by the adaptation laws, given by

$$\dot{\hat{\omega}}(t) = \Gamma\mathrm{Proj}\left(\hat{\omega}(t), -\tilde{x}^\top(t)Pbu(t)\right) \,, \quad \hat{\omega}(0) = \hat{\omega}_0 \,, \tag{S13}$$

$$\dot{\hat{\theta}}(t) = \Gamma\mathrm{Proj}\left(\hat{\theta}(t), -\tilde{x}^\top(t)Pbx(t)\right) \,, \quad \hat{\theta}(0) = \hat{\theta}_0 \,, \tag{S14}$$

$$\dot{\hat{\sigma}}(t) = \Gamma\mathrm{Proj}\left(\hat{\sigma}(t), -\tilde{x}^\top(t)Pb\right) \,, \quad \hat{\sigma}(0) = \hat{\sigma}_0 \,, \tag{S15}$$

where $\tilde{x}(t) \triangleq \hat{x}(t) - x(t)$, $\Gamma \in (0,\ \infty)$ is the adaptation gain, and the symmetric positive

definite matrix $P = P^\top > 0$ solves the Lyapunov equation $A_m^\top P + P A_m = -Q$ for arbitrary $Q = Q^\top > 0$. The adaptive control law is given by

$$u(s) = -kD(s)(\hat{\eta}(s) - k_g r(s))\,, \tag{S16}$$

where $k_g \triangleq -\frac{1}{c^\top A_m^{-1} b}$; $r(s)$ and $\hat{\eta}(s)$ are the Laplace transforms of $r(t)$ and

$$\hat{\eta}(t) \triangleq \hat{\omega}(t)u(t) + \hat{\theta}^\top(t)x(t) + \hat{\sigma}(t)\,.$$

The $\mathcal{L}_1$ reference system for this architecture is given by

$$\dot{x}_{\rm ref}(t) = A_m x_{\rm ref}(t) + b\big(\mu_{\rm ref}(t) + \theta^\top(t)x_{\rm ref}(t) + \sigma_0(t)\big)\,, \quad x_{\rm ref}(0) = x_0\,, \tag{S17}$$

$$\mu_{\rm ref}(s) = F(s)u_{\rm ref}(s)\,, \tag{S18}$$

$$u_{\rm ref}(s) = C_u(s)(k_g r(s) - \eta_{\rm ref}(s))\,, \tag{S19}$$

$$y_{\rm ref}(t) = c^\top x_{\rm ref}(t)\,, \tag{S20}$$

where $x_{\rm ref}(t) \in \mathbb{R}^n$ is the reference system state vector, and $\eta_{\rm ref}(s)$ is the Laplace transform of $\eta_{\rm ref}(t) \triangleq \theta^\top(t)x_{\rm ref}(t) + \sigma_0(t)$. To see how the refere

The next theorem summarizes the main result for this adaptive architecture.

Theorem 2 *[S9, Theorem 1] If the choice of k and $D(s)$ ensures that the $\mathcal{L}_1$–norm condition holds*

$$\|G(s)\|_{\mathcal{L}_1} L < 1\,, \tag{S21}$$

where

$$G(s) \triangleq (1 - C(s))H(s)\,, \quad H(s) \triangleq (s\mathbb{I} - A_m)^{-1}b\,, \quad L \triangleq \max_{\theta\in\Theta} \|\theta\|_1\,,$$

then we have

$$\|\tilde{x}\|_{\mathcal{L}_\infty} \leq \gamma_0\,,$$

$$\|x_{\rm ref} - x\|_{\mathcal{L}_\infty} \leq \gamma_1\,, \quad \|u_{\rm ref} - u\|_{\mathcal{L}_\infty} \leq \gamma_2\,,$$

where

$$\gamma_0 \triangleq \sqrt{\frac{\theta_m}{\lambda_{\min}(P)\Gamma}}\,,$$

$$\gamma_1 \triangleq \frac{\|C(s)\|_{\mathcal{L}_1}}{1 - \|G(s)\|_{\mathcal{L}_1}L}\gamma_0 + \beta\,, \quad \gamma_2 \triangleq \left\|\frac{C(s)}{F(s)}\right\| L\gamma_1 + \left\|\frac{C(s)c_0^\top}{c_0^\top H(s)}\right\|_{\mathcal{L}_1} \gamma_0\,,$$

and $\theta_m \in (0,\ \infty)$ *is a computable constant depending on the system uncertainties bounds,* $\beta \in (0,\ \infty)$ *is an arbitrary constant,* $c_0 \in \mathbb{R}^n$ *is a vector, which makes* $c_0^\top H(s)$ *minimum–phase and relative degree one.*

References

[S9] C. Cao and N. Hovakimyan, "$\mathcal{L}_1$ adaptive controller for systems in the presence of unmodelled actuator dynamics", in: *IEEE Conference on Decision and Control*, New Orleans, LA, 2007, pp. 891–896.

Sidebar 11. $\mathcal{L}_1$ Adaptive Output–Feedback Controller with Piecewise Constant Adaptation Laws

Consider the single–input single–output (SISO) system

$$y(s) = A(s)(u(s) + d(s))\,, \tag{S22}$$

where $u(t) \in \mathbb{R}$ is the control input; $y(t) \in \mathbb{R}$ is the system output; $A(s)$ is a strictly proper unknown transfer function of unknown relative degree n_r, for which only a known lower bound $1 < d_r \leq n_r$ is available; $d(s)$ is the Laplace transform of the time–varying uncertainties and disturbances $d(t) = f(t, y(t))$. We assume that there exist constants $L > 0$ and $L_0 > 0$ such that, for all time $t \geq 0$

$$|f(t, y_1) - f(t, y_2)| \leq L|y_1 - y_2|\,, \quad |f(t, y)| \leq L|y| + L_0\,. \tag{S23}$$

Let the desired performance specifications be given by a stable minimum–phase transfer function $M(s)$ of relative degree d_r, which does not need to be strictly positive real (SPR). Then the system equation (S22) in terms of the ideal model can be rewritten as

$$y(s) = M(s)(u(s) + \sigma(s))\,, \tag{S24}$$

$$\sigma(s) = \frac{(A(s) - M(s))u(s) + A(s)d(s)}{M(s)}\,. \tag{S25}$$

Let $(A_m,\ b,\ c^\top)$ be a minimal realization of $M(s)$, and A_m be Hurwitz. Then the system in (S24)

can be rewritten as

$$\dot{x}(t) = A_m x(t) + b(u(t) + \sigma(t))\,, \quad x(0) = 0\,, \tag{S26}$$
$$y(t) = c^\top x(t)\,.$$

The elements of $\mathcal{L}_1$ adaptive output–feedback controller are introduced next. The state predictor is given by

$$\dot{\hat{x}}(t) = A_m \hat{x}(t) + bu(t) + \hat{\sigma}(t)\,, \quad \hat{x}(0) = 0\,, \tag{S27}$$
$$\hat{y}(t) = c^\top \hat{x}(t)\,,$$

where $\hat{\sigma}(t) \in \mathbb{R}^n$ is the vector of adaptive parameters. Notice that while $\sigma(t) \in \mathbb{R}$ in (S26) is matched, the uncertainty estimation $\hat{\sigma}(t)$ in (S27) is unmatched.

The adaptation laws for this $\mathcal{L}_1$ architecture are sampled in time. The sampling period T_s is the fixed time–step during which the adaptive parameters in $\hat{\sigma}(t)$ take constant values during $[iT_s,\ (i+1)T_s)$ for every $i = 0, 1, \ldots$. Letting $\tilde{y}(t) \triangleq \hat{y}(t) - y(t)$ be the prediction error, and $\tilde{y}(iT_s)$, $i = 1,\ 2,\ \ldots$ be the sampled values of the prediction error, the update law for $\hat{\sigma}(t)$ is given by

$$\hat{\sigma}(t) = -\Phi^{-1}(T_s)\mu(T_s)\tilde{y}(iT_s)\,, \quad t \in [iT_s,\ (i+1)T_s)\,, \tag{S28}$$

where $\Phi^{-1}(T_s)\mu(T_s)$ represents the update law gain, with

$$\Phi(T_s) \triangleq \int_0^{T_s} \mathrm{e}^{\Lambda A_m \Lambda^{-1}(T_s - \tau)} \Lambda d\tau\,,$$
$$\mu(T_s) \triangleq \mathrm{e}^{\Lambda A_m \Lambda^{-1} T_s} \mathbf{1}_1\,.$$

Here $\mathbf{1}_1 \triangleq [1,\ 0,\ \ldots,\ 0]^\top \in \mathbb{R}^n$, and

$$\Lambda \triangleq \begin{bmatrix} c^\top \\ D\sqrt{P} \end{bmatrix},$$

where $P = P^\top > 0$ satisfies the algebraic Lyapunov equation

$$A_m^\top P + P A_m = -Q\,, \quad \text{for arbitrary} \quad Q = Q^\top > 0\,,$$

and D is a $(n-1) \times n$ matrix that contains the null–space of $c^\top(\sqrt{P})^{-1}$, that is,

$$D(c^\top(\sqrt{P})^{-1})^\top = 0\,.$$

Notice that reduction of T_s increases the values of the adaptation gains in $\Phi^{-1}(T_s)$, which imposes hardware requirements.

The control law is given by

$$u(s) = C(s)r(s) - \frac{C(s)}{c^\top(s\mathbb{I} - A_m)^{-1}b} c^\top(s\mathbb{I} - A_m)^{-1}\hat{\sigma}(s)\,, \tag{S29}$$

where $r(s)$ is the Laplace transform of a bounded reference signal, $C(s)$ is a strictly proper system of relative degree d_r, with $C(0) = 1$.

Similar to the state feedback case we consider the the ideal control signal

$$u_{\text{id}}(t) = r(t) - \sigma(t)\,,$$

which is the signal that leads to desired system response

$$y_{\rm id}(s) = M(s)r(s)$$

by canceling the uncertainties exactly. Next we define a filtered version of the ideal control law. This control law cancels only the uncertainties within the bandwidth of the filter $C(s)$ compatible with the control channel specifications, and leads to the $\mathcal{L}_1$ reference system

$$y_{\rm ref}(s) = M(s)(u_{\rm ref}(s) + \sigma_{\rm ref}(s))\,, \tag{S30}$$

$$u_{\rm ref}(s) = C(s)(r(s) - \sigma_{\rm ref}(s))\,, \tag{S31}$$

where

$$\sigma_{\rm ref}(s) \triangleq \frac{(A(s) - M(s))u_{\rm ref}(s) + A(s)d_{\rm ref}(s)}{M(s)}\,,$$

and $d_{\rm ref}(t) \triangleq f(t, y_{\rm ref}(t))$.

Notice that using the ideas discussed in "Bridging Adaptive and Robust Control", we can furhter rewrite the equations for the $\mathcal{L}_1$ reference system in (S30)–(S31) to obtain the reference controller in the form

$$u_{\rm ref}(s) = \frac{C(s)M(s)}{1 - C(s)}(M(s)r(s) - y_{\rm ref}(s))\,.$$

This control law is similar to the one in (S2), and its structure allows for the use of design methods from robust control toward the design of the filter for verification of the $\mathcal{L}_1$–norm stability condition in (S32) [S5].

The next theorem summarizes the main result for this adaptive architecture.

Theorem 3 *[S10, Theorem 1] If the choice of the lowpass filter $C(s)$ for the given $M(s)$ ensures stability of*

$$H(s) \triangleq \frac{A(s)M(s)}{C(s)A(s) + (1 - C(s))M(s)}\,,$$

and satisfies the $\mathcal{L}_1$–norm condition

$$\|G(s)\|_{\mathcal{L}_1} L < 1\,, \tag{S32}$$

where $G(s) \triangleq H(s)(1 - C(s))$, and L is defined in (S23)*, then the reference system in* (S30)–(S31) *is stable. Further if we choose sufficiently small T_s to ensure*

$$\gamma_0(T_s) < \bar{\gamma}_0\,,$$

where $\gamma_0(T_s)$ is a computable class $\mathcal{K}$ function of T_s, and $\bar{\gamma}_0$ is an arbitrary positive constant, then

$$\|\tilde{y}\|_{\mathcal{L}_\infty} < \bar{\gamma}_0\,, \tag{S33}$$

$$\|y_{\rm ref} - y\|_{\mathcal{L}_\infty} \leq \gamma_1(T_s)\,, \quad \|u_{\rm ref} - u\|_{\mathcal{L}_\infty} \leq \gamma_2(T_s)\,, \tag{S34}$$

where $\gamma_1(T_s)$, and $\gamma_2(T_s)$ are computable class $\mathcal{K}$ functions of T_s.

Thus, the tracking error between $y(t)$ and $y_{\rm ref}(t)$, as well between $u(t)$ and $u_{\rm ref}(t)$, is uniformly bounded by a constant proportional to T_s. This fact implies that during the transient phase, it is possible to achieve arbitrary improvement of tracking performance by uniformly reducing T_s. These results are consistent with the results in section "Adaptive Control in the Presence of Unknown Input Gain", where improvement of the transient performance is achieved

by increasing the adaptation rate in the projection–based integral adaptive laws.

References

[S5] K. K. K. Kim, E. Kharisov, and N. Hovakimyan, "Filter design for $\mathcal{L}_1$ adaptive output–feedback controller", in: *American Control Conference*, Submitted, San Francisco, CA, 2011.

[S10] C. Cao and N. Hovakimyan, "$\mathcal{L}_1$ adaptive output-feedback controller for non-stricly-positive-real reference systems: missile longitudinal autopilot design", *AIAA Journal of Guidance, Control, and Dynamics*, vol. 32, no. 3, pp. 717–726, 2009.

Sidebar 12. NASA's Airborne Subscale Transport Aircraft Research

Loss of control (LOC) is one of the leading contributors to the fatal accident rate of large commercial transport airplanes. These types of accidents are of great concern because they are usually catastrophic, involving loss of aircraft and lives. LOC accidents are complex in that they typically have many causal factors and precursors, and they are difficult to analyze because they often involve excursions beyond the normal flight envelope. For example, LOC accidents are known to exhibit post–stall angles of attack or steep pitch and bank attitudes, which can make recovery to normal flight difficult.

Flight validation of control technologies aimed at the loss–of–control problem is recognized as a significant challenge due to the difficulties and risks associated with full–scale testing of transport airplanes in abnormal flight regimes. The Airborne Subscale Transport for Aircraft Research (AirSTAR) is a state–of–the–art facility specifically, designed for the purpose of investigating and validating high–payoff technologies aimed at the LOC problem using subscale flight vehicles for effective validation without excessive risk [S11, S12]. The AirSTAR infrastructure is designed to support the aeronautics research under adverse conditions. These conditions include upsets, such as unusual attitudes and post–stall flight, control surface faults, damage, such as missing wing segments, and sensor failures. Some of the key research areas are adaptive flight controls technologies, system identification, flight dynamics modeling, data mining, and fault detection methods. AirSTAR vehicles are designed for testing in regimes beyond the normal flight envelope or with degraded control characteristics, such as hardware failures or system faults.

The AirSTAR infrastructure is comprised of a research flight vehicle shown in the

Figure S3, the mobile operation station (MOS), and the safety pilot. The MOS is comprised of a flight test control room and a research pilot station as well as systems and engineering stations. Takeoff and landing is accomplished by a safety pilot using direct visual contact and conventional radio control equipment. A research pilot executes flight test maneuvers from inside the MOS, using a synthetic vision display drawn from telemetry data and a local terrain database, while remaining within visual range of the safety pilot. Actuator commands from research pilot inputs and the ground–based flight control computer are transmitted to the aircraft by an L–band telemetry link. Computers in the MOS execute research flight control laws and interface with the research pilot station using direct connection. Sensor feedback from the aircraft to flight control system is done by S–band telemetry link. While the model is being controlled from the research pilot station, a reversionary flight control capability is provided by a safety pilot. If a problem were to arise, the safety pilot can override the research pilot control inputs and fly using a hobbyist radio–control interface. This design provides a flexible environment to conduct flight research and rapidly evaluate research flight control laws with minimal risk.

The primary test aircraft is a 5.5% dynamically scaled, which is similitude using equal Froude number and relative density between model–scale and full–scale Froude–scaled twin–turbine powered generic transport model (GTM). Dynamic scaling allows subscale flight test results to be applied to full–scale aircraft. This model with tail number T2 has a 6.5 ft wingspan, weighs 54 lbs at takeoff, and has a flight time of approximately 18 minutes. The aircraft is outfitted with full flight test instrumentation, including angle of attack and angle of sideslip vanes, static and dynamic pressure, control surface positions, rate gyros and accelerometers, a 6–DOF INS/GPS package, and engine instrumentation. Downlink data update rates vary from 5 Hz on the GPS data to 200 Hz on the analog sensors. Uplink commands are received at

200 Hz. Aircraft dynamic failures are emulated using software to schedule appropriate actuators to provide desired degradation. For example longitudinal stability degradation is achieved by commandeering 2 of the 4 elevator segments from the control law path and schedule these with angle of attack to adversely change pitching moment, thus reducing available pitch control authority by 50% and destabilizing the aircraft by some prescribed amount. Spoilers scheduled with roll rate are used to degrade lateral–directional stability.

The vehicles and operational concept used by AirSTAR present some unique challenges: First and foremost, dynamically scaling an aircraft results in increased model airspeed, angular rates, wind loading, and increased pilot workload relative to a model that is, only geometrically scaled. These factors make a dynamically scaled model more challenging to fly and less forgiving of mistakes. Second, under the current AirSTAR concept of operations, the aircraft must remain within visual range of the safety pilot, effectively limiting the test volume to an approximately $1/2$–mile radius circle around the safety pilot, extending to ≈ 2000 ft above the surface in altitude. Limited test volume combined with the high airspeeds of the test aircraft adds to the pilot's workload. Third, the primary purpose of AirSTAR is to perform flight research and flight validation of multiple research control laws in adverse flight conditions, which presents unique challenges to flight testing in an efficient and safe manner.

References

[S11] K. Cunningham, J. V. Foster, E. A. Morelli, and A. M. Murch, “Practical application of a subscale transport aircraft for flight research in control upset and failure conditions”, in: *AIAA Guidance, Navigation and Control Conference*, AIAA–2008–6200, Honolulu, HI, 2008.

[S12] A. M. Murch, “A flight control system architecture for the nasa airstar flight test infrastructure”, in: *AIAA Guidance, Navigation and Control Conference*, AIAA–2008–6990, Honolulu, HI, 2008.

Figure S3: AirSTAR flight test vehicle with tail number T2 performing takeoff (left) and landing (right). The test aircraft is a 5.5% dynamically scaled, twin–turbine powered generic transport model. The model has a 6.5 ft wingspan, weighs 54 lbs at takeoff, and has a flight time of approximately 18 minutes. The aircraft is outfitted with full flight test instrumentation, including angle of attack and angle of sideslip vanes, static and dynamic pressure, control surface positions, rate gyros and accelerometers, a 6–DOF INS/GPS package, and engine instrumentation. Downlink data update rates vary from 5 Hz on the GPS data to 200 Hz on the analog sensors. Uplink commands are received at 200 Hz.

Sidebar 13. $\mathcal{L}_1$ Adaptive Controller for Systems with Unmatched Uncertainties

Consider the class of systems with unmatched nonlinear uncertainties and with unmodeled dynamics, [S13]

$$\dot{x}(t) = A_m x(t) + B_m \omega u(t) + f(t, x(t), z(t)) \,, \quad x(0) = x_0 \,, \tag{S35}$$

$$y(t) = Cx(t) \,, \tag{S36}$$

where $x(t) \in \mathbb{R}^n$ is the system state vector (measured); $u(t) \in \mathbb{R}^m$ is the control signal; $y(t) \in \mathbb{R}^m$ is the regulated output; $A_m \in \mathbb{R}^{n\times n}$ is a known Hurwitz matrix that defines the desired dynamics for the closed–loop system; $B_m \in \mathbb{R}^{n\times m}$ and $C \in \mathbb{R}^{m\times n}$ are known full–rank constant matrices; $\omega \in \mathbb{R}^{m\times m}$ is the uncertain system input gain matrix; $f : \mathbb{R} \times \mathbb{R}^n \times \mathbb{R}^p \to \mathbb{R}^n$ is unknown nonlinear function. The initial condition x_0 is assumed to be inside a known set, that is, $\|x_0\|_\infty \leq \rho_0 < \infty$ for some $\rho_0 > 0$. The signal $z(t) \in \mathbb{R}^p$ is the output of the unmodeled dynamcs, given by

$$\dot{x}_z(t) = g\left(t, x_z(t), x(t)\right) \,, \quad x_z(0) = x_{z0} \,, \tag{S37}$$

$$z(t) = g_o\left(t, x_z(t)\right) \,, \tag{S38}$$

where $x_z(t) \in \mathbb{R}^l$ is the state vector of internal unmodeled dynamics; $g_o : \mathbb{R} \times \mathbb{R}^l \to \mathbb{R}^p$, and $g : \mathbb{R} \times \mathbb{R}^l \times \mathbb{R}^n \to \mathbb{R}^l$ are unknown nonlinear functions, satisfying the standard assumptions on existence and uniqueness of solutions.

We rewrite the system in (S35)–(S36) as

$$\dot{x}(t) = A_m x(t) + B_m \left(\omega u(t) + f_1(t, x(t), z(t))\right) + B_{um} f_2(t, x(t), z(t)), \quad x(0) = x_0\,, \tag{S39}$$

$$y(t) = Cx(t)\,, \tag{S40}$$

where $B_{um} \in \mathbb{R}^{n\times(n-m)}$ is a constant matrix such that $B_m^\top B_{um} = 0$ and also $\mathrm{rank}([B_m,\ B_{um}]) = n$, while $f_1 : \mathbb{R}\times\mathbb{R}^n\times\mathbb{R}^p \to \mathbb{R}^m$ and $f_2 : \mathbb{R}\times\mathbb{R}^n\times\mathbb{R}^p \to \mathbb{R}^{(n-m)}$ are unknown nonlinear functions that verify

$$\begin{bmatrix} f_1(t, x(t), z(t)) \\ f_2(t, x(t), z(t)) \end{bmatrix} = B^{-1} f(t, x(t), z(t))\,, \quad B \triangleq \begin{bmatrix} B_m, & B_{um} \end{bmatrix}. \tag{S41}$$

In this problem formulation, $f_1(\cdot)$ represents the *matched component* of the uncertainties, which is in the span of matrix B_m, whereas $f_2(\cdot)$ represents the *unmatched component*, which enters the system dynamics orthogonally to the matrix B_m.

Let $X \triangleq [x^\top,\ z^\top]^\top$, and with a slight abuse of language let $f_i(t, X) \triangleq f_i(t, x, z)$, $i = 1, 2$. Then let $\|f_i(t, 0)\|_{\mathcal{L}_\infty} \le B_{i0}$ for all $t \ge 0$, $i = 1, 2$, where $B_{i0} > 0$ are known upper bounds. Next, assume that for arbitrary $\delta > 0$, there exist positive K_{1_δ}, K_{2_δ} such that

$$\|f_i(t, X_1) - f_i(t, X_2)\|_\infty \le K_{i_\delta}\|X_1 - X_2\|_\infty\,, i = 1, 2\,,$$

for all $\|X_j\|_\infty \le \delta$, $j = 1, 2$, uniformly in t. Further let the x_z–dynamics be stable in the sense

$$\|z_t\|_{\mathcal{L}_\infty} \le L_z\|x_t\|_{\mathcal{L}_\infty} + B_z\,, \quad \text{for all} \ \ t \ge 0$$

for some L_z, $B_z > 0$. The system input gain matrix ω is assumed to be an unknown (non–

singular) strictly row–diagonally dominant matrix with $\mathrm{sgn}(\omega_{ii})$ known. Also, we assume that there exists a known compact convex set Ω such that $\omega \in \Omega \subset \mathbb{R}^{m\times m}$, and that a nominal system input gain $\omega_0 \in \Omega$ is known. Finally assume that the transmission zeros of the transfer matrix $H_m(s) = C(s\mathbb{I} - A_m)^{-1}B_m$ lie in the open left–half plane.

Before we present the adaptive architecture and give an $\mathcal{L}_1$–norm stability condition, define

$$
\begin{aligned}
H_{xm}(s) &\triangleq (s\mathbb{I}_n - A_m)^{-1} B_m \,, \\
H_{xum}(s) &\triangleq (s\mathbb{I}_n - A_m)^{-1} B_{um} \,, \\
H_m(s) &\triangleq C H_{xm}(s) = C\,(s\mathbb{I}_n - A_m)^{-1} B_m \,, \\
H_{um}(s) &\triangleq C H_{xum}(s) = C\,(s\mathbb{I}_n - A_m)^{-1} B_{um} \,,
\end{aligned}
$$

and also define $\rho_{\text{in}} \triangleq \|s(s\mathbb{I} - A_m)^{-1}\|_{\mathcal{L}_1}\rho_0$, where $\rho_0 = \max \|x_0\|_\infty$. Further, for every $\delta > 0$, let

$$
L_{i\delta} \triangleq \frac{\bar{\delta}(\delta)}{\delta} K_{i\bar{\delta}(\delta)} \,, \quad \bar{\delta}(\delta) \triangleq \max\{\delta + \bar{\gamma}_1,\ L_z(\delta + \bar{\gamma}_1) + B_z\} \,, \tag{S42}
$$

where $\bar{\gamma}_1$ is an arbitrary small positive constant. The design of the $\mathcal{L}_1$ adaptive controller involves a feedback gain matrix $K \in \mathbb{R}^{m\times m}$ and an $m \times m$ strictly proper transfer matrix $D(s)$, which lead, for all $\omega \in \Omega$, to a strictly proper stable

$$
C(s) \triangleq \omega K D(s)\,(\mathbb{I}_m + \omega K D(s))^{-1} \tag{S43}
$$

with DC gain $C(0) = \mathbb{I}_m$. The choice of K and $D(s)$ also needs to ensure also that $C(s)H_m^{-1}(s)$ is a proper stable transfer matrix and for a given ρ_0, there exists $\rho_r > \rho_{\text{in}}$ such that the $\mathcal{L}_1$–norm

condition holds

$$\|G_m(s)\|_{\mathcal{L}_1} + \|G_{um}(s)\|_{\mathcal{L}_1}\ell_0 < \frac{\rho_r - \|H_{xm}(s)C(s)K_g(s)\|_{\mathcal{L}_1}\|r\|_{\mathcal{L}_\infty} - \rho_{\text{in}}}{L_{1\rho_r}\rho_r + B_0}\,, \tag{S44}$$

where

$$G_m(s) \triangleq H_{xm}(s)\left(\mathbb{I}_m - C(s)\right)\,,$$

$$G_{um}(s) \triangleq \left(\mathbb{I}_n - H_{xm}(s)C(s)H_m^{-1}(s)C\right)H_{xum}(s)\,,$$

while

$$\ell_0 \triangleq \frac{L_{2\rho_r}}{L_{1\rho_r}}\,, \quad B_0 \triangleq \max\left\{B_{10},\ \frac{B_{20}}{\ell_0}\right\}\,,$$

and $K_g(s)$ is the stable feedforward prefilter.

The elements of the $\mathcal{L}_1$ adaptive control architecture are introduced next. The state–predictor is given by

$$\dot{\hat{x}}(t) = A_m\hat{x}(t) + B_m\left(\omega_0 u(t) + \hat{\sigma}_1(t)\right) + B_{um}\hat{\sigma}_2(t)\,, \quad \hat{x}(0) = x_0\,, \tag{S45}$$

$$\hat{y}(t) = C\hat{x}(t)\,, \tag{S46}$$

where $\hat{\sigma}_1(t) \in \mathbb{R}^m$ and $\hat{\sigma}_2(t) \in \mathbb{R}^{n-m}$ are the adaptive estimates of the matched and unmatched uncertainties driven by the adaptation laws

$$\begin{bmatrix} \hat{\sigma}_1(t) \\ \hat{\sigma}_2(t) \end{bmatrix} = -\begin{bmatrix} \mathbb{I}_m & 0 \\ 0 & \mathbb{I}_{n-m} \end{bmatrix} B^{-1}\Phi^{-1}(T_s)\mu(T_s)\tilde{x}(iT_s)\,, \quad t \in [iT_s, (i+1)T_s)\,, \tag{S47}$$

for $i = 0, 1, 2, \ldots$, where $\tilde{x}(t) = \hat{x}(t) - x(t)$, B is introduced in (S41), and

$$\Phi(T_s) \triangleq A_m^{-1} \left(\mathrm{e}^{A_m T_s} - \mathbb{I} \right) ,$$

while

$$\mu(T_s) = \mathrm{e}^{A_m T_s} ,$$

The control law is given by

$$u(s) = -KD(s)\hat{\eta}(s) , \tag{S48}$$

where $\hat{\eta}(s)$ is the Laplace transform of the signal

$$\hat{\eta}(t) \triangleq \omega_0 u(t) + \hat{\eta}_1(t) + \hat{\eta}_{2m}(t) - r_g(t) , \tag{S49}$$

with $r_g(s) \triangleq K_g(s) r(s)$, $\hat{\eta}_{2m}(s) \triangleq H_m^{-1}(s) H_{um}(s) \hat{\eta}_2(s)$ capturing the estimation of the unmatched uncertainties, where $\hat{\eta}_2(t) \triangleq \hat{\sigma}_2(t)$, and with $\hat{\eta}_1(t) \triangleq \hat{\sigma}_1(t)$ estimating the matched uncertainties.

Notice that conventional design methods from multivariable control theory can be used to design the prefilter $K_g(s)$ to achieve desired decoupling properties. As an example, if we choose $K_g(s)$ as the constant matrix $K_g = -(CA_m^{-1}B_m)^{-1}$, then the diagonal elements of the desired transfer matrix $M(s) = C(s\mathbb{I}_n - A_m)^{-1} B_m K_g$ have dc gain equal to one, while the off–diagonal elements have zero DC gain.

The $\mathcal{L}_1$ reference system for this architecture is given by

$$\dot{x}_{\rm ref}(t) = A_m x_{\rm ref}(t) + B_m \left(\omega u_{\rm ref}(t) + f_1(t, x_{\rm ref}(t), z(t))\right) \tag{S50}$$

$$+ B_{um} f_2(t, x_{\rm ref}(t), z(t)) \,, \quad x_{\rm ref}(0) = x_0 \,, \tag{S51}$$

$$u_{\rm ref}(s) = -\omega^{-1} C(s) \big(\eta_{1\rm ref}(s) + H_m^{-1}(s) H_{um}(s) \eta_{2\rm ref}(s) - K_g(s) r(s)\big) \,, \tag{S52}$$

$$y_{\rm ref}(t) = C x_{\rm ref}(t) \,, \tag{S53}$$

where $\eta_{i\rm ref}(s)$ is the Laplace transform of $\eta_{i\rm ref}(t) \triangleq f_i(t, x_{\rm ref}(t), z(t))$, $i = 1,\ 2$.

Again notice that using the ideas discussed in "Bridging Adaptive and Robust Control", we can derive the reference controller from the equations of the $\mathcal{L}_1$ reference system in (S51)–(S52) and arrive at

$$u_{\rm ref}(s) = k D(s) H_m^{-1}(s) (H_m(s) K_g(s) r(s) - C x_{\rm ref}(s)) \,,$$

which is similar to the reference controller for the state feedback with matched uncertainties in (S5). Due to this structural equivalence between $\mathcal{L}_1$ reference controller and a linear internal model controller, robust control methods can be applied for design a lowpass filter that satisfies the $\mathcal{L}_1$ norm stability condition in (S44).

The next theorem summarizes the main result for this adaptive architecture.

Theorem 4 *[S13, Theorem 1] Let the feedback gain K and the filter $D(s)$ be chosen to satisfy the $\mathcal{L}_1$–norm condition in* (S44)*. Then the reference system in* (S51)–(S53) *is stable.*

Further if the the adaptation rate is chosen to satisfy

$$\gamma_0(T_s) < \bar{\gamma}_0 \,,$$

where $\gamma_0(T_s)$ *is a known computable class* $\mathcal{K}$ *function of* T_s*, then we have*

$$\|\tilde{x}\|_{\mathcal{L}_\infty} \leq \gamma_0(T_s) \,, \tag{S54}$$

$$\|x_{\rm ref} - x\|_{\mathcal{L}_\infty} \leq \gamma_1(T_s) \,, \quad \|u_{\rm ref} - u\|_{\mathcal{L}_\infty} \leq \gamma_2(T_s) \,, \tag{S55}$$

$$\tag{S56}$$

where $\gamma_1(T_s)$ *and* $\gamma_2(T_s)$ *are known computable class* $\mathcal{K}$ *functions of* T_s*.*

Thus, the tracking error between $y(t)$ and $y_{\rm ref}(t)$, as well as $u(t)$ and $u_{\rm ref}(t)$, is uniformly bounded by an arbitrarily small constant, which implies that both in transient and steady state arbitrary close tracking performance can be achieved for both signals simultaneously by reducing T_s. These results are consistent with the results in "$\mathcal{L}_1$ Adaptive Output–Feedback Controller with Piecewise Constant Adaptation Laws", where we could achieve arbitrary performance bounds by choosing appropriate value of the sampling time T_s.

References

[S13] E. Xargay, N. Hovakimyan, and C. Cao, "$\mathcal{L}_1$ adaptive controller for multi–input multi–output systems in the presence of nonlinear unmatched uncertainties", in: *American Control Conference*, Baltimore, MD, 2010, pp. 874–879.

Sidebar 14. Aircraft Handling Qualities and Their Specifications

Handling qualities involves the study and evaluation of the stability and control characteristics of an aircraft [S14]. They have a critical bearing on the safety of flight and on the ease of controlling an airplane in steady flight and in maneuvers. The stability characteristics of airplanes can be separated into longitudinal and lateral groups with the corresponding modes of motion. The longitudinal modes of a statically stable airplane following a disturbance consist of a long–period oscillation called the phugoid oscillation, usually with a period in seconds about one–quarter of the airspeed in miles per hour and a short–period oscillation with a period of only a few seconds. The lateral motion has three modes of motion: an aperiodic mode called the spiral mode that can be a divergence or subsidence, a heavily damped aperiodic mode called the roll subsidence, and a short–period oscillation, usually lightly damped, called the Dutch roll mode.

In an attempt to provide guidance for stability and control of an aircraft, whether stable bare airframe, one with feedback stability augmentation system or full authority command augmentation, US Military Specifications (Mil–Specs) are described in [S15]. These specifications establish the relationships between pilot ratings, phases of flight, aircraft class, flight envelopes and aircraft states. Moreover, they provide very specific guidelines on the desired dynamics for specific longitudinal and lateral motions of the aircraft as well as the simplified dynamics that can express these dynamics, known as low order equivalent systems. These Mil–Spec guidelines are used in both civilian and military aircraft to shape dynamics associated with good handling qualities for both piloted and unmanned aircraft. The evaluation of how well a piloted aircraft behavior follows these guidelines is done using the Cooper–Harper scale.

The Cooper–Harper scale is universally used to enable the pilot to award a number to an aircraft to allow comparison with other aircraft or to show compliance with specifications. The scale has ten points, where 1 indicates excellent and 10 the worst qualities possible — uncontrollable aircraft resulting in a crash. The scale is dichotomous, which results in improved repeatability by leading the evaluation pilot through a series of decisions regarding the task performance and pilot workload. The latter is subjective but the task performance is reasonably repeatable provided that the task is well–defined. Note that the rating is task specific, which implies that although the aircraft may be controllable and flyable, the specific task rating might be very poor. Such a result would indicate a constraint on the aircraft performance and maneuverability and would typically be a result of a fault or failure.

References

[S14] J. Hodgkinson, *Aircraft Handling Qualities*, AIAA Educational Series, 1999.

[S15] Anonymous, *Mil–SPEC–1797A: Military Standard, Flying Qualities of Piloted Vehicles*, 1990.

Author Information

Naira Hovakimyan (nhovakim@illinois.edu) received her Ph.D. in Physics and Mathematics in 1992, in Moscow, from the Institute of Applied Mathematics of Russian Academy of Sciences. In 1997 she has been awarded a governmental postdoctoral scholarship to work in INRIA, France. She is the recipient of the SICE International scholarship for the best paper of a young investigator in the VII ISDG Symposium (Japan, 1996). Since 2008 she is on the faculty of Mechanical Science and Engineering of University of Illinois at Urbana–Champaign, where she is a professor and Schaller faculty scholar. She is also affiliated with Aerospace Engineering, Electrical and Computer Engineering, Coordinated Science Labs and Information Thrust Institute. She is the author of over 200 refereed publications. She is senior member of the IEEE (CSS, NNS), Associate fellow of AIAA, member of AMS, SIAM, ISDG, and is serving as Associate Editor for the IEEE Control Systems Society, IEEE Transactions on Control Systems Technology, Computational Management Science of Springer, Mathematics in Engineering, Science and Aerospace. She is the 2004, 2005 and 2007 recipient of Pride@Boeing award, the plenary speaker of 2007 SIAM Conference on Control and Its Applications, 2009 IASTED Conference on Identification and Control Applications, 2010 International Symposium on Systems and Control in Aeronautics and Astronautics, 2010 ICNPAA World Congress. In 2008 she received Dean's Award for Research Excellence at Virginia Tech. She was named outstanding reviewer for AIAA Journal of Guidance, Control and Dynamics in 2008 and 2009. Her current interests are in the theory of robust adaptive control and estimation with an emphasis on aerospace applications, control in the presence of limited information, networks of autonomous systems and game theory.

Chengyu Cao is Assistant Professor of Mechanical Engineering at the University of Connecticut.

His research interests are in the areas of dynamics and control, adaptive and intelligent systems, and mechatronics, with focus on unmanned systems and aerospace applications. He is the author of more than 100 publications in journals and peer-reviewed conference proceedings.

Evgeny Kharisov is a Ph.D. candidate at the Department of Aerospace Engineering at University of Illinois at Urbana–Champaign. He received the Bachelor's and Master's degrees from the Department of Informatics and Control Systems at Bauman Moscow State Technical University in 2004 and 2007 respectively. His research interests include adaptive control, robust control, multi–agent systems, and automatic control in aerospace systems.

Enric Xargay please write your bio here

Irene M. Gregory is a Senior Research Engineer at NASA Langley Research Center, Dynamic Systems and Control Branch. She has received a S.B. in Aeronautics and Astronautics from the Massachusetts Institute of Technology in 1988, M.S. in 1990 and a Ph.D. in Control and Dynamical Systems from California Institute of Technology in 2004. Her research included advanced flight control for hypersonic, supersonic, subsonic flight regimes, aircraft, launch vehicles, and UAVs. Her current interests are adaptive, nonlinear control, their robustness and performance measures for real systems as well as autonomy and safe flight in Next Generation National Aerospace System. She is an Associate Fellow of AIAA and a member of IEEE.